

University Of Jordan

Faculty Of Graduate Studies



**Numerical Study Of  
Impinging Jets In Cross-Flow  
Relevant To Short Take-Off And Vertical Landing Aircraft**

**By**

**Baha Mahmoud Mousa Suleiman**

عميد كلية الدراسات العليا



**Supervised By**

**Dr. Bassam Ali Jubran**

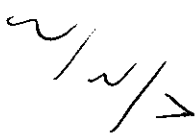


Submitted in Partial Fulfillment of the Requirements for the Degree of Master of  
Science in Mechanical Engineering

Faculty Of Graduate Studies

University Of Jordan

May, 1994



This thesis was defended successfully on 15/5/1994.

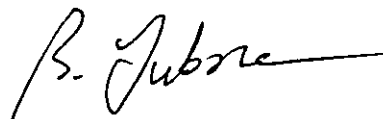
Committee Members

Signature

Dr. Bassam Ali Jubran

Department of Mech. Engineering  
University of Jordan

Chairman of committee



Dr. Nasri J. Rabadi

Department of Mech. Engineering  
University of Jordan

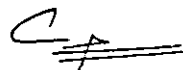
Member of committee



Dr. Saad Al Habali

Department of Mech. Engineering  
University of Jordan

Member of committee



## ACKNOWLEDGMENTS

The author wishes to express his thanks and appreciation for his supervisor Dr. Bassam Ali Jubran for his help, guidance and encouragement through the work of this thesis. Thanks are also due to Dr. Bassam Kakhaleh, the head of the computer lab of the Faculty of Engineering and Technology for his valuable assistance and support in regards to the computer facilities. Also, worthy of mentioning is the computer lab operators.

Special thanks are due to the author's family for their support and encouragement. Finally, word of thanks are due to the author's colleagues and friends, who were interested in this work.

## ***Table of contents***

Committee decision	II
Acknowledgments	III
Table of contents	IV
List of tables	VII
List of figures	VIII
Nomenclature	X
Abstract	XIII
Chapter 1	
Introduction	1
1.1 Introduction	1
1.2 Basic flow fields	2
1.3 Hot gas ingestion	4
1.4 Induced pressures and forces	6
1.5 Thesis objective and layout	7
Chapter 2	
Literature Survey	12
2.1 Introduction	12
2.2 Experimental Studies	12
2.2 Numerical Studies	21
Chapter 3	
Mathematical Modeling	32
3.1 Introduction	32
3.2 Governing equations	33
3.3 Grid Layout	35
3.4 Finite volume equations	35
3.5 The solution procedure	38

3.6 Boundary Conditions	38
3.7 Convergence monitoring	40
3.8 Impinging jet in cross-flow modeling	41
3.8.1 Cross-flow modeling	41
3.8.2 Boundary conditions	42
3.8.3 Solution domain	43
3.8.4 Convergence monitoring and under-relaxation	44
Chapter 4	
Results and Discussion	48
4.1 Introduction	48
4.2 Pressure coefficient distributions and velocity vectors	51
4.3 Ground vortex self similarity	52
4.4 Effect of effective Velocity ratio	53
4.5 Effect of height	58
4.6 Effect of nozzle pressure ratio	60
4.7 Effect of jet temperature	61
4.8 Effect of the intake (engine inlet)	62
4.8.1 Effect of intake mass flow rate	63
4.8.2 Effect of intake location	63
4.9 Hot gas environment	65
4.9.1 Temperature contours	65
4.9.2 Hot gas ingestion	66
Chapter 5	
Conclusions and Recommendations	88
5.1 Introduction	88
5.2 Summery and Assessment of the Present Investigation	88
5.3 Conclusions	89
5.4 Recommendations	91
References	92

<b>Appendix A</b>	
<b>Calculation of jet exit conditions</b>	<b>97</b>
<b>Appendix B</b>	
<b>Structure and Modifications of the computer code TEAM</b>	<b>99</b>
<b>Appendix C</b>	
<b>Preparing the I file</b>	<b>105</b>
<b>Appendix D</b>	
<b>List of Modified Subroutines and samples of Input/Output files</b>	<b>110</b>
<b>Abstract in Arabic</b>	<b>156</b>

## ***List of tables***

Table 3.1:	Exchange coefficients and sources.	33
Table 3.2:	Standard turbulence constants and Prandtl number.	34
Table 3.3:	Source term treatment	36
Table 4.1:	The ranges of parameters used in numerical modeling.	48
Table 4.2:	Predicted results for the cases of low jet temperature and no intake present.	49
Table 4.3:	Predicted results for the cases of high jet temperature and no intake present.	50
Table 4.4:	Predicted results for the cases of high jet temperature and intake present.	50

## List of figures

Figure 1.1:	Research topics associated with <i>STOVL</i> aircraft hovering in ground effect.	9
Figure 1.2:	Subsonic turbulent free jet.	10
Figure 1.3:	Subsonic turbulent impinging jet.	10
Figure 1.4:	Subsonic turbulent impinging jet in cross-flow.	11
Figure 3.1:	Grid layout used for numerical modeling.	44
Figure 3.2:	Boundary conditions for modeling impinging jet in cross-flow.	46
Figure 3.3:	Grid used for modeling impinging jet in cross-flow.	47
Figure 4.1:	Typical ground plane $C_p$ distribution for impinging jet in cross-flow (case 8).	68
Figure 4.2:	Typical velocity vectors for impinging jet in cross-flow (case 8).	68
Figure 4.3:	Enlarged ground vortex region of figure 4.2 (case 8).	69
Figure 4.4:	Effect of $Ve$ on $C_p$ distribution.	69
Figure 4.5:	Effect of $Ve$ on $x_p/d$ at different values of $h/d$ .	70
Figure 4.6:	Enlarged ground vortex region (case 6).	70
Figure 4.7:	Enlarged ground vortex region (case 7).	71
Figure 4.8:	Effect of $Ve$ on $y_v/d$ at different values of $h/d$ .	71
Figure 4.9:	Effect of $Ve$ on $x_p/d$ (comparison between experimental and numerical works).	72
Figure 4.10:	Effect of $h/d$ on $C_p$ distribution.	72
Figure 4.11:	Effect of $h/d$ on $x_p/d$ at different values of $Ve$ .	73
Figure 4.12:	Effect of $h/d$ on $x_p/d$ (comparison between experimental and numerical works).	73



Figure 4.13: Effect of $h/d$ on $x_p/d$ (comparison between experimental and numerical works).	74
Figure 4.14: Effect of $h/d$ on $x_p/d$ (comparison between numerical works).	74
Figure 4.15: Effect of $pr$ on $C_p$ distribution.	75
Figure 4.16: Effect of $pr$ on $x_p/d$ .	75
Figure 4.17: Effect of $T_j/T_\infty$ on $C_p$ distribution.	76
Figure 4.18: Effect of $T_j/T_\infty$ on $x_p/d$ at different values of $Ve$ .	76
Figure 4.19: Effect of $m_j/m_j$ on $C_p$ distribution.	77
Figure 4.20: Effect of $m_j/m_j$ on $C_p$ distribution.	77
Figure 4.21: Enlarged ground vortex region (case 26).	78
Figure 4.22: Effect of $m_j/m_j$ on $x_p/d$ .	78
Figure 4.23: Effect of $l/d$ on $C_p$ distribution.	79
Figure 4.24: Effect of $l/d$ on $x_p/d$ .	79
Figure 4.25: Effect of $l/d$ on $C_p$ distribution.	80
Figure 4.26: Enlarged ground vortex region (case 37).	80
Figure 4.27: Velocity vectors (case 37).	81
Figure 4.28: Temperature contours (case 18).	81
Figure 4.29: Temperature contours (case 19).	82
Figure 4.30: Temperature contours (case 20).	82
Figure 4.31: Temperature contours (case 22).	83
Figure 4.32: Temperature contours (case 24).	83
Figure 4.33: Temperature contours (case 26).	84
Figure 4.34: Temperature contours (case 37).	84
Figure 4.35: Temperature contours (case 34).	85
Figure 4.36: Effect of $Ve$ on $x_{ph}/d$ .	85
Figure 4.37: Relation between $x_{ph}/d$ and $x_p/d$ .	86
Figure 4.38: Effect of $m_j/m_j$ on $Tn_i$ .	86
Figure 4.39: Effect of $l/d$ on $Tn_i$ .	87

# Nomenclature

## Abbreviations

<i>ASTOVL</i>	Advanced Short Take-Off and Vertical Landing
<i>CFD</i>	Computational Fluid Dynamics
<i>HGI</i>	Hot Gas Ingestion
<i>LID</i>	Lift Improvement Device
<i>PLDS</i>	Power Law Differencing Scheme
<i>QUICK</i>	Quadratic Upstream-Weighted Differencing Scheme
<i>STOVL</i>	Short Take-Off and Vertical Landing
<i>VTOL</i>	Vertical Take-Off and Landing
<i>V/STOL</i>	Vertical or Short Take-Off and Landing

## Symbols

$a$	numerical coefficient (combined diffusion and convection coefficient)
$c_p$	constant pressure heat capacity
$C_p$	coefficient of pressure = $(p - p_\infty)/(0.5\rho_\infty V_\infty^2)$
$C_{p_{max}}$	maximum $C_p$ on the ground plane
$C_{p_{min}}$	minimum $C_p$ on the ground plane
$C_1$ and $C_2$	Standard turbulence coefficients
$d$	nozzle diameter
$G$	turbulence generation
$h_c$	ground vortex height, critical nozzle height
$h$	nozzle height above the ground plane
$k$	turbulent kinetic energy
$l$	horizontal distance between the nozzle and the intake
$m$	mass flow rate

$p$	pressure
$pr$	pressure ratio
$q$	dynamic pressure
$S$	source term
$S_p$ and $S_u$	linearized source terms
$T$	temperature
$TU$	turbulence intensity
$u$	$x$ -axis velocity component
$urf$	Under-relaxation factor
$v$	$y$ -axis velocity component
$V$	velocity in vector form
$V_0$	wind speed at which no more <i>HGI</i> occurs
$V_e$	effective velocity ratio = $\sqrt{(\frac{1}{2}\rho_j V_j^2)/(\frac{1}{2}\rho_\infty V_\infty^2)}$
$V_j$	jet exit velocity
$V_\infty$	cross-flow velocity
$x$	horizontal distance (measured against the cross-flow)
$y$	Vertical distance (measured against the free jet flow)

Greek symbols

$\varepsilon$	eddy dissipation of turbulent kinetic energy
$\phi$	general variable ( $\phi = I, u, v, k, \varepsilon$ or $T$ )
$\gamma$	Isentropic ratio
$I$	turbulent exchange coefficient
$\mu_l$	laminar viscosity
$\mu_t$	turbulent viscosity
$\mu_{eff}$	effective viscosity
$\rho$	density
$\sigma_\varepsilon$ and $\sigma_k$	standard turbulent constants

$\sigma_T$       Frandtl number

**Common Subscripts**

*i*            intake conditions  
*j*            jet exit conditions  
*p*            maximum penetration point  
*ph*          hot gases penetration  
*m*            maximum  
*s*            separation point  
*v*            ground vortex core  
 $\infty$           ambient (cross-flow) conditions

## **Abstract**

***Title: "Numerical Study Of Impinging Jets In Cross-Flow Relevant To Short Take-Off And Vertical Landing Aircraft"***

***Prepared By: Baha Mahmoud Suleiman***

***Supervised By: Dr. Bassam Ali Jubran***

In this study, the flow field due to a single impinging jet in cross-flow has been investigated numerically, using a 2-D axi-symmetric model. The parameters studied are; the effective velocity ratio ( $Ve = 14.4$  to  $26.1$ ), the nozzle height ( $h/d = 2.0$  to  $10.0$ ), the nozzle pressure ratio ( $pr = 1.05$  to  $1.6$ ), the intake location ( $l/d = 10.5$  to  $22.5$ ), the intake mass flow rate ( $m_i/m_j = 0.25$  to  $4.0$ ) and the jet temperature ( $T_j/T_\infty = 0.89$ - $3.2$ ). The effect of the above parameters on the ground vortex location, size and strength as well as on the temperature distribution in the flow field have been investigated. It is interesting to note that even with the 2-D modeling limitations, the modeling produced similar flow fields to those obtained experimentally, in terms of both velocity vectors and ground plane pressure coefficient distributions. The ground vortex self similarity relations are reasonably and accurately predicted.

The effective velocity ratio ( $Ve$ ) was found to be the most important parameter that affects the flow field. The ground vortex maximum penetration point ( $x_p$ ) is found to increase steadily as  $Ve$  is increased. It has been found that  $x_p = 0.86 Ve$ , where  $x_p$  is overpredicted by about 25% compared with 40-50% in previous numerical studies. The ground vortex strength and size also increase with increasing  $Ve$ . The temperature distribution in the flow field is greatly affected by  $Ve$ , where the penetration of hot gases increase with increasing  $Ve$ . Furthermore, it is found that the maximum penetration point is equal to the hot gases penetration.

The effect of jet temperature on the flow field is found to be minor at a constant  $V_e$  in terms of the ground vortex geometry and strength, and temperature distribution, since the temperature effect is included in  $V_e$ . For the range investigated in this study, nozzle height is found to have a little effect on the ground vortex geometry and strength, and on the penetration of hot gases, but it has a significant effect on the temperature at the impingement point. Nozzle pressure ratio effect (in the subsonic range) is found to be insignificant at constant  $V_e$ .

The ground vortex strength increases a little with increasing the intake mass flow rate while the mass flow rate has a minor effect on the ground vortex geometry and on the penetration of hot gases. Hot gas ingestion decreases a little with increasing mass flow rate. The intake location is found to have a significant effect on the ground vortex strength and on the stagnation pressure, provided it is located beyond the ground vortex core but with a little effect on the temperature distribution. Hot gas ingestion decreases clearly with increasing the intake location.

# Chapter 1

## Introduction

### 1.1 Introduction

A primary design consideration in a short take-off and vertical landing (*STOVL*) aircraft is the aerodynamic interaction between airframe undersurface and the ground in the presence of lift jets during hover and low speed operation. The performance of a *STOVL* aircraft in ground effect is highly dependent on the details of the design. Improvements in *STOVL* performance is translated into fuel savings, which yield either increased range or payload [1]. The areas of concern that associated with jet lift aircraft in ground effect are [2]; airframe airloads, hot gas ingestion (*HGI*), ground erosion, ground crew safety, and noise and airframe acoustic fatigue, see figure 1.1.

The first two areas are considered to be the major areas and have been the subject of many experimental and numerical studies over the past 20 to 30 years. These may be explained by the fact that the turbulent lifting jets mix with their surroundings leading to an induced down flow of air around the aircraft (entrainment) and a resulting suckdown force (figure 1.1). The impingement of the high velocity jet exhaust flow on the ground results in the formation of a wall jet that flows radially from the point of impingement along the ground surface which causes the entrainment of the surrounding flow to increase rapidly. In the presence

of a cross-flow, the wall jet is opposed by the cross-flow and a ground vortex is created. The cross-flow could be present due to either horizontal movement of the aircraft or due to the presence of a head wind. The ground vortex is a major source of the induced flow on *STOVL* aircraft operating in ground effect. The ground vortex is also a source of *HGI*, where the hot exhaust gases are recirculated and ingested by the engine inlets. The ingestion of only a small portion of the exhaust gas into the engine inlets can result in a significant thrust loss. With multiple jet impingement, wall jets collide with each other to form fountain flows that impinge on the fuselage. This can create a significant upload on the aircraft that oppose suckdown effects. However, the fountain flow has many disadvantages since it is highly unsteady and is a major source of *HGI*.

## **1.2 Basic flow fields**

### **The free jet**

The subsonic free jet is characterized by a potential core surrounded by a shear layer where viscous mixing between the jet and the ambient fluid takes place and the velocity drops to zero at the outer edge of the shear layer, see figure 1.2. The potential core region extends about six jet diameters ( $6d$ ) downstream the jet exit [3], beyond which the potential core no longer exists, and the maximum velocity ( $v_m$ ) and the maximum temperature ( $T_m$ ) at the jet centerline decay with vertical distance. The mixing region spreads out due to the entrainment action and the velocity and temperature profiles approach self similar shapes.



### The impinging jet

The flow field of a subsonic impinging jet on a ground plane is characterized by three distinct flow modules (figure 1.3):

1. A free turbulent jet upstream of the plate where the flow characteristics are the same as of a free jet.
2. A stagnation flow near the plate (impingement region) where the jet undergoes a considerable deflection and the pressure gradients dominate that the flow can be considered to act in an invicid manner. The impingement region extends upstream of the ground to a location where the mean properties of the flow deviate by 2% from what value the free jet would have had at the same location [3].
3. A wall jet region where the jet becomes almost parallel to the wall and the effects of impingement are no longer significant. In the wall jet, two separate regions can be identified, an outer region which has characteristics similar to that of a free turbulent jet and an inner region where the frictional effects are significant. The maximum velocity ( $u_m$ ) and the maximum temperature ( $T_m$ ) decrease with the horizontal distance  $x$  due to the effect of entrainment and turbulent mixing.

### The impinging jet in cross-flow

The flow structure of an impinging jet in cross-flow is similar to that of an impinging jet, regarding the free jet region, impingement region and the wall jet region. The interaction of the wall jet with a cross-flow results in the formation of a stagnation line and an unsteady three dimensional ground vortex (figure 1.4). The stagnation line is generally of the shape of front half of an ellipse whose major axis is aligned with the cross-flow. The maximum pressure coefficient  $Cp_{max}$  on the ground plane corresponds to the maximum penetration point (stagnation point,  $x_p$ ) of the ground vortex, the minimum pressure coefficient  $Cp_{min}$  corresponds to the

ground vortex core ( $x_v$ ) and the zero  $C_p$  corresponds to the separation point ( $x_s$ ) [4] and [5].

Using invicid and incompressible flow assumptions (ideal flow), the flow field was solved analytically by Bray [5] for the purpose of comparison between theoretical and experimental ground vortex characteristics, it was found that :

$$x_p/d = \frac{1}{8D} V_j/V_\alpha \quad (1.1)$$

where  $V_j$  is the jet velocity,  $V_\alpha$  is the cross-flow velocity,  $d$  is the nozzle diameter and  $D$  is a constant. It can be seen that the ground vortex core location is proportional to the ratio of the jet to cross-flow velocities.

### 1.3 Hot gas Ingestion

*HGI* is a term that describes the flow when the hot exhaust gases from a propulsive jet return to the air intake. The inlets act as sinks that draw inward air from all directions. The effectiveness of these sinks in drawing in hot gases depends on the proximity to the hot gases flow and on the direction and energy of the hot gases stream [6]. Avoidance of excessive *HGI* is critical for safe *STOVL* operation. The *HGI* is an extremely complex process affected by, the inlet and nozzle design and location, the engine performance characteristics, the aircraft velocity and the instantaneous value of separation of the aircraft from the ground [7]. The *HGI* can affect the aircraft in several mechanisms [8], namely;

1. Warmer air is less dense which causes the mass flow rate to decrease resulting in a loss of thrust.
2. The distortion of air temperature in space and time may cause compressor stall.
3. High inlet air temperature causes high temperatures in the turbine, and to prevent this, thrust demand must be reduced.

An increase in the temperature of the inlet air of only  $10\text{ }^{\circ}\text{C}$  can cause a thrust loss of 2-5% depending on the engine type [6]. The flow associated with *HGI* can be divided into two types; near field and far field ingestion.

*Near field ingestion* arises with multiple jet configuration where a fountain flow is formed that impinges on the underside of the fuselage, then flows along the bottom of the fuselage to the vicinity of the inlets and eventually finds its way into the inlets. The temperature rise associated with this type of ingestion is high, so it is more severe than far field ingestion. This type of ingestion is strongly fuselage geometry dependent and can be controlled by appropriate fuselage design. For example, the addition of lift improvement devices (*LID's*) to the Harrier aircraft results in at least  $80\text{ }^{\circ}\text{F}$  ( $44.5\text{ }^{\circ}\text{C}$ ) reduction in inlet temperature rise [1]. To minimize *HGI*, jet exit arrangement should be designed to produce only spanwise fountain and the inlets should be as high as possible. Deflectors (shields) should be located where the fountain impinges on the aircraft.

*Far field ingestion* occurs when the radially flowing wall jet separates from the ground due to the effect of buoyancy forces and rises to mix with ambient air, then drawn into the engine inlets. This type of ingestion can be more critical in the presence of a cross wind where a ground vortex is formed. The amount of far field *HGI* is dependent on the location and the size of the ground vortex which are dependent on so many flow and geometrical parameters. The main two parameters are the height of the aircraft over the ground and the wind speed.

The maximum temperature rise in the engine inlet decreases as the height of the aircraft above the ground increases until a height is reached where no more *HGI* occurs. This height is called the critical height ( $h_c$ ) which corresponds to the ground vortex height (see figure 1.4). The maximum temperature rise first increases with increasing the wind speed then decreases until a velocity is reached ( $V_0$ ) where no more *HGI* occurs,  $V_0$  decreases with increasing the height. If the inlets are located above the critical height, there will be no *HGI* [6].

The forward projection of the ground vortex ( $x_p$ ) generated by a single vertical jet (figure 1.4), is directly proportional to  $V_e$ , which is the square root of the ratio of jet exit dynamic pressure to the freestream dynamic pressure ( $V_e$ ). The critical height ( $h_c$ ) is about half the forward projection of the ground vortex [6]. For a test in a wind tunnel or for an aircraft hovering in a head wind,

$$h_c/d = 0.45V_e \quad (1.2)$$

For an aircraft moving forward with no wind,

$$h_c/d = 0.27V_e \quad (1.3)$$

### **1.4 Induced pressures and forces**

For an aircraft hovering out of ground effect, a small lift loss is induced by the entrainment action of the jet, but for an aircraft hovering in ground effect, the download force is considerably much larger due to the presence of the wall jet which increases the entrainment area. With multiple jets, a fountain is created which produces a lifting force when it impinges on the aircraft. The Addition of *LID's* to the Harrier aircraft increases the fountain lift by 5% [1]. In the presence of a cross wind, a ground vortex is formed which induces an additional download. The strength of the ground vortex decreases rapidly at larger heights and there is a height where impingement no longer occurs and the ground vortex does not form [9].

## 1.5 Thesis objective and layout

The objective of this thesis is to investigate numerically the various parameters that influence the location and size of the ground vortex and the hot gas ingestion with reference to *STOVL* aircraft. The effect of the effective velocity ratio, jet height, jet temperature, nozzle pressure ratio, intake mass flow rate and the location of the intake are to be studied in this work. Comparisons with other experimental and numerical works are provided. The studied parameters are all defined in non-dimensionalized forms, as follows:

- Effective velocity ratio:  $Ve = \sqrt{(1/2\rho_j V_j^2)/(1/2\rho_\infty V_\infty^2)}$ .
- Nozzle pressure ratio:  $pr = p_0/p_\infty$ .
- Temperature ratio:  $T_j/T_\infty$ .
- Nozzle height (normalized):  $h/d$ .
- Intake location (normalized):  $l/d$ .
- Mass flow rate ratio:  $m_i/m_j$ .

where,

$V_j$  and  $V_\infty$  are the velocities of the jet and the cross-flow, respectively.

$\rho_j$  and  $\rho_\infty$  are the jet density and the ambient/cross-flow density, respectively.

$p_0$  and  $p_\infty$  are the nozzle stagnation pressure and the ambient/cross-flow pressure, respectively.

$T_j$  and  $T_\infty$  are the temperatures of the jet and the cross-flow, respectively.

$h$  is the height of the nozzle above the ground plane.

$l$  is the horizontal distance between the intake and the nozzle.

$m_i$  and  $m_j$  are the mass flow rates of the intake and the jet, respectively.

436779

The thesis consists of five *chapters*, of which this introduction is the first. *Chapter 2* is a literature survey of previous experimental and numerical works. *Chapter 3* describes the mathematical modeling of the problem and the computer code used to solve it numerically. *Chapter 4* includes the presentation and the discussion of the results. Finally, *chapter 5* reports the concluding remarks gained from the present investigation, followed by recommendations for future work.

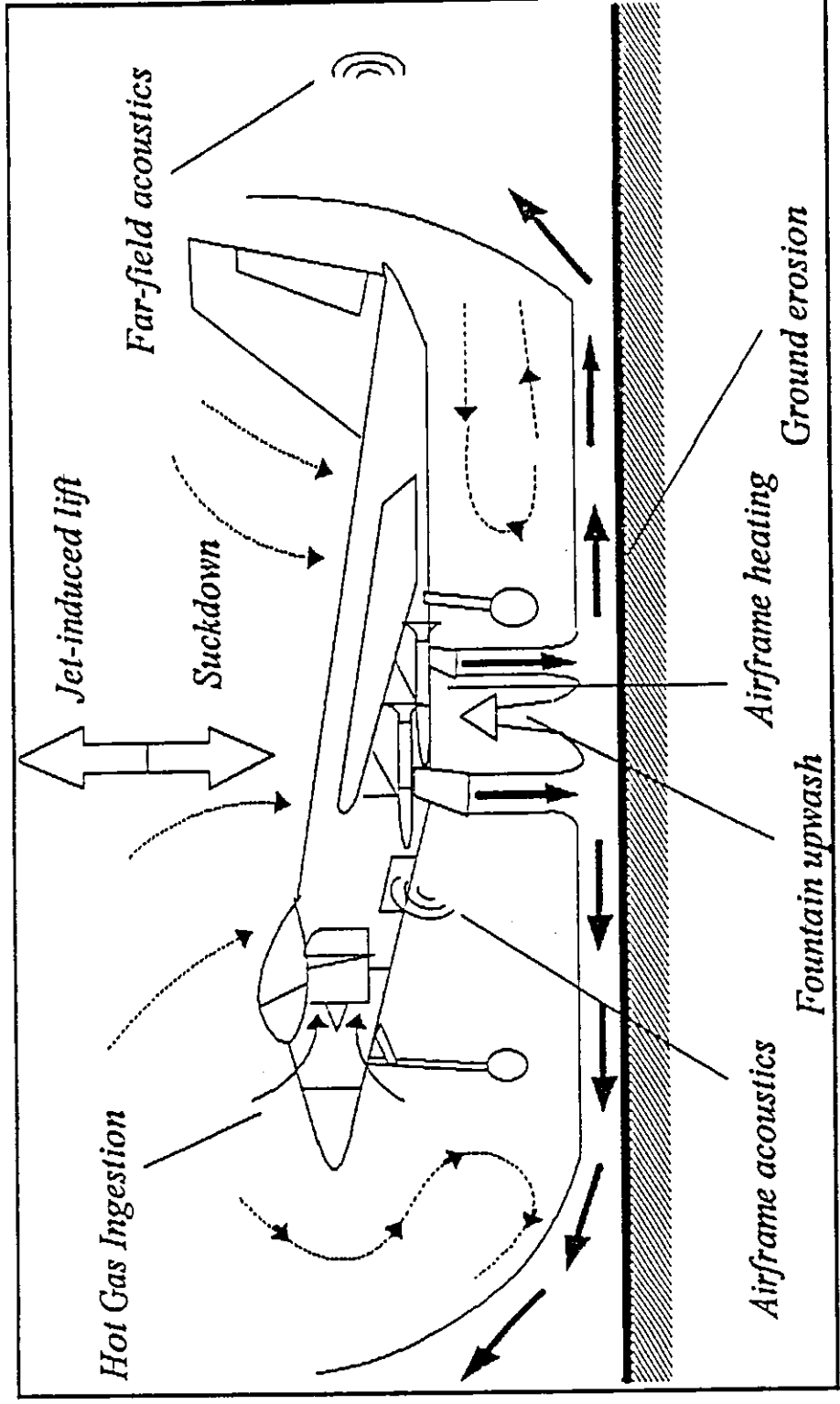


Figure 1.1: Research topics associated with STOVL aircraft hovering in ground effect.

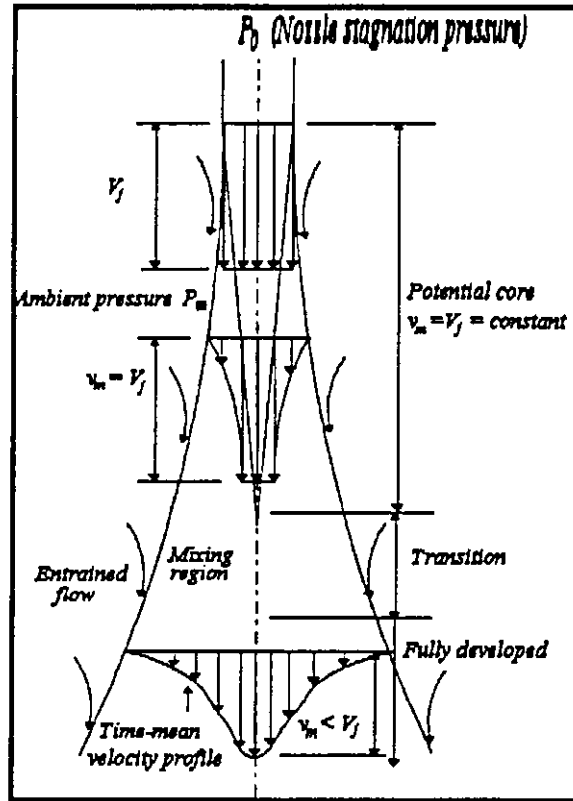


Figure 1.2: Subsonic turbulent free jet.

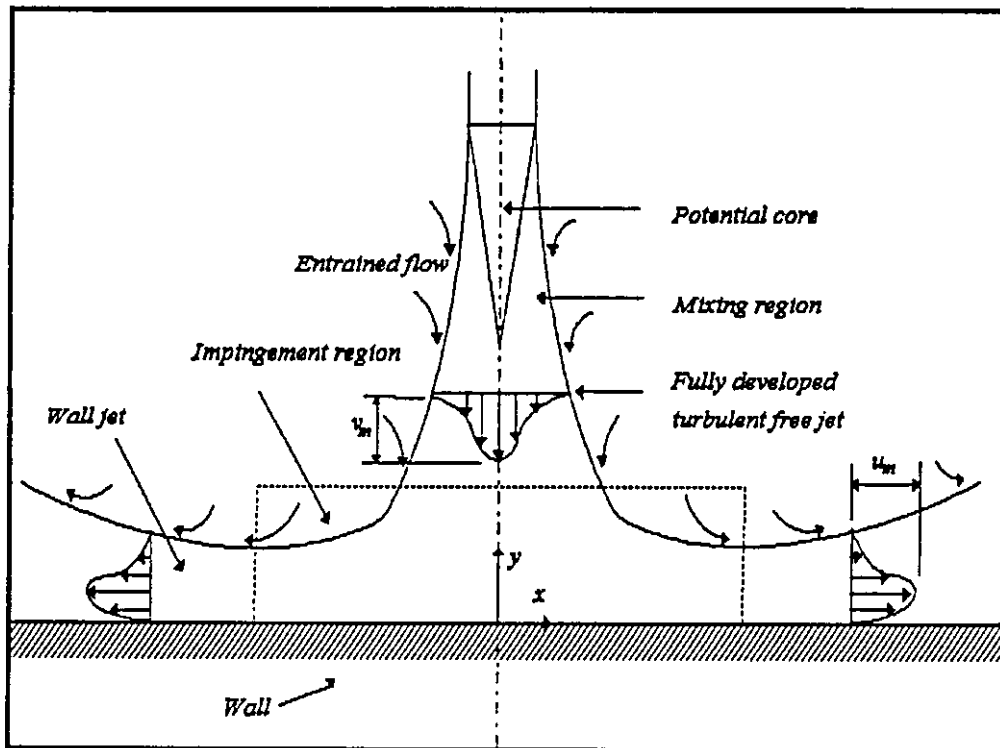


Figure 1.3: Subsonic turbulent impinging jet.



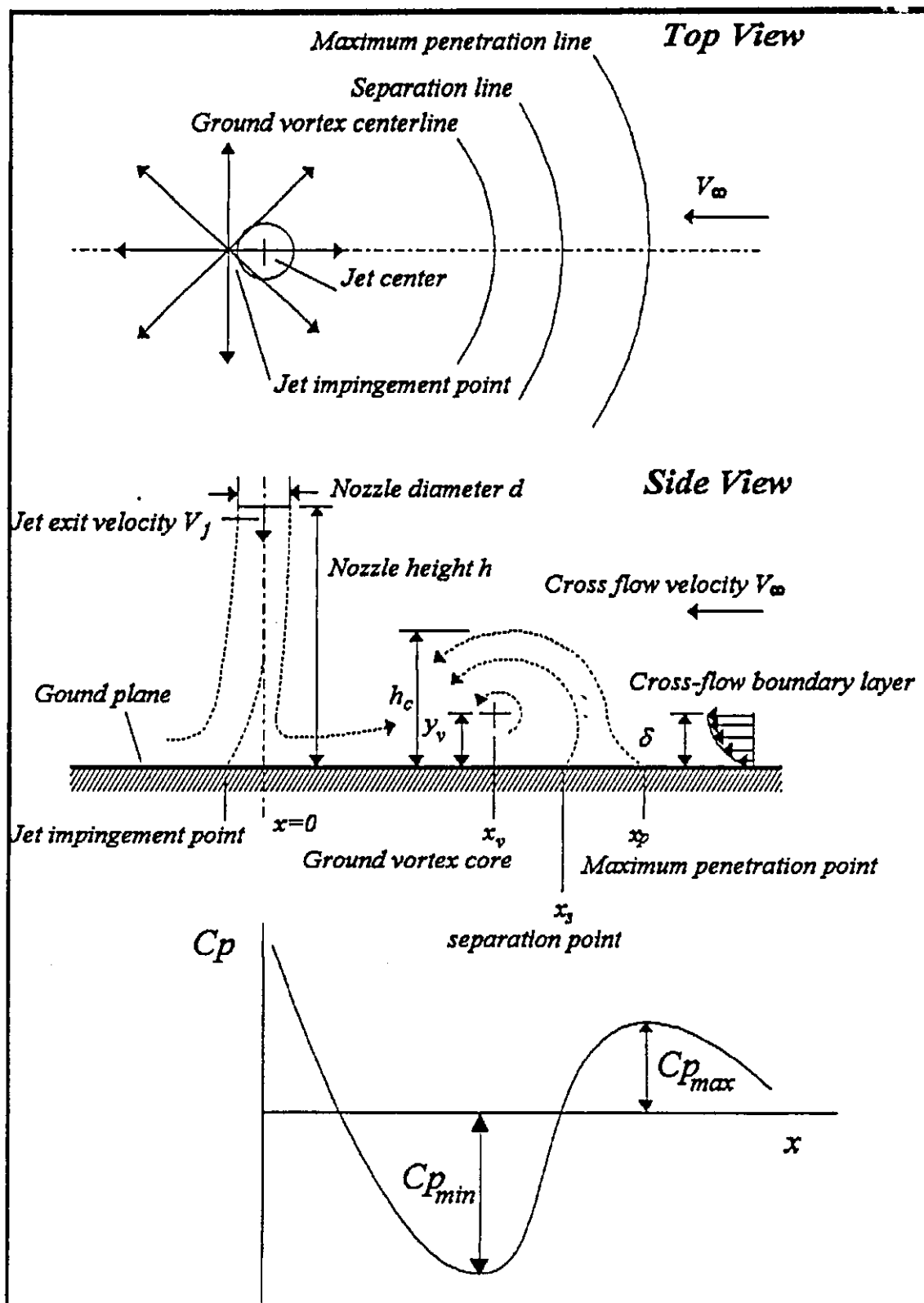


Figure 1.4: Subsonic turbulent impinging jet in cross-flow.

## Chapter 2

### Literature Survey

#### 2.1 Introduction

This thesis is mainly directed towards the numerical investigation of jets in cross-flow, together with the basic flow fields that are strongly related to it, namely; the free jets and the impinging jets. Although the present investigation is a numerical one, the literature survey will also include a review on the experimental and numerical investigations for the purposes of comparison with the present numerical predictions as well as providing a better understanding of the flow fields of interest. The literature survey will emphasize the physical aspects of the flow fields of interest together with the various parameters that affect them. Particularly, the effects of the jet to cross-flow velocity ratio, the height of the jet above the ground plane, the nozzle pressure ratio, the jet temperature and the conditions at the intake.

#### 2.2 Experimental Studies

Cimbala *et al.* [4] conducted experimental investigations in a wind tunnel to model the impingement of high velocity jet exhaust flow on the ground, as encountered by vertical or short take-off and landing (*V/STOL*) aircraft. A constant

jet velocity was maintained ( $45.7 \text{ m/s}$ ) while varying the wind tunnel cross-flow velocity (velocity ratios of  $0.1$ ,  $0.15$ ,  $0.2$ ,  $0.3$  and  $0.4$ ), upstream boundary layer thickness and height from the ground to the jet exit plane ( $h/d = 1, 2, 3$  and  $4$ ). It was found that the ground vortex decreases in size and moves further downstream as the cross-flow velocity increases and that the freestream apparently flows over the vortex as it would flow over a solid body obstruction in the flow. Photographs for the flow field revealed the flow field to be quiet unsteady and three dimensional. It appeared that installing a jet plate around the nozzle exit causes the separation bubble (ground vortex) to decrease significantly in size and the separation point moves further downstream. Thickening of the oncoming boundary layer resulted in further penetration of the wall jet but it was not enough to account for the large scatter in data from various facilities. As the height of the jet or the velocity ratio is increased, the impingement point moves downstream.

Cimbala *et al.* [10] studied experimentally the ground vortex formed by a jet in the presence of a cross-flow. High speed motion pictures and spectral measurements were obtained to study the unsteady features of the flow field. In all cases the freestream velocity was  $4.6 \text{ m/s}$ , while the jet velocity was maintained at  $45.7 \text{ m/s}$  at a fixed height of nozzle from the ground ( $h/d$  of  $3.0$ ). It was concluded that the ground vortex is extremely unsteady in terms of size, shape and location, it is also three dimensional. The ground vortex unsteadiness could not be correlated with disturbances in the cross-flow, jet, wake of the jet tube or the approaching boundary layer.

Abbott [11] carried out model tests with single and twin nozzle arrangements at different inclinations, jet temperatures and nozzle heights above the ground. Moving and stationary nozzle configurations were used. The nozzle speed was varied between  $1.52$  to  $5.18 \text{ m/s}$ . The upwind extent of the flow from these nozzles has been measured and an attempt has been made to correlate these

readings with the steady state decay of dynamic head of the jets from the respective stationary nozzle arrangement. Flow visualization techniques were used, with a *cine* camera and chalk dust. For the impinging jets (steady state tests), it was found that  $(q_{mx}/q_j)^{1/2}$  which represents the decay of the wall jet maximum dynamic pressure ( $q_{mx}$ ) along the ground plane relative to the jet exit dynamic pressure ( $q_j$ ), is independent of the jet dynamic head and the jet temperature. Straight line relation was found to exist between the dynamic head decay and the radial distance from the impingement point ( $x$ ). For vertical jets or behind an inclined jet, it was found that there will be no apparent effect of the nozzle height. Abbott used a moving model to study the effect of impinging jets in cross-flow (taxiing model tests). He conducted both cold and hot jet tests. It was concluded that the parameter defining the extent of the jet (maximum penetration point) is  $(q_\infty/q_j)^{1/2}$  and not  $V_\infty/V_j$ , where  $V_\infty$  is the cross wind velocity,  $V_j$  is the jet velocity and  $q_\infty$  is the cross-flow dynamic head. Abbott also concluded that the jet extends forward to a point at which the maximum dynamic head for the stationary nozzle arrangement would be four times the dynamic head of the still air relative to the moving nozzle. No effect of height was found at low velocity ratios.

Miller *et al.* [12] conducted flow visualization experiments in a water tunnel to study the interaction of three dimensional impinging jets for potential *STOVL* aircraft applications. The flow field behavior was studied as a function of model height above a ground plane, jet nozzle spacing, jet exit velocity, angle of attack, and cross-flow velocity. The jet Reynolds numbers were 6,200, 16,000, and 18,600 while the freestream Reynolds numbers were varied between 0 to 48,000. It was found that the ground vortex appeared to change in size and strength in a semi periodic fashion. At the lowest heights ( $h < 1.25$  inches), the jet flows were observed to move outwards at high speeds and in some cases curved back over the top of the model which suggests that strong "suckdown" and potential exhaust re-ingestion problems might exist. As the height was increased or jet mass flow rates

decreased, the suckdown magnitude diminished. It was concluded that only minor effects in the flow behavior were noted as a result of installation and operation of the simulated engine inlets. The effect of suckdown and re-ingestion problems were observed at low heights ( $h < 2.5$  inches).

Catalano *et al.* [13] carried out both experimental and numerical studies for the flow of a turbulent jet discharging into a confined cross-flow, mean velocity ratios of 2, 4, and 6 were examined and a comparison was made between the calculated results and experimental data. It was concluded that the flow near the jet exit is anisotropic and that the maximum turbulent stresses occur at approximately the same location as the maximum velocity gradients indicating the existence of a large transfer of kinetic energy from the mean flow to the turbulent flow. The highest shearing rate exists near the jet entrance to the flow.

Barata *et al.* [14] studied the flow field resulting from the impingement of a single axisymmetric jet against a wall after penetrating a confined cross-flowing stream using Laser Doppler Anemometry. The jet Reynolds number was 60,000 and the jet turbulent intensity was 2% while the cross-flow turbulence intensity was 18%. The jet to cross-flow velocity ratio was 30. The results showed an initial potential core jet region and an impingement region characterized by considerable deflection of the jet which is only slightly distorted by the cross-flow. Turbulence measurements show that the shear layer surrounding the impinging jet and the impingement zone is characterized by intense velocity fluctuations with its maximum value is coincident with the highest mean velocity gradients.

Araujo *et al.* [15] conducted an experimental study of a developing jet that was impinging normally and obliquely on a smooth wall. The nozzle used was of 14.0 mm diameter, and the velocity of the jet was 50 m/s. The height of the nozzle above the ground was 12d. The Reynolds numbers of the jet were 32,000 and

42,500. For the impinging jets, it was found that self similarity was achieved at a distance of  $8d$  from the nozzle and that the turbulence intensity and the Reynolds number at the jet exit have influence on the initial spreading of the jet. Empirical relations were given for jet spreading rate and velocity decay with distance from the nozzle. The turbulence intensity at the jet center line of the free jet was 20%. For  $h/d > 8.3$ , the development of the impinging region and wall jet is independent of the nozzle height  $h/d$ . For the wall jet with normal impingement, it was found that self similarity was achieved at radial distance  $x/d = 9$ . Empirical relations were given for the wall jet spreading rate and velocity decay with the radial distance measured from the virtual wall jet origin. The turbulence intensity was found to reach self similarity at  $x/d = 6$  where the fluctuations were smeared out and the minimum turbulence intensity was found at the location of maximum velocity. The entrainment of quiet fluid was found to occur deep inside the flow. The outer shear layer was found to have important role on the turbulent mixing process.

Bradbury [16] studied the impact of an axisymmetric jet into a ground board. He presented a simple argument for correlating data obtained in the impact region for different nozzle configurations and for different nozzle heights above the ground. The argument was applied, in particular, to the static pressure on the ground board and to the peak dynamic head in the flow over the ground plane. Tests were conducted with jet velocities up to about  $120 \text{ m/s}$ , and the distance between the nozzle and the ground ranged from  $50.8$  to  $254 \text{ mm}$ . For the free jet, it was found that the potential core extended up to six diameters from the nozzle where the flow became fully developed and self similarity for the mean velocity was achieved. In this region, the thickness of the jet width becomes directly proportional to the vertical distance and the mean velocity becomes inversely proportional to the vertical distance. Empirical relations were given for the above relations. For the impinging jet, it was argued that the flow in the impact region is dominated by the high pressure gradient terms so that the fluid in this region

behaves in almost an invicid manner in which the total head along streamlines will be nearly constant. Away from the impact region ( $x/d > 1.5$ ), the decay of the peak dynamic head will arise from turbulence mixing.

Knowles and Bray [17, 18] and Knowles *et al.* [19] studied the flow fields associated with single and twin jets impinging in cross-flows. The parameters which affect the position of the ground vortex have been investigated, namely, cross-flow to jet velocity ratio, cross-flow boundary layer thickness, nozzle height, nozzle pressure ratio, vector angle and nozzle splay with both fixed and moving ground planes. Results show that the ground vortex moves away from the nozzle center line as the cross-flow to jet velocity ratio is decreased, the rate of change of position, however is dependent on other parameters. In this regard, the definition of the nozzle equivalent velocity and cross-flow velocity ratio were seen to be important. The influence of the nozzle height on the vortex position was seen to be extremely difficult to isolate accurately. For single nozzles, increasing nozzle height above the ground appeared to cause little consistent variation in the vortex position where vortex penetration was increased for initial height increases, followed by a reduction in penetration once jet deflection becomes significant. For all cases, there is an increase in penetration with increasing nozzle pressure ratio up to choking, with the subsequent behavior dependent on the definition of the nozzle equivalent velocity and cross-flow velocity ratio. The effect of the moving ground plane is to reduce vortex penetration by 24% on the average. It is also shown that the rig design can produce a blockage effect which moves the ground vortex significantly and can change other apparent parametric effects. Self similarity laws were proposed for the ground vortex and the wall jet. The flow was seen to be unsteady, especially in the presence of the twin jet fountain.

Smith *et al.* [20] studied the jet flow fields generated by advanced short take-off and vertical landing (ASTOVL) aircraft in ground effect experimentally and

computationally. The general aspects of single, twin and three jet impingement were described via experimental information obtained using Laser sheet and schlieren photography as well as ground and underfuselage surface measurements. Regarding the single nozzle jet impingement tests, subsonic free jets produced a self similar profile and displayed a steady decay with distance from nozzle. The impingement pressure produced by such jets showed a normal distribution and the peak pressure was dependent upon how much the jet has mixed upstream of the impingement. Supersonic jet impingement flows exhibited major differences from their subsonic counterparts. Regarding the single impinging jet in cross-flow, the flow separation distance increased by 10-25% with the moving ground belt compared with the fixed ground plane and the flow separation distances increased by 15-20% with cross-flow boundary layer suction. It was found that the relation between ground vortex core location, separation location and maximum penetration location could be correlated with straight line relationships independent of the flow variables. The non-dimensional parameter derived remains constant for a given rig configuration. It was stated that the ground vortex shows similarity of shape over the range of measured flow conditions and the slope of the straight line correlation is affected mainly by surface friction. If the pressure at the impingement surface is sufficiently high, a supersonic wall jet can be formed.

MacLean *et al.* [7] conducted an experimental investigation on a typical model configuration to establish the interactions between the jets, forward velocity, and the ground. The model consisted of a two inlet configuration with four low subsonic velocity jets impinging vertically on a flat plate, the vertical distance between the flat plate and model under surface being adjustable. The jet Reynolds number was about 20,000. The cross-flow velocity could be set at 0 to 0.1 times the jet velocity. It was concluded that at the higher velocity ratios ( $V_\infty/V_j > 0.06$ ), the ground vortex location appears to be independent of the inlet suction and the test model height. At the lower velocity ratios, the separation distance increases



with height. The ground vortex location was independent of height with the suction off. Inlet suction appeared to influence the ground vortex only at low heights.

Brady and Ludwig [21] studied the flow field under a uniform circular jet perpendicular to and impinging on the ground experimentally and theoretically in order to further the understanding of the aerodynamic processes associated with ground particle entrainment in the impinging downwash from *STOVL* aircraft. Experimental data have been obtained for the flow in the deflected jet and in the ground boundary layer for jet height to nozzle diameter ratios ( $h/d$ ) from 0.25 to 4 and for two mass flows. The boundary layer measurements were obtained at radial stations between one-half and four nozzle diameters from the stagnation point. It was found that at  $h/d = 2$  and 4, the velocity distribution at the jet exit was uniform but for  $h/d = 0.25, 0.5$  and 1.0, the velocity distribution was no longer uniform due to the effect of the ground. It was found that the ground board static pressure distribution is independent of the mass flow. The static pressure at the jet center line was essentially ambient for  $y/d > 1.5$  at  $h/d \geq 1.5$ . The velocity profiles obtained at several radial distances indicated that up to  $x/d = 0.83$ , the boundary layer was laminar where the pressure gradients are large. A transition to turbulent flow occurred in the range  $0.8 < x/d < 2.0$ . Beyond  $x/d = 2$  the flow is turbulent and the pressure is constant.

Bray [5] investigated the flow fields associated with single and twin jets impinging in a cross-flow experimentally and numerically. Parameters which affect the position and strength of the ground vortex have been investigated, namely, nozzle height ( $h/d = 2$  to 12), nozzle pressure ratio ( $p_r = 1.05$  to 4.0), effective velocity ratio ( $V_e = 7.08$  to 75.75), vector angle and nozzle splay with both fixed and moving ground planes. It was concluded that:

- Vortex penetration increases in a reasonably linear fashion with effective velocity ratio. This is the dominant scaling factor, though it is not the only one.
- Penetration decreases significantly when a moving ground plane is used.
- Nozzle height is a secondary factor for single nozzles and difficult to isolate from rig interference effect. Vortex penetration tends to increase with increasing height until a critical height is reached, it then reduces with further height increases. The low height effect appears to be due to more efficient turning process in the impingement region while the upper height effect is due to an increasing dominance of free jet deflation, especially once out of the blocking effect of the ground vortex.
- The size of the cross-flow boundary layer is only a very minor scaling factor consideration, provided that it is only a few  $d$  thick.
- A forward vectoring of the nozzles into the cross-flow results in an increase of vortex penetration.
- Penetration increases with nozzle pressure ratio (at constant  $Ve$ ) up to choking, it decreases at higher pressure ratios but with a second lower peak around  $pr = 3.0$ .
- There is a fixed relationship between the characteristic ground vortex locations which can be described by  $x_s = 0.805 x_p$  and  $x_s = 1.28 x_v$ . This relationship is independent of all flow field variables tested against, including the different nozzle configurations

## 2.2 Numerical Studies

Catalano *et al.* [22] carried out both experimental and numerical studies for the flow of a turbulent jet discharging into a confined cross-flow with mean velocity ratios of 2, 4, and 6. Predicted results were obtained by solving the steady three dimensional elliptic forms of the Reynolds equations coupled with a two equation  $k$ - $\epsilon$  model of turbulence. Finite difference equations were formulated by the finite volume method. The combined effects of convection and diffusion between adjacent grid points were expressed using a power law scheme. A staggered grid arrangement was utilized with the pressure and other dependent variables stored in the main grid points and the velocities in staggered locations. At the wall boundaries, two layer model of the wall function was utilized. It was found that in the initial region ( $x/d = 0.5$ ), the cross-flow was accelerated around the jet and a reverse flow existed behind the jet (wake) similar to the flow around a cylinder. This acceleration increased with the velocity ratio. It was concluded that the velocity ratio determines the existence and location of impingement. The agreement between predicted and experimental results is generally fair. The relatively poor agreement between predicted and measured results near the jet exit suggests the anisotropic nature of this portion of the flow field.

Hwang and Liu [23] solved the Reynolds-averaged compressible Navier stokes, continuity, and energy equations in conjunction with a two-equation ( $k$ - $\epsilon$ ) turbulence model for two dimensional impinging jet flow fields relevant to vertical take-off and landing (VTOL) aircraft. Beam and Warming implicit finite difference scheme with implicit boundary treatment was introduced. For the laminar impinging jet with upper flat plate, the effect of the height of the jet above the ground plane on the flow behavior was obtained ( $h = 2.0, 4.0, 6.0, 8.0$ ). It was found that for smaller  $h$ , the static pressure at the stagnation point became high. The ground plane static pressures at either side of the stagnation point were below

ambient which suggest a strong acceleration in the impingement flow to either side of the stagnation point. Negative pressures occurred along the upper flat surface which suggest the induced suck downloads for *VTOL* aircraft. The negative pressure distributions along the upper flat surface became significant when the distance between the jet and ground plane was small.

Agarwal and Bower [24] solved the planar mass averaged Navier stokes and energy equations in stream function/vorticity form in conjunction with a two equation  $k$ - $\epsilon$  turbulence model for impinging jet configurations relevant to *VTOL* aircraft design. The physical domain was mapped conformally into a rectangular computational region. An augmented central difference scheme was used to preserve the diagonal dominance character of the difference equations at high Reynolds numbers. The resulting difference equations were solved by successive point relaxation. This investigation was the first attempt in the direction of utilizing two equation turbulence model for jet impingement flows. The computed solutions were in good agreement with the experimental data for ground plane pressure, airframe undersurface pressure, and velocity decay along the jet axis. The computed turbulent kinetic energy along the jet axis, however, has a larger overshoot near the ground plane than indicated by the experimental data. This difference was attributed to deficiency in the turbulence model and the fine tuning of the various constants used in the model may be required. The model, however appeared to satisfactory predict the pressure distribution and the velocity field which are the quantities of primary interest in *VTOL* design. The two equation turbulence model was found to be superior in lift-jet predictions than the one equation turbulence model used in previous studies. For these class of flows, there is no single dominant flow direction and there is a large recirculating region, so there is a necessity of a two or higher equation turbulence models. It was concluded that it is unlikely that the pressure, the velocity field, the skin friction, and the heating rate can all be predicted accurately using  $k$ - $\epsilon$  model.

Hwang *et al.* [25] solved the Euler/Reynolds averaged compressible Navier Stokes, continuity and energy equations in conjunction with a two equation  $k-\varepsilon$  turbulence model for two dimensional flows related to  $V/STOL$  aircraft. Two major problems, airfoil/jet/ground interaction flow fields and planar jet issuing from fuselage undersurface in ground effect, were investigated. Beam and warming, implicit, factored scheme with central difference and explicit boundary treatments were introduced. For the airfoil/jet/ground interaction flow fields, the invicid and laminar flows were considered. It was found for the invicid case that the blockage effect of the impinging jet divided the flow field into two major regions between ground and lower surface of the airfoil, as well as five vortices were formulated. The viscous laminar flow patterns obtained did not change very much except near the airfoil and ground plane. The cross-flow Reynolds numbers used were 20,000 and 5,000 and the temperature ratios ( $T_j/T_\infty$ ) were 1.0 and 1.5. For the small cross-flow Reynolds values, it was found that the boundary layer was thicker, the depth of jet penetration was increased and the magnitude of the velocity of the cross-flow ahead of the jet decreases due to the larger effect of the solid blockage. When the temperature of the jet was increased, the jet strength was reduced due to the smaller value of density at the plane of entering jet. For the turbulent impinging jet with curved fuselage undersurface, the two equation  $k-\varepsilon$  model was employed to study the turbulent effect. The adiabatic wall condition was assumed along the solid surface. The basic flow behaviors, such as wall jet, entrainment and impingement of flow, were clearly demonstrated.

Barata *et al.* [14] studied numerically and experimentally the flow field resulting from the impingement of a single axisymmetric jet against a wall after penetrating a confined cross-flowing stream. Calculations were presented for the three dimensional flow that characterized the experimental work for the purpose of evaluation of the accuracy of the turbulence models. A standard  $k-\varepsilon$  turbulence

model was used in the calculations. The difficulty of assessing the turbulence model performance in these complex flows due to numerical diffusion errors was demonstrated by comparing predictions on both coarse and fine meshes and improving accuracy of the discretisation of the convection terms using the high order *QUICK* method. The hybrid scheme was implemented in a coarse mesh of  $30 \times 17 \times 17$  and in a fine mesh of  $60 \times 34 \times 34$ . It was found that the use of the high order *QUICK* method improves considerably the numerical simulations of the flow field even with the coarse meshes. The shear stress in the impingement zone was not predicted correctly and this was independent of numerical influences and confirms that this zone is not represented by a turbulent viscosity hypothesis.

Bray and Knowles [26] used the *PHOENICS* finite volume code for the 2-D modeling of a single, round, impinging jet in cross-flow. It was possible to replicate the effects of parameters such as jet pressure ratio, jet height, jet/cross-flow velocity ratio and ground plane conditions on the resultant ground vortex. The numerical modeling, using only standard  $k-\varepsilon$  turbulence model, produced an essentially similar flow field to that observed experimentally, in terms of both velocity vectors and the ground plane pressure coefficient distribution. The output demonstrated that the vortex core and maximum penetration points are coincident with ground plane minimum and maximum penetration positions. The results, however, show that the vortex separation is overpredicted by around 7 jet diameters in the worst case, this being primarily attributable to the 2-D modeling assumptions. The correct trend of increasing vortex penetration with increasing effective velocity ratio is predicted reasonably well. The modeling also shows the correct trend regarding moving ground plane operation, though the reduction in vortex separation is slightly underpredicted. The apparent jet height effects predicted were believed to be due to inaccuracies in the free jet turbulence modeling. The modeling also indicates the correct low jet pressure ratio effect, i.e.

slightly increasing separation with increasing pressure ratio with a larger increase evident at choked conditions.

Smith *et al.* [20] studied the jet flow fields generated by *ASTOVL* aircraft in ground effect experimentally and computationally. *CFD* models of the flow fields have been developed using *FloSYS* and *PHOENICS* general purpose *CFD* packages. Both codes have shown good agreement with experimental data when considering the flow characteristics. It was found that the use of a  $k-\varepsilon$  turbulence model results in a more rapid mixing of the jet. It was believed that the discrepancies arising from the use of the standard  $k-\varepsilon$  model can be improved relatively simply by modifying turbulence constants. *CFD* predictions of the full scale arrangements of the *ASTOVL* aircraft were carried out. Using a three jet impingement model, the full scale sizes and temperatures were simulated. A crude intake effect was modeled by applying a mass-sink boundary condition across the aircraft ahead of the front nozzle. The rear nozzle flow temperature was set to about  $1200\text{ K}$  whereas the front nozzle temperature was around  $500\text{ K}$ . The predictions were carried out using a coarse grid for heights of 6, 4, and 2 rear nozzle diameters above the ground. The predicted temperature rise at  $h/d = 4$  in the intake was approximately  $180\text{ }^\circ\text{C}$  maximum.

VanOverbeke and Holdeman [27] used a 3-D turbulent flow *CFD* code to predict the hot gas environment around a *STOVL* aircraft operating in ground proximity. The calculations were performed with a 3-D subsonic *TEACH*-type turbulent viscous flow code. This code solves the time averaged Navier stokes or Reynolds equations. The  $k-\varepsilon$  turbulence model was used to provide closure. Equations were differenced over small control volumes. A hybrid numerical differencing scheme was used. The *SIMPLE* algorithm of Patankar was used to provide the pressure field. Calculations were performed for a generic four jet, side inlet *STOVL* aircraft configuration. The entire calculation domain grid was 80-84

( $x$ )  $\times$  47 ( $y$ )  $\times$  34 ( $z$ ). A non-uniform grid was used to concentrate cells in regions where large gradients in temperature and/or velocity were expected. The freestream temperature was 70 F (21.1 °C) and velocity was either 30 or 90.5 m/s. A uniform temperature of 1000 F (538 °C) and velocity of 1000 ft/s (304.8 m/s) were specified for the vertical lift jets. Convergence within 5 % residual was typical. The parameters varied were the distance from the exhaust lift jets to the ground plane, ( $h/d = 2$  and  $4$ ), and the velocity ratio ( $V_\infty/V_j = 0.03$  and  $0.09$ ). It was concluded that the primary flow path for ingestion was underneath the front part of the fuselage. With strong head winds, the hot gas ingestion was a combination of flow directly along the bottom of the fuselage and hot flow from the lift jet area stagnating slightly upwind of the inlet engine underneath the front part of the fuselage. Weaker head winds allowed the forward flow from the fountain area to penetrate much farther upwind allowing the hot flow to mix around the side of the forward part of the fuselage where some of it was ingested. Direct ingestion from the fountain lift jet area was seen for all cases. The mean inlet temperature rise increased with decreasing head wind and decreasing distance from the ground.

Tafti and Vanka [28] solved the Navier Stokes equations governing the hot gas ingestion flow field by an efficient finite difference calculation procedure. The complete geometry including the head wind, fuselage and multiple impinging jets were simulated and the temperature fields close to the engine inlet face were studied. Four demonstration calculations with variations in the height of the fuselage and head wind velocity were presented. The authors demonstrated the applicability of a solution algorithm which is based on the concept of multiple levels of grids to obtain faster convergence. The authors simulated the same configurations studied by VanOvebeke and Holdeman [27] for the purpose of comparison. The equations were finite differenced by a hybrid scheme. The principle behind the multi-grid procedure is that for elliptic equations, single grid techniques converge poorly when the finite difference grid contains a large number



of mesh points, but in the multi-grid concept, a series of fine and coarse grids is used and the solution is switched between the coarse and fine grids such that errors of all frequencies converge at the same rate. The velocities and pressures were obtained by a block implicit solution procedure of the momentum and continuity equations. The computational domain was divided into 100 computational cells in the  $x$ -direction, 44 in the  $y$ -direction and 48 in the  $z$ -direction. It was found that the solution converges to the required tolerance of 1% in approximately 150 iterations compared with 2000 iterations mentioned in reference [27]. It was concluded that *HGI* from the fountain flow was severe while the *HGI* due to the recirculating flow is not as severe. The effect of the head wind to jet velocity was clearly evident, for strong head wind, the ground vortex can be pushed behind the engine inlets so that no hot gases are ingested. For low velocity ratios, *HGI* occurred from the top, bottom and side of the fuselage but for high velocity ratios, *HGI* occurred from the bottom and side of the fuselage. It was found that the effect of the height on the flow field is not as strong. For low  $h/d$ , a smaller area is available between the fuselage and the ground and consequently the radial momentum of the hot gas is larger, so the radial flow penetration will be increased. The trend indicated by experiments (increased upstream penetration with increased height) was the opposite of what the numerical calculations indicated. This was attributed due to the turbulence modeling. The  $k$ - $\epsilon$  turbulence model is unable to accurately capture the full extent of turbulence production caused by the stagnating jets. The turbulent kinetic energy is severely underpredicted, particularly close to the ground but the velocity field is reasonably well predicted. The non-dimensionalized inlet temperature rise was found to decrease with increasing height and decrease with increasing the velocity ratio.

Van Dalsem *et al.* [29] studied the flows inherent in *V/STOL* operations, the jet in ground effect with a cross-flow using Fortified Navier stokes (*FNS*) scheme. The jet in ground effect flow, for the velocity ratio  $V_\infty/V_j = 0.223$  and  $h/d =$

3 was studied extensively. The experimentally measured velocity profile was inserted at the nozzle exit. A large number of grid points were required to resolve the numerous high gradient regions (e.g. ground boundary layer and the ground vortex). A number of flow field parameters were varied, namely; the initial jet profile and the Reynolds number. Various far field boundary conditions were also studied. In general, it was found that the ground vortex location is relatively insensitive to all of these variations. The calculated ground vortex location was very sensitive to the level of mixing in the boundary layer produced by the fraction of the jet which moves upstream and forms the ground vortex. If the flow is assumed entirely laminar, then the ground vortex moves far upstream. If the turbulence intensity is greater than calculated by the Baldwin-Lomax model, then the ground vortex moves back past the location that was observed experimentally. The Baldwin-Lomax turbulence model was found not accurate in predicting the correct eddy viscosity for this flow, so the ground vortex location was overpredicted. For the case of  $V_\infty/V_j = 0.1$  m/s, the ground vortex was much larger and penetrated further upstream and a high frequency flow unsteadiness was observed. The pressures induced on the surface of the jet by the freestream were similar to those induced on a cylinder in cross-flow. It was concluded that an elliptic jet with the major axis aligned with the cross-flow, may for practical V/STOL applications, has advantage over a circular jet in terms of reduced jet deformation and the size and the shape of the resulting ground vortex. The flow produced by a circular jet with  $V_\infty/V_j = 0.223$  was also computed at an  $h/d = 6$ . It was found that the jet impinges on the wall, but a ground vortex does form. It was found that jet impingement may begin at  $h/d = 10$  while the ground vortex does not form until  $h/d = 4$ .

Van Dalsem *et al.* [1] described the progress to date in NASA's Ames research center involving the application of CFD for the prediction of flows encountered by powered-lift aircraft operating in ground effect. Over the last five

years, work has progressed from simulating the interaction of a single impinging jet, through the simulation of a delta planform with multiple jets in ground effect, to an ongoing effort to simulate the complete flow about a *Harrier AV-8B* in ground effect. These flows require the solution of the general Navier Stokes equations, with turbulence closure models. A time-accurate, partially flux-split, two factor scheme is used. A range of turbulence models have been implemented, including Baldwin-Lomax model,  $k-\varepsilon$  model and a sub-grid scale model. For the delta planform with multiple jets in ground effect, it was found that as the height above the ground is reduced, the lift coefficient first increases (the ground cushion effect) and then rapidly drops (the suckdown effect). The effect of jet temperature was studied ( $T_j/T_\infty = 3.0$ ). The buoyancy terms have been added to the Navier Stokes equations. Results indicated that the jet temperature has little effect on the flow structure or global force coefficients, such as lift coefficient. Hence, it appeared that cold jet experiments can be used to study the ground environment, excluding heating effects.

Bray [5] used the commercially available *PHOENICS* computational fluid dynamics package for the modeling of free jets, impinging jets and impinging jets in cross-flow. *PHOENICS* uses a finite volume numerical modeling formulation of the conservation differential equations involving mass, momentum, energy and turbulence quantities. The turbulence model used was the standard  $k-\varepsilon$  model. The logarithmic law of the wall was used near the solid boundaries and the perfect gas equation was used to calculate the fluid density. The combined effects of convection and diffusion between adjacent grid points were expressed using a power law scheme. The resultant difference equations were solved through the *SIMPLEST* algorithm, which is a variation of *SIMPLE*. Regarding the free jet modeling, the predicted velocity profiles agreed well with experiment. It was found that the solution divergence increased with all of the followings; decreasing the turbulence intensity, increasing turbulent length scale and increasing nozzle

pressure ratio. The predicted velocity decay and the spreading rate were heavily dependent upon turbulent intensity, both increased by increasing turbulence intensity. The axial velocity decay and the spreading rate were overpredicted as compared with experiment. Increasing the length scale increased the velocity decay and the spreading rate. A decrease in pressure ratio increased the axial velocity decay. The modeling accuracy was improved when using a length scale of  $0.035d$  rather than  $0.1d$ . Regarding the impinging jet, convergence was only achieved with heavy under-relaxation of the flow equations. The turbulence quantities were the most difficult to converge satisfactorily. The initial wall jet was too thick while its velocity was too low. The rate of wall jet thickness growth was slightly underpredicted and this was attributed to inaccuracies in  $k-\varepsilon$  model and the logarithmic law of the wall. The velocity distribution was poorly predicted in the near wall region. The growth rate appeared to be insignificantly effected by the jet height, but the initial wall jet thickness increased with increasing the height due to the overprediction in the free jet spreading rate. The effect of the jet exit turbulence intensity and pressure ratio appeared to be negligible. The velocity decay rate was significantly underpredicted in the impingement region. Regarding the impinging jet in cross-flow, over 30 cases have been run, mostly with a standard turbulent compressible model based on a 2-D ( $49 \times 51$ ) polar axisymmetric grid. The parameters used were jet pressure ratio  $pr = 1.05$  to  $2.0$ , nozzle height normalized by the nozzle diameter  $h/d = 2.5$  to  $10.0$ , freestream velocity  $V_\infty = 3.9$  to  $25.0$  and ground plane velocity of  $V_\infty$  or  $0$ . Heavy under-relaxation was required in each case. The turbulence quantities were usually the most difficult to converge to acceptable residual levels. By the time the turbulence quantities were solved within, say 20%, the continuity and momentum equation residuals were usually below around 0.1%. Any further turbulence convergence did not lead to any measurable changes in the pressure and velocity output fields and, consequently, relatively high turbulence equation residuals were sometimes considered satisfactory. The following results were obtained:

- The modeling produced a similar flow field to that observed experimentally, in terms of both velocity vectors and the ground plane pressure coefficients distribution.
- The vortex core and maximum penetration results were coincident with ground plane minimum and maximum pressure coefficient points respectively.
- The predicted vortex self similarity laws agreed fairly well with experiment.
- Vortex separation was overpredicted by between  $5d$  and  $6d$ , this being primarily due to the  $2-D$  modeling assumptions. The correct trend of increasing vortex penetration with increasing  $Ve$  was predicted reasonably well.
- Regarding the pressure ratio effects, the modeling indicated the correct trend, i.e. a slight increase in separation with increasing pressure ratio with a larger increase at choked  $pr$ .
- Regarding the height effect, in all cases, vortex penetration slightly reduces with increasing height, by typically  $1.5d$  over the given height range. The predicted nozzle height effects are probably due to inaccuracies in the free jet turbulence modeling.

## Chapter 3

# Mathematical Modeling

### 3.1 Introduction

In many areas of aerospace design, computational fluid dynamics (*CFD*), is being accepted as an effective tool with the existing experimental and analytic design tools [1]. For some applications, it is possible to begin with simple and inexpensive techniques and obtain predictions of adequate accuracy for engineering use. The simple methods can eventually be replaced with more accurate and general techniques. In this way, *CFD* has become an integral part of the design cycle in many portions of aerospace engineering.

All the *CFD* predictions in the present work have been carried out using a preliminary copy of the *TEAM* computer code. *TEAM* is a finite difference/finite volume computer code for the simulation of steady two dimensional turbulent elliptic flows.

The computer code *TEAM*, an acronym for *Turbulent Elliptic Algorithm-Manchester* is developed from the known *TEACH* code in an attempt to overcome some of its disadvantages. The code can be applied to both plane and axisymmetric flows. A flow boundary can be a wall, a plane or axis of symmetry or an entrainment boundary along which the static or stagnation pressure is generally known.

### 3.2 Governing equations

The steady conservation equations for any general scalar variable  $\phi$  can be expressed as:

$$\text{div}(\rho V \phi) = \text{div}(\Gamma^\phi \text{grad} \phi) + S^\phi \quad (3.1)$$

For plane or axi-symmetric geometry, the equation can be written as:

$$\frac{\partial}{\partial x} (\rho r^j u \phi) + \frac{\partial}{\partial y} (\rho r^j v \phi) = \frac{\partial}{\partial x} (r^j \Gamma^\phi \frac{\partial \phi}{\partial x}) + \frac{\partial}{\partial y} (r^j \Gamma^\phi \frac{\partial \phi}{\partial y}) + r^j S^\phi \quad (3.2)$$

where  $x$  and  $y$  ( $y = r$ , for axisymmetric case) are coordinate directions,  $u$  and  $v$  are the local time-averaged velocities in  $x$  and  $y$  directions respectively,  $\rho$  is the fluid density,  $\Gamma^\phi$  and  $S^\phi$  are the turbulent exchange coefficient and the source term, respectively for the general variable  $\phi$ ,  $j=1$  for axi-symmetric case and  $j=0$  for the plane case. Table (3.1) lists the expressions for  $\Gamma^\phi$  and  $S^\phi$  which arise when  $\phi$  relates to density, momentum, temperature and the turbulence quantities  $k$  and  $\varepsilon$ .

Table 3.1: Exchange coefficients and sources.

Equation	$\phi$	$\Gamma^\phi$	$S^\phi$
Continuity	1	0	0
x-Momentum	$u$	$\mu_\sigma$	$-\frac{\partial p}{\partial x} + \frac{\partial}{\partial x} (\mu_\sigma \frac{\partial u}{\partial x}) + \frac{1}{r^j} \frac{\partial}{\partial y} (r^j \mu_\sigma \frac{\partial v}{\partial x})$
y-Momentum	$v$	$\mu_\sigma$	$-\frac{\partial p}{\partial y} + \frac{\partial}{\partial x} (\mu_\sigma \frac{\partial u}{\partial y}) + \frac{1}{r^j} \frac{\partial}{\partial y} (r^j \mu_\sigma \frac{\partial v}{\partial y}) - \frac{2j\mu_\sigma v}{r^2}$
Turbulence Energy	$k$	$\mu_\sigma / \sigma_k$	$G - \rho \varepsilon$
Eddy Dissipation	$\varepsilon$	$\mu_\sigma / \sigma_\varepsilon$	$\frac{\varepsilon}{k} (C_1 G - C_2 \rho \varepsilon)$
Energy	$T$	$\mu_\sigma / \sigma_T$	0

In table 3.1,  $G$  is the turbulence generation defined as follows:

$$G = \mu_t \left\{ 2 \left[ \left( \frac{\partial u}{\partial x} \right)^2 + \left( \frac{\partial v}{\partial y} \right)^2 + f \left( \frac{v}{r} \right)^2 \right] + \left( \frac{\partial u}{\partial y} + \frac{\partial v}{\partial x} \right)^2 \right\} \quad (3.3)$$

### Turbulence modeling

The turbulence model used here is the  $k$ - $\varepsilon$  model. The effective viscosity  $\mu_{eff}$  is calculated from the local values of the turbulent kinetic energy  $k$  and its dissipation rate  $\varepsilon$  via:

$$\mu_{eff} = \mu_l + \mu_t = \mu_l + C_\mu \rho \frac{k^2}{\varepsilon} \quad (3.4)$$

where  $\mu_t$  and  $\mu_l$  are the turbulent and molecular viscosity, respectively. The constants ( $C_1$ ,  $C_2$ ,  $C_\mu$ ,  $\sigma_k$ ,  $\sigma_\varepsilon$  and  $\sigma_T$ ) are given in table (3.2).

Table 3.2: Standard turbulence constants and Prandtl number.

$C_1$	$C_2$	$C_\mu$	$\sigma_k$	$\sigma_\varepsilon$	$\sigma_T$
1.44	1.92	0.09	1.0	1.22	0.6

$\sigma_T$  is the Prandtl number of the fluid.

### Compressible flow modeling

The present preliminary copy of the *TEAM* code does not include the compressibility effect, so the present author incorporated the compressibility effect into the code by using the perfect gas equation for calculating the density of the compressible fluid:

$$\rho = \frac{p}{\mathcal{R}T} \quad (3.5)$$

where:

$p$  and  $T$  are the pressure and temperature of the fluid, respectively and  $\mathcal{R}$  is the ideal gas constant



### 3.3 Grid Layout

A staggered grid system is used in *TEAM*. Scalar quantities such as  $p$ ,  $k$ ,  $\epsilon$  and  $I$  are stored at the intersection of grid lines, velocities are stored at the control volume faces, as shown in figure 3.1. Control volumes for  $u$  and  $v$  arise through placing their faces at pressure (scalar) nodes, the major advantage being that the primary pressure-gradient source revert, after discretization, to simple differences of nodal pressures.

The practice used in *TEAM* involves defining the control volumes over the solution domain and placing the associated grid nodes in the volume centers. This practice is believed to give better resolution in turbulent flow calculations and offer a more convenient way of discretising the flow configuration.

### 3.4 Finite volume equations

*TEAM* uses a finite volume numerical modeling formulation to convert the differential transport equations into a set of algebraic finite difference equations. The finite difference equations are derived by integration of the differential equations over the control volumes.

The most difficult task in this integration is the approximation of the value of  $\phi$  at the control volume faces. *TEAM* has the option of employing the Power Law Differencing Scheme (*PLDS*) or the Quadratic Upstream-Weighted Differencing Scheme (*QUICK*). *PLDS* is believed to be most stable, but false diffusion is associated with it. *QUICK* seems to be the most accurate but tends to exhibit overshoots and is not as stable as *PLDS*.

The Discretized source term is obtained by assuming  $S^\phi$  to be uniform over the control volume. Regardless of the nature of  $S^\phi$ , the discretized form is always represented in the linearized form:

$$S^\dagger = S_p^\dagger \phi_p + S_v^\dagger \quad (3.6)$$

Table 3.3 lists the most suitable combinations of the source term treatment for the various dependent variables.

Table 3.3: Source term treatment..

$\phi$	$S_p^\dagger$	$S_v^\dagger$
$u$	0	$-\frac{\partial p}{\partial x} + \frac{\partial}{\partial x} (\mu_\sigma \frac{\partial u}{\partial x}) + \frac{1}{r'} \frac{\partial}{\partial y} (r' \mu_\sigma \frac{\partial u}{\partial y})$
$v$	$-\frac{2j\mu_\sigma}{r'}$	$-\frac{\partial p}{\partial y} + \frac{\partial}{\partial x} (\mu_\sigma \frac{\partial v}{\partial x}) + \frac{1}{r'} \frac{\partial}{\partial y} (r' \mu_\sigma \frac{\partial v}{\partial y})$
$k$	$-C_p \rho^2 k / \mu_t$	$G$
$\epsilon$	$-C_\epsilon C_p \rho^2 k / \mu_t$	$C_\epsilon C_p \rho^2 k G / \mu_t$

The final form of the discretized equations follows as:

$$a_p^\dagger \phi_p = a_E^\dagger \phi_E + a_W^\dagger \phi_W + a_N^\dagger \phi_N + a_S^\dagger \phi_S + S_v^\dagger \Delta x \Delta y \quad (3.7)$$

$$a_E^\dagger = D_x^\dagger A(|P_x^\dagger|) + [[-F_x, 0]] \quad (3.8a)$$

$$a_W^\dagger = D_w^\dagger A(|P_w^\dagger|) + [[F_w, 0]] \quad (3.8b)$$

$$a_N^\dagger = D_n^\dagger A(|P_n^\dagger|) + [[-F_n, 0]] \quad (3.8c)$$

$$a_S^\dagger = D_s^\dagger A(|P_s^\dagger|) + [[F_s, 0]] \quad (3.8d)$$

$$a_p^\dagger = a_E^\dagger + a_W^\dagger + a_N^\dagger + a_S^\dagger - S_p^\dagger \Delta x \Delta y \quad (3.8e)$$

$$F_x = (\rho u)_x \Delta y, D_x^\dagger = \frac{\Gamma_x^\dagger \Delta y}{(\Delta x)_x}, P_x^\dagger = \frac{F_x}{D_x^\dagger} \quad (3.9a)$$

$$F_w = (\rho u)_w \Delta y, D_w^\phi = \frac{\Gamma_w^\phi \Delta y}{(\Delta x)_w}, P_w^\phi = \frac{F_w}{D_w^\phi} \quad (3.9b)$$

$$F_n = (\rho v)_n \Delta x, D_n^\phi = \frac{\Gamma_n^\phi \Delta x}{(\Delta y)_n}, P_n^\phi = \frac{F_n}{D_n^\phi} \quad (3.9c)$$

$$F_s = (\rho v)_s \Delta x, D_s^\phi = \frac{\Gamma_s^\phi \Delta x}{(\Delta y)_s}, P_s^\phi = \frac{F_s}{D_s^\phi} \quad (3.9d)$$

where:

$\phi_P, \phi_E, \phi_W, \phi_N$  and  $\phi_S$  are the values of the variable  $\phi$  at the nodes:  $P, E, W, N$  and  $S$ , respectively (see figure 3.1).

$a_P^\phi, a_E^\phi, a_W^\phi, a_N^\phi$  and  $a_S^\phi$  are the combined convection and diffusion coefficients of the variable  $\phi$  at the nodes:  $P, E, W, N$  and  $S$ , respectively.

$F_e, F_w, F_n$  and  $F_s$  are the mass flow rates through the east, west, north and south faces of the control volume, respectively.

$D_e^\phi, D_w^\phi, D_n^\phi$  and  $D_s^\phi$  are the diffusion conductances of the variable  $\phi$  at the east, west, north and south faces of the control volume, respectively.

$P_e^\phi, P_w^\phi, P_n^\phi$  and  $P_s^\phi$  are the Peclet numbers of the variable  $\phi$  at the east, west, north and south faces of the control volume, respectively.

$\Delta x$  and  $\Delta y$  are the width and the height of the control volume, respectively.

$(\Delta x)_e, (\Delta x)_w, (\Delta y)_n$  and  $(\Delta y)_s$  are the distances between the node  $P$  and the nodes  $E, W, N$  and  $S$ , respectively.

The symbol  $[[a, b]]$  is defined to denote the greater of  $a$  and  $b$ .

$A(|P|)$  is a function that depends on the difference scheme. For the power law difference scheme (PLDS), we can write:

$$A(|P|) = \left[ \left[ 0, (1 - 0.1|P|)^5 \right] \right] \quad (3.10)$$

### 3.5 The solution procedure

The resulting finite difference equations are solved by a line-iterative method using a *Tri-diagonal Matrix Algorithm (TDMA)* with alternating sweep directions. This is closely akin to the *ADI* technique.

A difficulty arises due to the absence of an equation explicitly governing the pressure. The momentum equations for the velocity components join a common pressure and they must jointly satisfy the continuity equation. Indirect methods are used to obtain the pressure field. *TEAM* incorporates two algorithms for handling the velocity-pressure linkage, the "*Semi Implicit Method for Pressure Linked Equations*" method (*SIMPLE*) and the "*Pressure Implicit Solution by Split Operator*" method (*PISO*).

### 3.6 Boundary Conditions

Because of the elliptic nature of the governing differential equations, boundary conditions are required along all domain boundaries for all the dependent variables. Boundaries may be of five types discussed below.

- *Fluid entry plane*: All fluid and flow properties must be known and prescribed along this boundary, ( $\phi = \text{constant}$ )
- *Axis of symmetry*: Along this boundary, the gradients of all properties normal to the axis are zero, ( $\partial\phi/\partial n = 0$ ).
- *Fluid exit plane*: Across the exit, the flow direction must be uniform. The exit boundary is usually positioned in such a way that the flow there can be assumed to be uniform. In this case, zero streamwise gradients of all properties may be implemented ( $\partial\phi/\partial s = 0$ ) and a uniform pressure is prescribed along the exit plane ( $p = \text{constant}$ ).

- **Walls:** At walls, the velocity components and the turbulent quantities are zero due to the no-slip condition ( $u = v = k = \varepsilon = 0$ ). Near the walls, the "Wall-Function Method" is used to bridge the gap between the fully turbulent region and the wall. The approach used in the present code is the logarithmic law of the wall function.
- **Entrainment boundary:** Along this boundary, a uniform pressure is specified ( $p = \text{constant}$ ) and the gradient of the tangential velocity component is set to zero ( $\partial u / \partial y = 0$ , for horizontal boundary). The normal velocity component ( $v$ , for horizontal boundary) is calculated by direct application of the mass continuity principle.

### 3.7 Convergence monitoring

#### Convergence criteria

The iterative procedure is considered to yield a converged solution if the absolute normalized residuals for  $u$ ,  $v$ ,  $k$  and  $\varepsilon$  as well as the mass source are less than prescribed small values. The residual of each variable is summed over all the domain nodes. The normalizing factor of  $u$  and  $v$  equals to the total inflow of momentum. For  $k$  and  $\varepsilon$ -equations, the normalizing factors represent the products of the total volumetric inflow and inlet values of  $k$  and  $\varepsilon$ , respectively. The mass source is normalized by the total inflow of mass. The prescribed convergence criterion varies from case to case and is dependent on requirement of the user.

#### Under-relaxation

Under-relaxation is a means of slowing down the rate of convergence of the solution process. Under-relaxation is found to be necessary to ensure convergence. It avoids steep rates of change in the variables and provides a means for equalizing the rates of convergence of the various coupled equations. *TEAM* uses a linear under-relaxation which is introduced in an implicit fashion. The under-relaxation factors vary from case to case and the optimum values of the under-relaxation factors are a matter of trial and error and experience. The linear under-relaxation is done as follows:

$$\phi^{i+1} = \phi^i + urf(\phi^{i+1} - \phi^i) \quad (3.11)$$

where  $\phi^i$  is the value of the general variable  $\phi$  at iteration number  $i$ ,  $\phi^{i+1}$  is the value of  $\phi$  at iteration number  $i+1$  and  $urf$  is the under-relaxation factor.

### **3.8 Impinging Jet In cross-flow modeling**

This section describes the numerical modeling of a single impinging jet in cross-flow using the *TEAM* code. A 2-D axisymmetric coordinate system was used as it is ideally suited to the modeling of round jets. This approach, though having some drawbacks, is still able to represent the general structures of the flow field of interest in a relatively quick and economic way.

As a start, the simple impinging jet with no cross-flow was modeled in order to get familiar with the code and its capabilities as well as to get some experience about the convergence problems and when they occurred. The complexity was then added to the code by modeling the impinging jet in cross-flow. For both cases, a great number of preliminary runs were conducted in an attempt to test the code reliability and to explore the range of flow parameters to be tested. Moreover, these preliminary runs aimed to reach a reliable resolution of the grid used to simulate the flow field.

#### **3.8.1 Cross-flow modeling**

The cross-flow-flow which causes the ground vortex phenomena may be either due to *ambient wind* or due to *motion of the aircraft* through the still air [5], combinations of the two may also occur. If due to ambient wind, there will be a cross-flow boundary layer. If due to aircraft motion, there will be no relative motion between onset flow and ground plane, and there will be no cross-flow boundary layer.

The *ambient wind case* can be modeled using a fixed nozzle and ground plane in the presence of a head wind, as done by the present work and most of the previous numerical and experimental works.

The *motion of the aircraft case* can be modeled either by using a moving nozzle and a fixed ground plane, where the nozzle moves at the same velocity of

the head wind, as done by Abbott [11], or by using a fixed nozzle and a moving ground plane that moves at the same velocity of the head wind.

In the second case (motion of the aircraft), the cross-flow boundary layer is removed and the wall jet penetration is expected to reduce due to the increased opposing cross-flow velocities.

### 3.8.2 Boundary conditions

The boundary conditions for the impinging jet in cross-flow are shown in figure 3.2. At the inlet of the of the cross-flow, uniform velocity and temperature conditions are prescribed and the turbulent intensity was assumed to be three percent. The turbulence intensity of the cross-flow was changed so many times to explore its effect and it was found to have a little effect on the flow field. The position of the cross-flow inlet boundary was varied to investigate its effect on the ground vortex flow field. It was found that its effect is minor as long as it is positioned far enough from the ground vortex location. At the ground plane (bottom wall), wall boundary conditions are implemented, namely; the no slip condition is prescribed where the velocity components and the turbulence quantities are set to zero. The wall is assumed to have zero heat loss (adiabatic) and the logarithmic law of the wall is used in vicinity of the wall. At the upper boundary, a free surface was prescribed where the pressure was uniform and the gradients of the tangential velocity and the turbulence quantities were set to zero, the normal velocity was calculated by direct applying the continuity equation at the near boundary cell. At the left hand side boundary, symmetry boundary condition was applied where the gradients of all the variables were set to zero and the normal velocity was also set to zero. At the jet exit, the velocity ( $V_j$ ) profile and the pressure ( $p_j$ ) were assumed to be uniform. The jet exit boundary conditions for turbulent kinetic energy,  $k_j$  and its rate of dissipation  $\epsilon_j$ , were formulated in a similar way to that has been done in Bray [5], namely;



$$k_j = (TU_j V_j)^2 \quad (3.12)$$

$$\epsilon_j = \frac{0.015 k_j^{3/2}}{0.035 d} \quad (3.13)$$

where,  $TU_j$  is the turbulence intensity at the jet exit. The length scale was set at 3.5% of  $d$ . The turbulence intensity at the jet exit was varied several times to study its effect. It was found to have a little effect on the flow field. This is consistent with that found in Bray [5], where the turbulence intensity at the jet exit was found to have a significant effect on the flow fields of free jets, but has a negligible effect on the flow field of impinging jets. At the nozzle tube wall, wall boundary conditions were implemented, the wall was assumed to be adiabatic with the logarithmic law of the wall applied near the wall. For the cases where the intake was simulated, uniform pressure and velocity were prescribed at the intake. The uniform velocity was prescribed in such away to satisfy the intake to jet mass flow rate ratio ( $m_i/m_j$ ). The gradients of all scalar variables were set to zero.

### 3.8.3 Solution domain

After many trials, it was settled to use an identical solution domain of  $52 \times 34$  ( $x \times y$ ). For the intake cases, the grid became  $58 \times 34$  and the intake position could be varied along the  $x$  direction (different  $l/d$ ). Smaller cell sizes were used in those areas where the gradients were expected to be great, namely; the free jet region, the wall jet region and the intake region. The different jet heights were modeled simply by varying the nozzle tube length. The overall grid dimensions were  $1.016 \text{ m}$  ( $x$ )  $\times$   $0.254 \text{ m}$  ( $y$ ) or  $40d \times 10d$  for a nozzle diameter,  $d = 0.0254 \text{ m}$ . The grid used for the modeling is shown in figure 3.3.

### 3.8.4 Convergence monitoring and under-relaxation

Under-relaxation was needed for each case ( $urf = 0.25 - 0.75$ ). More under-relaxation was needed for the turbulence quantities, particularly the dissipation rate  $\epsilon$ . The continuity and the momentum equations residuals were much faster to converge. A convergence criteria of the residuals of 1% was typical for most of the cases, but by the time the turbulence quantities residuals were converged to within this criteria, the continuity and momentum equations residuals were usually below around 0.01%. In some cases, the turbulence quantities residuals could not be converged to less than 1% while the other residuals were well converged, nevertheless, any further iterations and convergence of the turbulence quantities did not lead to any measurable changes in the pressure and velocity fields which are the primary areas of interest. Consequently, relatively high turbulence residuals (2 - 10 %) can be considered acceptable. It is worth noting that similar trends regarding convergence were experienced by Bray [5]. The present predictions were carried out on VAX 8700 at the University of Jordan. A typical iteration of an intake case (58 (x)  $\times$  34 (y)) consumed about .03 s of CPU time. Full convergence of a non-intake case usually needed 3000 to 6000 iterations. The intake cases were very difficult to converge and usually needed at least 9000 iterations to converge.

The author introduced the restart capability to the code in order to overcome some of the convergence problems since previously solved flow fields can be considered as initial conditions for the similar flow fields. For example, the cold jet cases results can be entered as initial conditions for the hot jet runs, also, the non-intake cases results can be considered as initial conditions for the intake cases. The restart capability also makes it possible to change the under-relaxation factors during the runs whenever necessary. For example, the case can be run for 100 iterations and the residuals are monitored, accordingly, the under-relaxation factors can be either decreased or increased. By this way, many of the divergent cases could be driven to get converged.

Another method introduced by the author is modifying the code to automatically monitor the residuals for all the variables after each iteration and to record the number of times the residual has converged in the last 15 iterations, for example. Accordingly, the under-relaxation factor can be modified automatically to improve the convergence, some of the cases could not be converged without this method.

The convergence was also improved by satisfying the overall continuity equation in the solution domain. In the present solution domain, it can be noticed that the only boundary the flow can exit from is the upper free boundary. In this case, the inflow mass flow rate (from the cross-flow and the jet) can be calculated and stored, and after each iteration, the outflow (through the upper free surface) can be calculated and an increment can be added to the normal velocity exiting from the free surface in order to force the outflow to be equal to the inflow. By using this method, the convergence became faster.

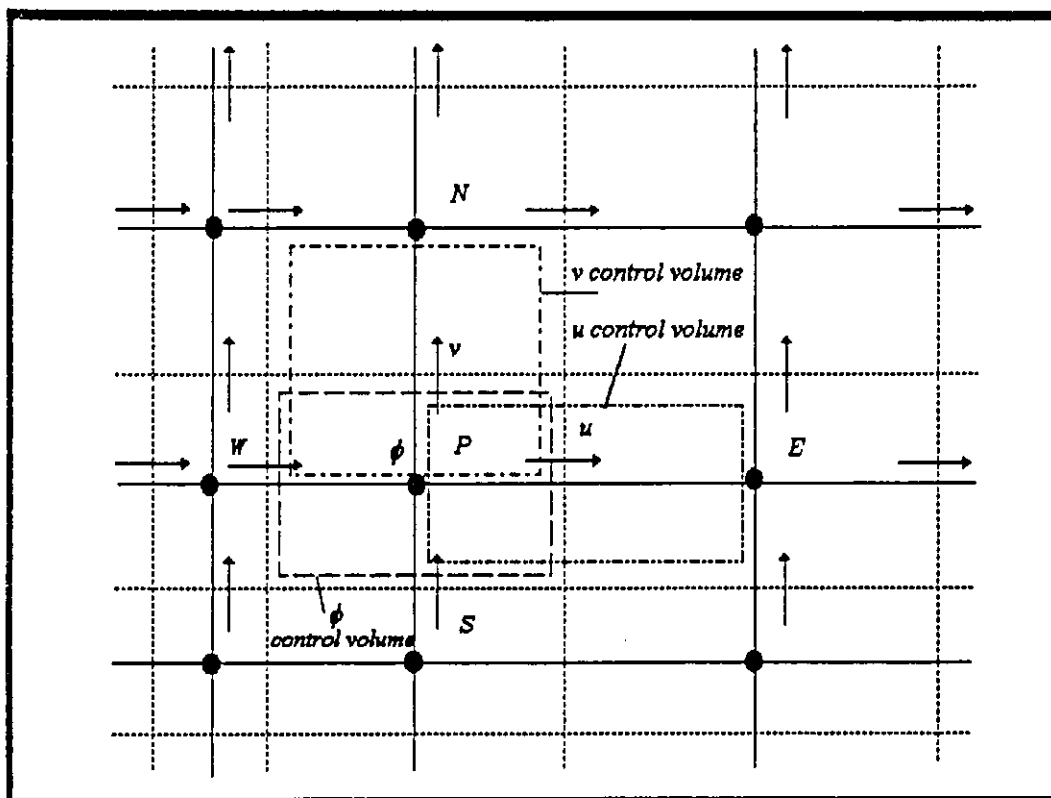


Figure 3.1: Grid layout used for numerical modeling.

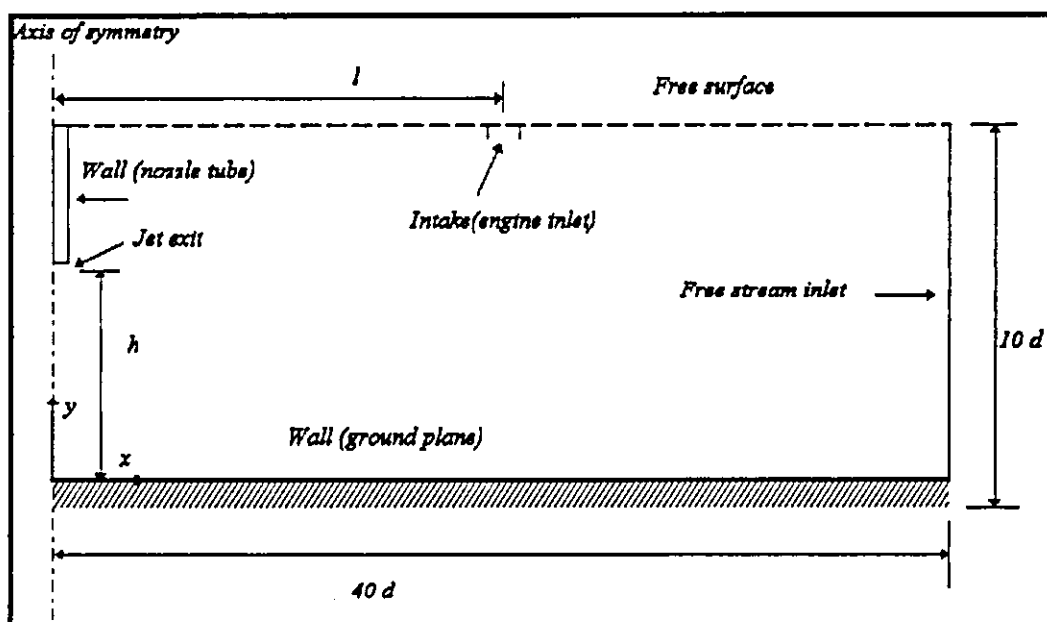


Figure 3.2: Boundary conditions for modeling impinging jet in cross-flow.

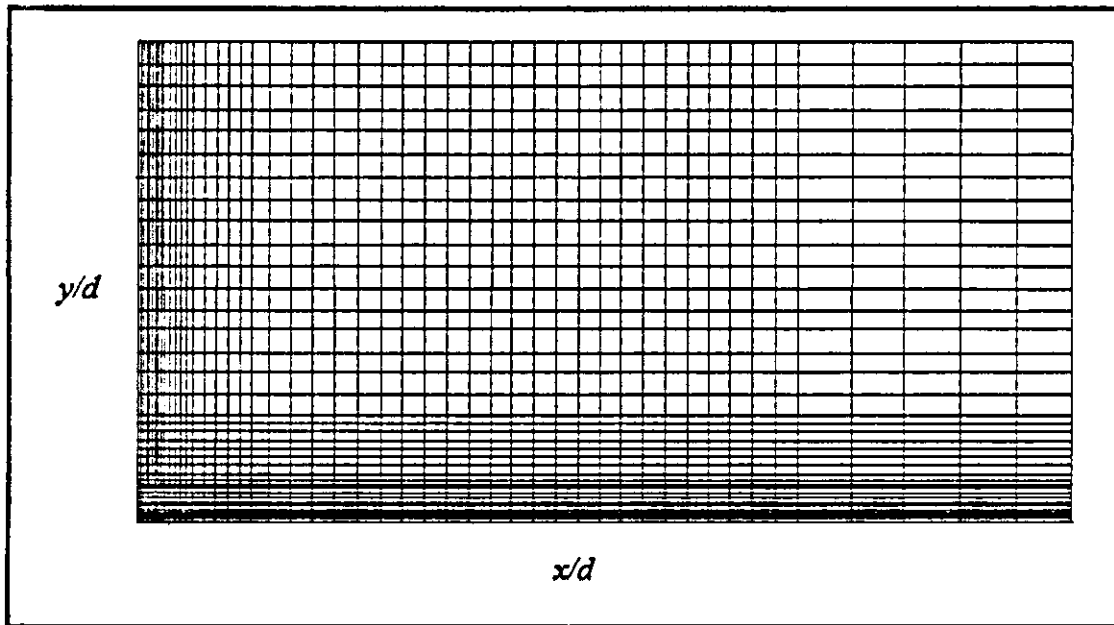


Figure 3.3: Grid used for modeling impinging jet in cross-flow.

## Chapter 4

### Results and Discussion

#### 4.1 Introduction

Much time was initially spent on the preliminary tests to explore the grid dependence and the number of iterations of the predicted solutions. The main problem is to provide a parametric study of the effect of  $Ve$ ,  $h/d$ ,  $Pr$ ,  $T_j/T_\infty$ ,  $m_1/m_2$  and  $l/d$  on the flow field of interest. The ranges of these parameters were varied in such a manner to compare the present results with previous numerical and experimental results, especially that of Bray [5]. The number of cases which have been successfully completed was 37. The parameters used in these runs are given in table 4.1.

Table 4.1: The ranges of parameters used in numerical modeling

Parameter	Range
$Ve$	14.4, 17.9, 25.1 and 26.1
$pr$	1.05, 1.2, 1.5 and 1.6
$h/d$	2.0, 2.5, 4.0, 5.0, 6.0, 7.5, 8.0 and 10
$T_j/T_\infty$	0.89, 2.4 and 3.2
$m_1/m_2$	0 (no intake), 0.25, 0.5, 1.0, 1.5, 2.0, 2.5, 3.0 and 4.0
$l/d$	10.5, 13.5, 16.5 and 22.5

Table 4.2 presents the predicted results for the cases when the jet temperature is low ( $T_j/T_\infty = 0.89$ ) and when the intake (engine inlet) is not present. Table 4.3 presents the predicted results for the cases when the jet temperatures is high ( $T_j/T_\infty = 2.14$  and  $3.20$ ) and when the intake is not present. Table 4.4 presents the predicted results for the cases when the jet temperature is high and when the intake is present. Included in these tables are the vortex core horizontal position  $x_v/d$ , the vortex core vertical position  $y_v/d$  and the vortex maximum penetration position  $x_p/d$ .

Table 4.2: Predicted results for the cases of low jet temperature and no intake present.

Case	$h/d$	$pr$	$T_j/T_\infty$	$Ve$	$x_v/d$	$x_p/d$	$y_v/d$
1	2	1.5	0.89	26.12	13.5	20.5	2.2
2	2.5	1.5	0.89	17.91	10.5	16.5	1.7
3	2.5	1.5	0.89	14.35	8.5	14.5	1.5
4	2.5	1.5	0.89	25.08	13.5	20.5	2.3
5	4	1.5	0.89	26.12	13.5	20.5	2.3
6	5	1.5	0.89	17.97	10.5	16.5	1.7
7	5	1.5	0.89	14.35	8.5	13.5	1.5
8	5	1.5	0.89	25.08	13.5	20.5	2.2
9	6	1.5	0.89	26.12	13.5	20.5	2.2
10	7.5	1.5	0.89	17.89	9.5	15.5	1.8
11	7.5	1.5	0.89	14.35	7.5	13.5	1.5
12	7.5	1.5	0.89	25.08	12.5	19.5	2.2
13	8	1.5	0.89	26.12	12.5	19.5	2.2
14	10	1.5	0.89	14.35	7.5	13.5	1.8
15	5	1.05	0.89	14.4	8.5	14.5	1.4
16	5	1.2	0.89	14.4	8.5	14.5	1.4
17	5	1.6	0.89	14.4	8.5	13.5	1.4

Table 4.3: Predicted results for the cases of high jet temperature and no intake present.

Case	$h/d$	$pr$	$T_j/T_a$	$Ve$	$x_j/d$	$x_p/d$	$y_j/d$
18	5	1.5	3.2	14.36	9.5	14.5	1.4
19	5	1.5	2.14	14.36	8.5	16.5	1.4
20	5	1.5	3.2	17.89	10.5	16.5	1.5
21	5	1.5	2.14	17.89	10.5	16.5	1.6
22	5	1.5	3.2	25.08	13.5	20.5	2.1
23	5	1.5	2.14	25.08	13.5	20.5	2.3
24	8	1.5	3.2	26.12	13.5	20.5	2.2
25	8	1.5	2.14	26.12	13.5	20.5	2.3

Table 4.4: Predicted results for the cases of high jet temperature and intake present.

Case	$h/d$	$pr$	$T_j/T_a$	$Ve$	$h/d$	$m/m_0$	$x_j/d$	$x_p/d$	$y_j/d$	$Tr$
26	8	1.5	3.2	26.12	13.5	1	13.44	21.5	2.4	0.0175
27	8	1.5	3.2	26.12	10.5	1	13.5	20.5	2.3	0.0217
28	8	1.5	3.2	26.12	16.5	1	14.5	21.5	2.3	0.0144
29	8	1.5	3.2	26.12	13.5	1.5	13.56	21.5	2.4	0.0166
30	8	1.5	3.2	26.12	13.5	2	13.18	21.5	2.5	0.0163
31	8	1.5	3.2	26.12	13.5	3	13.188	20.5	2.3	0.0164
32	6	1.5	3.2	26.12	13.5	1	14.5	21.5	2.2	0.0173
33	8	1.5	3.2	26.12	13.5	2.5	13.18	20.5	2.2	0.0164
34	8	1.5	3.2	26.12	13.5	4	13.188	20.5	2.2	0.0159
35	8	1.5	3.2	26.12	13.5	0.5	13.81	21.5	2.4	0.0179
36	8	1.5	3.2	26.12	13.5	0.25	13.8	21.5	2.4	0.0181
37	8	1.5	3.2	26.12	22.5	1	12.5	20.5	2.2	0.005



## 4.2 Pressure coefficient distributions and velocity vectors

The pressure coefficient distribution for the domain cells nearest to the ground plane and the velocity vector output for case (8) where  $h/d = 5.0$ ,  $pr = 1.5$  and  $Ve = 25.1$  are given in figures 4.1 and 4.2 respectively. The vortex region has been enlarged in figure 4.3, which clearly shows that the minimum  $C_p$  position at  $x/d = 13.5$  coincides with the vortex core position. Similarly, the maximum  $C_p$  position at  $x/d = 20.5$  coincides with the maximum penetration position. This justifies the definitions of  $x_v$  and  $x_p$  used in tables 4.1 to 4.3. The above argument is typical for all the cases that have been studied.

From the velocity vectors of figures 4.2 and 4.3, it can be seen that the freestream flows over the ground vortex in a similar manner as the freestream would flow over a solid body obstruction placed in the flow. This was also observed by Cimbala *et al.* [4].

When the jet impinges on the ground plane, it stagnates and deflects to the right, forming a wall jet that meets the freestream where a stagnation point is formed and the wall jet is deflected backwards. Part of this back-flowing fluid is entrained again into the wall jet forming a ground vortex region. The freestream fluid that passes over the ground vortex reaches the free jet area where part of it is entrained into the free jet. Part of the freestream fluid collides with the nozzle tube wall, where it stagnates and deflects upwards. The interaction of the freestream with the free jet is supposed to deflect the free jet, but due to the existence of the axis of symmetry on the left hand side boundary, this deflection is not possible. This is a drawback of the 2-D modeling, another drawback of this modeling is that the only way the fluid can exit the flow domain is through the upper free surface. When the freestream flows over the ground vortex, it is forced to deflect upwards strongly with no sideways deflection possible due to the 2-D numerical modeling.

The position of the upper free surface was varied intentionally in order to investigate its effect. It was found that it has a great effect on the flow field, the

ground vortex was found not to form when the free surface was near the ground and that it must be positioned as far as possible from the ground.

### 4.3 Ground vortex self similarity

The numerical predictions presented in tables 4.2 to 4.4 reveal the existence of a fixed relation between  $x_v$  and  $x_p$  as determined from the static pressure distribution. By averaging the values presented in the tables 4.2 to 4.4, it can be concluded that,

$$x_p / x_v \approx 1.58 \quad (4.1)$$

This is so close to the experimental relation given by Bray [5]:

$$x_p / x_v = 1.592 \quad (4.2)$$

It is to be noted here that both  $x_v$  and  $x_p$  are overpredicted (25% overprediction), but the relation between  $x_v$  and  $x_p$  is accurately predicted (error = 0.75 % only). This relationship is independent of the flow parameters, which implies that the ground vortex can be described by any of its characteristic positions since any one of these positions can be deduced from the other. Another relation that can be found between  $y_v$  and  $x_v$ . By averaging the values of  $y_v/d$  and  $x_v/d$  presented in these tables, it can be concluded that:

$$y_v / x_v \approx 0.184 \quad (4.3)$$

The values of  $y_v/d$  in tables 4.2 to 4.4 are found from the velocity vectors.

#### 4.4 Effect of effective velocity ratio

The effective velocity ratio ( $V_e$ ) is defined as the square root of the ratio of the dynamic head of the jet ( $q_j$ ) to the dynamic head of the cross-flow ( $q_\infty$ ). This definition is found to be more representative than the definition used by some investigators, namely,  $V_j/V_\infty$  for the reasons that will be discussed in a later section. The effective velocity ratio  $V_e$  is the most important parameter that effect the ground vortex geometry. This is due to the fact that the maximum penetration distance increases clearly with increasing the effective velocity ratio. This can be demonstrated by referring to figure 4.4 where it can be seen that the position of  $C_{p_{max}}$  increases with increasing  $V_e$ . The same trend was found to apply to all other cases studied. The rate of increase of  $x_p/d$  with  $V_e$  is nearly independent of the nozzle height as can be shown in figure 4.5. The values of  $x_p/d$  and  $V_e$  presented in tables 4.2 to 4.4 were averaged and the following relation was found;

$$x_p/d \approx 0.86V_e \quad (4.4)$$

The ground vortex size which is described by  $y_v/d$  also increases by increasing  $V_e$ . This can be seen clearly by comparing figures 4.3, 4.6 and 4.7 for the cases 8, 6 and 7 where  $V_e = 25.1, 17.9$  and  $14.4$  respectively and  $h/d = 5$ . The rate of increase is also independent of the nozzle height as shown in figure 4.8. The relation between the vortex core height and  $V_e$  was found after averaging the values of  $y_v/d$  and  $V_e$  presented in the tables to be:

$$y_v/d \approx 0.1V_e \quad (4.5)$$

This relation is also independent of the height, for the range investigated in this study ( $h/d = 2.0 - 10.0$ ).

The strength of the ground vortex which is proportional to the absolute value of  $Cp_{min}$ , [4], increases by increasing  $Ve$  as can be seen in figure 4.4. The same trend was found to hold for the other values of  $h/d$ . This is consistent with the experimental results presented in [4]. Although  $Cp_{min}$  increases by increasing  $Ve$ , it can be seen from figure 4.4 that  $Cp_{max}$  does not change significantly.

The trend of increasing  $x_p/d$  with  $Ve$  was found in all the previous numerical and experimental studies, such as [4], [5] and [11]. Nevertheless, there was a significant disagreement among the investigators regarding the rate of increase. This may be partially attributed to the different freestream boundary layer thickness. A comparison between the present predictions with the experimental and numerical results of Bray [5] is shown in figure 4.9. It is seen clearly that the rate of increase of  $x_p/d$  with  $Ve$  is well predicted, although the absolute values of  $x_p/d$  are overpredicted. However, the present predictions are closer to the experimental values than Bray's predictions. The present predictions overpredict the vortex penetration by about 25% while Bray's predictions overpredict the vortex penetration by about 40%. The difference in overpredicting the results by the present work and that of Bray may be attributed to different numerical schemes used to interpolate the values of the scalar variables at the control volume faces. Bray used the *PLDS* scheme for all the variables while the present author used the *QUICK* scheme for the velocity components and the *PLDS* scheme for all the other scalar variables. The *QUICK* scheme is known to cause less numerical diffusion than the *PLDS* scheme [14]. In general, the overprediction in vortex penetration can be attributed to two reasons. The first one is the deficiency of the  $k-\epsilon$  turbulence model where generally, it is known to overpredict the vortex penetration between 40 to 50% [30]. The second reason is the effect of the 2-D modeling. As was mentioned earlier, the freestream is forced to exit the flow domain through the upper freestream with no possible sideways turning, thus detracting from the horizontal freestream momentum component which stagnates the wall jet.

Furthermore, the free jet deflection is not possible due to the presence of the axis of symmetry at the left hand side boundary.

Abbott [11] found the following experimental relation regarding the impinging jets (fixed nozzle),

$$(q_{mx}/q_j)^{1/2} = \frac{1}{x/d} \quad (4.6)$$

where  $q_j$  is the dynamic pressure of the jet and  $q_{mx}$  is the maximum dynamic head of the wall jet at the distance  $x$  along the ground plane (based on the maximum velocity  $u_m$ , see figure 1.3). As mentioned earlier in chapter 3, Abbott used a moving nozzle in still air for modeling impinging jets in cross-flow (cross-flow boundary layer does not exist), he found that the wall jet extends forward (against cross-flow) to a point at which the maximum dynamic head for an impinging jet (fixed nozzle) would be four times the dynamic head of the still air relative to the moving nozzle. In other words, we can write the following relation;

$$(q_\infty/q_{mxp})^{1/2} = 0.5 \quad (4.7)$$

where  $q_\infty$  is the dynamic head of the cross-flow (or the dynamic head of the still air relative to the moving nozzle) and  $q_{mxp}$  is the maximum dynamic head of an impinging jet (fixed nozzle) at the maximum penetration point  $x_p$  of the wall jet (moving nozzle). By combining equations 4.6 and 4.7, it follows that:

$$x_p/d = 0.5(q_j/q_\infty)^{1/2} = 0.5Ve \quad (4.8)$$

This equation is independent of the nozzle height  $h/d$ .

The author averaged 42 points of  $x_p/d$  and  $Ve$  from Bray's experimental work [5] for moving ground plane arrangement (cross-flow boundary layer does not exist) and found the following relation:

$$x_p/d \approx 0.546Ve \quad (4.9a)$$

which is close to equation 4.8 deduced from Abbott's work. The author also averaged 120 points of Bray's experimental work for fixed ground plane arrangement with head wind (cross-flow boundary layer exist) and found the following relation:

$$x_p/d \approx 0.698Ve \quad (4.9b)$$

Moreover, the author averaged 17 points of Bray's numerical work for fixed ground plane arrangement with head wind (cross-flow boundary layer exist). and found the following relation:

$$x_p/d \approx 1.05Ve \quad (4.9c)$$

It is worth noting here that using a moving nozzle in still air [11] or a fixed nozzle with moving ground plane [5] is the correct method to model an aircraft hovering forward in still air. As mentioned in chapter 1, Kuhn [6] stated that for an aircraft hovering with no head wind (cross-flow boundary layer does not exist),  $h_c/d = 0.27Ve$ , where  $h_c/d$  is the critical vortex height, also stated that the critical height ( $h_c/d$ ) is about half the forward projection, which means that :

$$x_p/d = 2.0 \times h_c/d = 0.54Ve \quad (4.10)$$

This equation is so close to equation 4.9a deduced from Bray's experimental work. Equations 4.8, 4.9a and 4.10 can be combined as follows:

$$x_p/d = K_1 Ve \quad (4.11a)$$

where  $K_1 = 0.5 - 0.55$ . Equation 4.11a provides an experimental estimation of  $x_p/d$  for the case of no cross-flow boundary layer present.

Comparing equations 4.9a and 4.9b deduced from Bray's work [5], we can conclude that using a fixed ground plane arrangement with head wind (cross-flow boundary layer exists) leads to approximately 28% increase in  $x_p/d$  relative to the moving ground plane arrangement (cross-flow boundary layer does not exist). Equation 4.11a can be corrected by a factor 1.28 to give:

$$x_p/d = 1.28 \times K_1 Ve = K_2 Ve \quad (4.11b)$$

where  $K_2 = 0.64 - 0.7$ . Equation 4.11b provides an experimental estimation of  $x_p/d$  for the case of cross-flow boundary layer present.

It is generally known that the  $k-\varepsilon$  model leads to an overprediction of vortex simulation between 40 to 50% [30], so equation 4.11b can be corrected by a factor of 1.4-1.5 to give:

$$x_p/d = (1.4 - 1.5) \times K_2 Ve = K_3 Ve \quad (4.12a)$$

where  $K_3 = 0.9 - 1.1$ . Equation 4.12a provides a numerical estimation of  $x_p/d$  for the case of cross-flow boundary layer present using a  $k-\varepsilon$  turbulence model, it can be noticed that equation 4.9c deduced from Bray's numerical work fits in the range of equation 4.12a.

For the present predictions, it was shown that the overprediction due to the use of the  $k-\varepsilon$  turbulence model is only 25%, so equation 4.11b can be corrected by a factor of 1.25 to give:

$$x_p/d = 1.25 \times K_2 Ve = K_4 Ve \quad (4.12b)$$

where  $K_4 = 0.8 - 0.88$ . Equation 4.12a provides a numerical estimation of  $x_p/d$  for the case of cross-flow boundary layer present using a  $k-\varepsilon$  turbulence model, it can be noticed that equation 4.4 deduced from the present work fits in the range of equation 4.12b.

#### 4.5 Effect of height

The effect of height ( $h/d$ ) on the pressure distribution can be seen to be insignificant as shown in figure 4.10 where the positions and the values of  $Cp_{max}$  and  $Cp_{min}$  clearly do not change significantly with increasing  $h/d$  from 2 to 8 when  $Ve$  is kept constant. This little effect of  $h/d$  is independent of  $Ve$  as shown in figure 4.11. It can also be seen that a decrease of only  $1d$  occurs over the given height range. A comparison between the numerical and experimental works is given in figure 4.12. It can be seen that both the present numerical predictions and that of Bray show a slight decrease in vortex penetration with increasing  $h/d$ . This is not consistent with the experimental results where there is a slight increase in vortex penetration with increasing height until a critical height is reached, after that a slight decrease in vortex penetration occurs. For both the numerical and experimental results, the increase or decrease of vortex penetration is slight, so the height of the nozzle can be considered to be a secondary factor for a single nozzle configuration. Again, it can be seen that the overprediction in vortex penetration is less severe for the present predictions than that of Bray's predictions [5]. More



comparisons with Bray's experimental and numerical works at different  $V_e$  values are given in *figures 4.13* and *4.14* respectively. Once more, it is shown that the present predictions overpredict the vortex penetration while still less severe than those of Bray's predictions.

The little effect of  $h/d$  here could be attributed to inaccuracies in the  $k-\epsilon$  model [5]. It also should be noted that the physical situation was not accurately modeled due to 2-D effect where the jet deflection is not possible. The jet deflection may be responsible for the vortex penetration reduction at higher heights, while at lower heights the jet deflection does not occur due to the ground vortex blockage effect. Hence, as the height is increased, the vortex penetration is increased due to the efficient turning of the jet (less collision losses) [5] until a height is reached where the jet deflection occurs, so the vortex penetration decreases with further height increase.

According to Bray [5], the effect of height is rig interference dependent. Physically, the rig is present due to the presence the aircraft fuselage and wings or due to the presence of the test rig. As the height is increased, the rig effects become minor and the ground vortex increases in size and penetration. At small heights, the ground vortex has no chance to increase in size due to the blockage effect of the rig, and it will be pushed downstream by the cross-flow, leading to a decrease in vortex penetration. This was noticed by Cimbala *et al.* [4] where it was found that as a jet plate was added around the jet nozzle, the separation bubble (ground vortex) decreases significantly in size and the separation point moves further downstream. The 2-D modeling does not include any rig effects, hence, the effect of  $h/d$  is insignificant.

Tafti and Vanka [28] found that the effect of the height on the flow fields is not as strong as the other flow parameters, such as  $V_j/V_\infty$ . Reilley "Bray [5]" stated that there was no correlation found between  $h/d$  and  $x_p/d$ .

## 4.6 Effect of nozzle pressure ratio

Figure 4.15 provides a comparison between the  $C_p$  plots of different  $pr$  cases at the same  $h/d$  and  $V_e$  values. The  $C_p$  plots are clearly seen to be similar in terms of the position and values of  $C_{p_{min}}$  and  $C_{p_{max}}$ . This indicates that  $pr$  has only little effect on the ground vortex strength and location. It is to be noted here that all  $pr$  values were chosen to fit in the subsonic range ( $pr < 1.89$ ). This was intended since the preliminary copy of the *TEAM* code used is not able to capture the shock structures that exist when using supersonic  $pr$  values. From figure 4.16, it can be shown that the vortex penetration decreases by only  $1d$  over the range of  $pr$  used here.

Bray [5] noticed experimentally that there is an increase in vortex penetration with increasing nozzle pressure ratio up to choking, at higher pressure ratios it decreases but with a second lower peak at  $pr = 3.0$ . Curtis "Bray [5]" studied the effect of  $pr$  where it was varied from 1.04 to 3.0, it was found that the wall jet characteristics are unaffected by  $pr$ . Glyn and Jal "Bray [5]" found that the effect of  $pr$  was very small.

Corsiglia *et al.* [31] conducted a series of experimental tests on circular plates and generic *STOVL* configurations. It was found that the effect of  $pr$  is small up to  $pr = 4.0$ , in terms of force and pressure data. It is worth noting here that these quantities (force and pressure) depend strongly on the flow structure, particularly, the location and size of the ground vortex.

As a numerical point of view, changing  $pr$  at constant stagnation temperature of the nozzle, will lead to a change in  $V_j$  and  $\rho_j$ . This means that the jet dynamic head  $q_j$ , will change also, but if the cross-flow velocity is changed in such a way that  $V_e$  remains constant,  $pr$  will have no effect, since its effect is included in  $V_e$ . This is strictly true in the range of subsonic flow ( $pr < 1.89$ ), since for supersonic flows, the flow structure will be completely different, and the shock waves and mach disks that form will change the flow behavior.

#### 4.7 Effect of Jet temperature

The effect of jet temperature can be seen to be minor as indicated by figure 4.17 for  $V_e = 25.1$ . The same effect was found to be true for the other velocity ratios. From a numerical point of view, increasing the jet temperature decreases the jet density and consequently decreases the jet dynamic pressure leading to a decrease in  $V_e$ . But, if the freestream velocity was decreased in such a way that  $V_e$  stays constant, there will be no effect of the temperature since the temperature effect is included in  $V_e$ . Hence,  $V_e$  is the proper non-dimensional parameter that must be used to model the flow field since it combines both the effect of jet to cross-flow velocity ratio along with the effect of compressibility that arises from using different jet and/or cross-flow temperatures. This argument was first noticed experimentally by Abbott [11] who tested the effect of different jet temperatures and found that the plots are independent of temperature when using  $V_e$ . Referring to figure 4.18, it can be seen that the effect of jet temperature on  $x_p/d$  is insignificant where a very little increase of vortex penetration is noticed by increasing the jet temperature.

The above findings were supported by the following investigators; Corsiglia *et al.* [31] noticed that the effect of jet temperature was found to be small on the force and pressure data. Reilly "Bray [5]" found that there is no effect of the jet temperature on the vortex penetration and vortex shape. Schwantes "Bray [5]" found that the jet temperature did not affect the position of the ground vortex.

Hwang *et al.* [25] studied numerically the two dimensional field relative to *V/STOL* aircraft, two temperature ratios were studied,  $T_j/T_\infty = 1.0$  and  $1.5$ , it was found that the jet strength decreases as the jet temperature is increased due to the smaller value of density.

Van Dalsem *et al.* [1] studied numerically the effect of jet temperature and buoyancy terms were added to the Navier Stokes equations. Results indicated that

the jet temperature has a little effect on the flow structure and on the global force coefficient.

#### **4.8 Effect of the Intake (engine Inlet)**

The effect of engine inlet on the vortex location and geometry did not receive enough attention in previous studies. The effect of inlet was mainly studied experimentally. MacLean *et al.* [7] conducted an experimental investigation on a typical model configuration. The test rig consisted of a two inlet configuration with four jets impinging on a flat plate. It was found that the inlet suction appeared to increase the ground vortex location only at low heights and low freestream to jet velocity ratios,  $V_\infty/V_j$ . Miller *et al.* [12] found that the installation and operation of the simulated engine inlets had minor effects on the flow behavior. VanOverbeke and Holdeman [27] and Tafti and Vanka [28], separately, studied numerically the hot gas environment around *STOVL* aircraft model. The configuration involved four impinging jets and two inlets. No parametric study of the effect of the inlet on the ground vortex was given.

It was necessary to study the effect of the engine inlet numerically and to make a parametric study of that effect on the ground vortex geometry and on *HGI*. There are two parameters that can be studied relating to the engine inlets, namely, the ratio of the engine inlet mass flow rate to the jet mass flow rate ( $m_i/m_j$ ), and the horizontal distance between the engine inlet and the nozzle jet location ( $l/d$ ).

Due to the 2-D limitations, the inlet was simulated as a horizontal mass sink on the top free surface at a height of  $10d$  above the ground plane. The mass flow rate of the engine inlet was prescribed in such a way to satisfy the ratio of  $m_i/m_j$ .

#### 4.8.1 Effect of intake mass flow rate

Brady and Ludwig [21] found that the ground board static pressure distribution is independent of the mass flow. By referring to figures 4.19 and 4.20, it can be shown that there is a negligible effect of  $m_i/m_j$  on the  $C_p$  distribution in terms of the position of  $C_{p_{min}}$  and  $C_{p_{max}}$ . It can be seen that increasing  $m_i/m_j$  tends to increase  $C_{p_{min}}$  and consequently increases the vortex strength, except for the case of zero  $m_i/m_j$  (no intake). However, the size of the ground vortex does not change with increasing  $m_i/m_j$  as long as  $Ve$  and  $l/d$  are the same. Figure 4.21 shows the velocity vectors (ground vortex region) for case 26 of  $m_i/m_j = 1.0$  and  $l/d = 13.5$ . Similar flow structures were found for the other cases of different  $m_i/m_j$  values at the same  $l/d$  of 13.5. The flow field structures for these cases are similar to the no intake case at the same  $Ve$  of 26.1. It is to be noted here that the location where the arrows are concentrated is the location where the engine inlet is installed. Figure 4.22 shows that  $x_p/d$  decreases only slightly with increasing  $m_i/m_j$ .

#### 4.8.2 Effect of intake location

The intake location,  $l/d$  was varied from 10.5 to 22.5 for a fixed value of  $m_i/m_j$  of 1.0. For the non intake case at the same  $Ve = 26.1$  and  $h/d$  of 8, the ground vortex core location ( $x_v/d$ ) is 13.5 and the ground vortex maximum penetration location ( $x_p/d$ ) is 20.5. So, for the intake case of  $l/d = 10.5$ , the intake is positioned downstream the ground vortex core (for a similar non intake case at the same  $Ve$ ). For the case of  $l/d = 13.5$ , the intake is located exactly above the ground vortex, for the case of  $l/d = 16.5$ , the intake is located between the ground vortex core and the maximum penetration point and for the case of  $l/d = 22.5$ , the intake is positioned upstream of the ground vortex maximum penetration point. Referring to figure 4.23, it can be seen that for the cases of  $l/d = 10.5$  and 13.5, the  $C_p$  plots are nearly the same in terms of the positions and the values of  $C_{p_{min}}$  and  $C_{p_{max}}$  which means that the ground vortex location and strength are the same for these cases. From the velocity vectors of the above three cases, it was found that the ground vortex

structures were similar to each other in terms of the ground vortex position, size and maximum penetration distance. From figure 4.24, it can be seen that the location of the inlet of the engine has a minor effect on  $x_p/d$  where it can be seen that  $x_p/d$  increases only slightly as  $l/d$  is increased.

For the cases of  $l/d = 16.5$  and  $22.5$  (figure 4.25), it can be seen that the  $C_p$  plots are different in terms of the values of  $C_{p_{min}}$  and  $C_{p_{max}}$ . For both cases,  $C_{p_{min}}$  is low compared with the other cases of  $l/d = 10.5$  and  $13.5$  which means that the ground vortex is weak. For the case of  $l/d = 22.5$ ,  $C_{p_{max}}$  is lower than that of the case of  $l/d = 16.5$ . The velocity vectors shown in figure 4.26 reveal that for the case of  $l/d = 22.5$  (case 37), there is a clear ground vortex and the self similarity laws are applicable. However, the ground vortex is weak and the stagnation pressure is low, as indicated from the  $C_p$  plots (figure 4.25). This may be explained by the fact that for  $l/d = 22.5$  (case 37), the cross-flow is strongly deflected upwards towards the upper free surface due to the existence of the suction of the inlet (see figure 4.27). This strong deflection leads to a reduction in the horizontal component of the cross-flow momentum and consequently leads to a reduction in collision losses with the wall jet and hence the stagnation pressure will be reduced and the ground vortex strength will be reduced also.

From the above argument, it is clearly seen that the cases where the intake is positioned beyond the ground vortex core, the suction effect of the intake will modify the flow structure leading to weaker vortices and/or lower  $C_{p_{max}}$ . It must be noted here that it is possible that the 2-D modeling is one of reasons for this behavior of the flow, since the flow can not be deflected sideways and it is forced to deflect upwards.

## 4.9 Hot gas environment

### 4.9.1 Temperature contours

The normalized temperature is expressed as  $Tn = (T - T_{\infty}) / (T_j - T_{\infty})$ , where  $T_{\infty}$  is the ambient temperature and  $T_j$  is the jet temperature at the nozzle exit. The range of  $Tn$  is always between 0 and 1.0. Contour plots of  $Tn$  are provided in order to investigate the distribution of the hot gases in the flow field. Figure 4.28 shows the temperature contours for case 18 of  $T_j/T_{\infty} = 3.2$ ,  $Ve = 14.4$  and  $h/d = 5$ . It can be clearly seen that at the centerline of the free jet region, the jet temperature decreases steadily with the vertical distance from the nozzle. At the jet exit,  $Tn = 1.0$ , while at the ground plane  $Tn = 0.6$ , which means that the jet temperature is reduced by 40%. Similarly, for the wall jet,  $Tn$  decreases steadily with distance from the impingement point where it eventually reaches a value of 0. The argument mentioned above is true for all the cases studied and it is independent of the jet temperature. This can be shown by figure 4.29 for the case of  $T_j/T_{\infty} = 2.14$  (case 19), where it can be seen that the temperature contours are very similar to those of figure 4.28 ( $T_j/T_{\infty} = 3.2$ ). The effective velocity ratio  $Ve$  has a significant effect on the temperature contours, where the penetration of the hot gases increases with increasing  $Ve$ . It can be seen from figure 4.30 for case 20 ( $Ve = 17.9$ ) that the hot gases in the wall jet penetrate to a greater distance than those of figure 4.28 ( $Ve = 14.4$ ). From figures 4.28 and 4.29 ( $Ve = 14.4$ ), it can be seen that the contour of  $Tn = 0.05$  penetrates to a distance of  $x/d = 14.4-14.7$  but from figure 4.30 ( $Ve = 17.9$ ), the penetration increases to a distance of  $x/d = 16.2$ , moreover, from figure 4.31 for case 22 ( $Ve = 25.1$ ), the penetration increases to a distance of  $x/d = 20.7$ .

The temperature reduction in both the free and the wall jets is attributed to the entrainment action and the turbulent mixing of the jets with the surrounding fluid. As the nozzle height is increased, more entrainment occurs in the free jet, so it is expected to have cooler jets at the impingement point for greater nozzle heights. This is exactly the case of figure 4.32 (case 24), where  $h/d$  is increased to

8.0 at  $Ve = 26.1$ . It can be seen that  $Tn$  at the ground is 0.4, compared to a value of 0.6 for  $h/d = 5.0$  at  $Ve = 25.1$  (figure 4.31). However, the penetration of the hot gases in the wall jet does not change significantly ( $x/d = 20.7-21$ ).

To study the effect of the location of the intake on the temperature distribution, refer to figures 4.33 and 4.34 showing the cases of  $l/d = 13.5$  (case 26) and 22.5 (case 37) respectively. Both cases are of  $Ve = 26.1$  and  $m_i/m_j = 1.0$ . It can be seen that the temperature contours are similar to those of figure 4.32 where the intake does not exist. The temperature contours are also independent of the mass flow rate as can be seen from figure 4.35 for the case of  $m_i/m_j = 4.0$ . It can be seen that increasing  $m_i/m_j$  from 1.0 (figure 4.33) to 4.0 (figure 4.35) did not introduce any significant changes on the temperature contours.

The penetration of the hot gases can be described by  $x_{pH}/d$  which indicates the distance at which the hot gases penetrate through the wall jet against the cross-flow, this can be found from the penetration distance of the contour of  $Tn = 0.05$ . By looking to figure 4.36, it can be seen that there is a straight line relation between  $x_{pH}/d$  and  $Ve$ .

An interesting relation concerning the temperature contours can be found from figure 4.37, which is a plot of  $x_{pH}/d$  against  $x_p/d$  for similar flow conditions. It can be noticed that the values of  $x_{pH}/d$  are very close to the values of  $x_p/d$ . This means that there exists a fixed correlation between  $x_{pH}/d$  and  $x_p/d$ , which is given by:

$$x_{pH}/d \approx x_p/d \quad (4.13)$$

#### 4.9.2 Hot gas ingestion

The HGI is quantified by the normalized average temperature rise at the inlet,  $Tn_i = (T_i - T_\infty)/(T_j - T_\infty)$ , where  $T_i$  is the average temperature at the inlet. Referring to figure 4.38, it can be seen that  $Tn_i$  decreases as  $m_i/m_j$  is increased. This can be explained by the fact that as the inlet mass flow rate ( $m_i$ ) is increased, the



suction effect of the inlet is increased and a larger quantity of cross-flow fluid is sucked into the inlet which leads to a decrease in the inlet temperature. The effect of  $l/d$  on  $HGI$  is shown in 4.39 where it can be seen that  $T_{n_i}$  decreases as  $l/d$  is increased, this is expected since as the inlet gets closer to the nozzle, it gets closer to the hot gases and consequently the suction of the hot gases becomes greater leading to an increase of the inlet temperature.

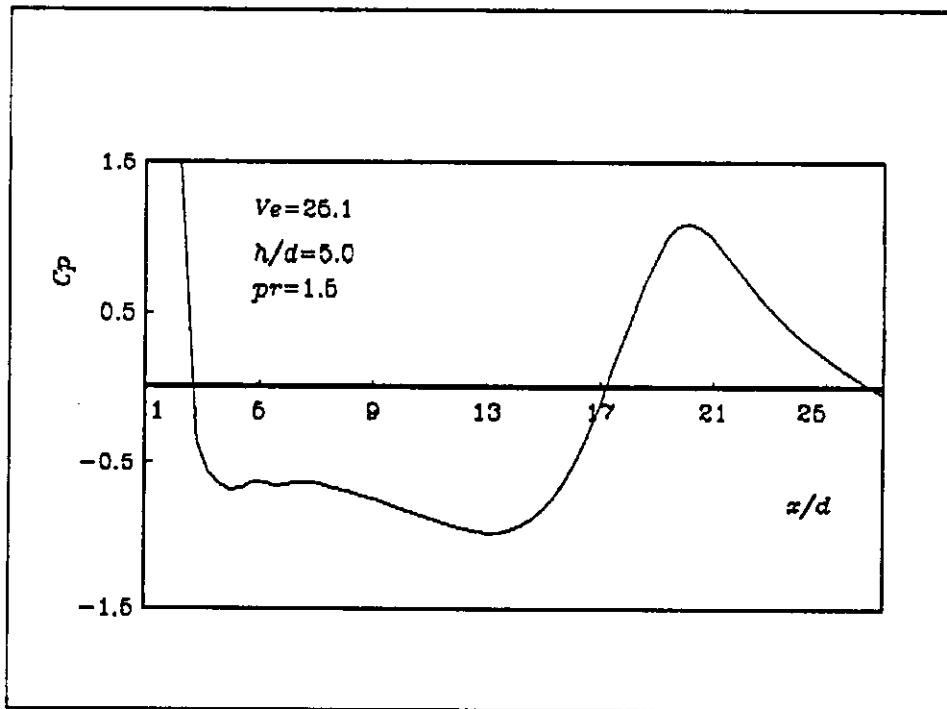


Figure 4.1: Typical ground plane  $C_p$  distribution for impinging jet in cross-flow (case 8).

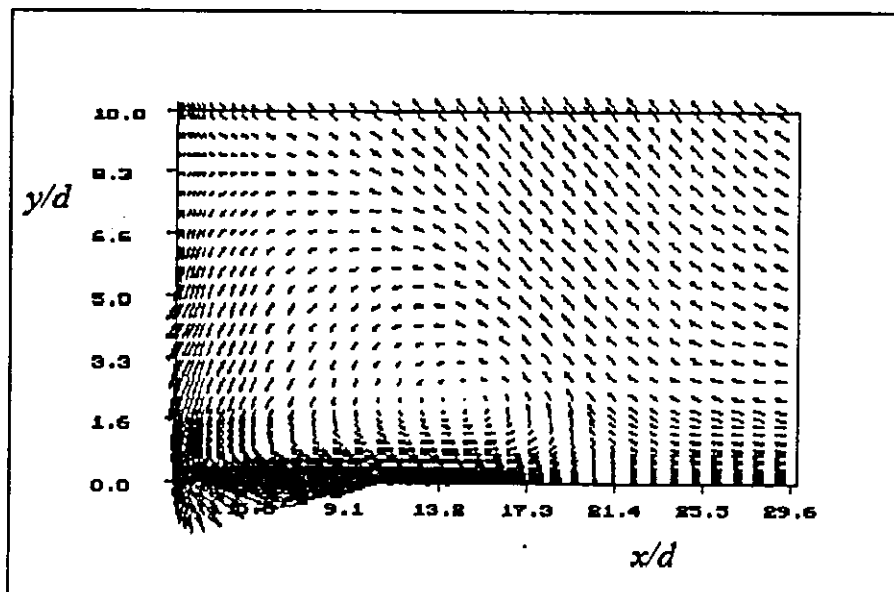


Figure 4.2: Typical velocity vectors for impinging jet in cross-flow (case 8).

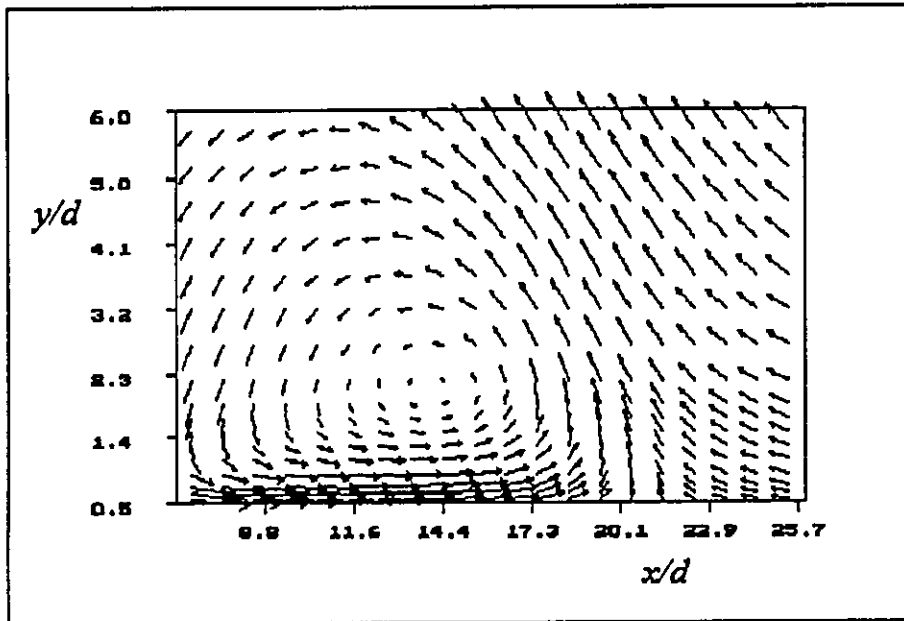


Figure 4.3: Enlarged ground vortex region of figure 4.2 (case 8).

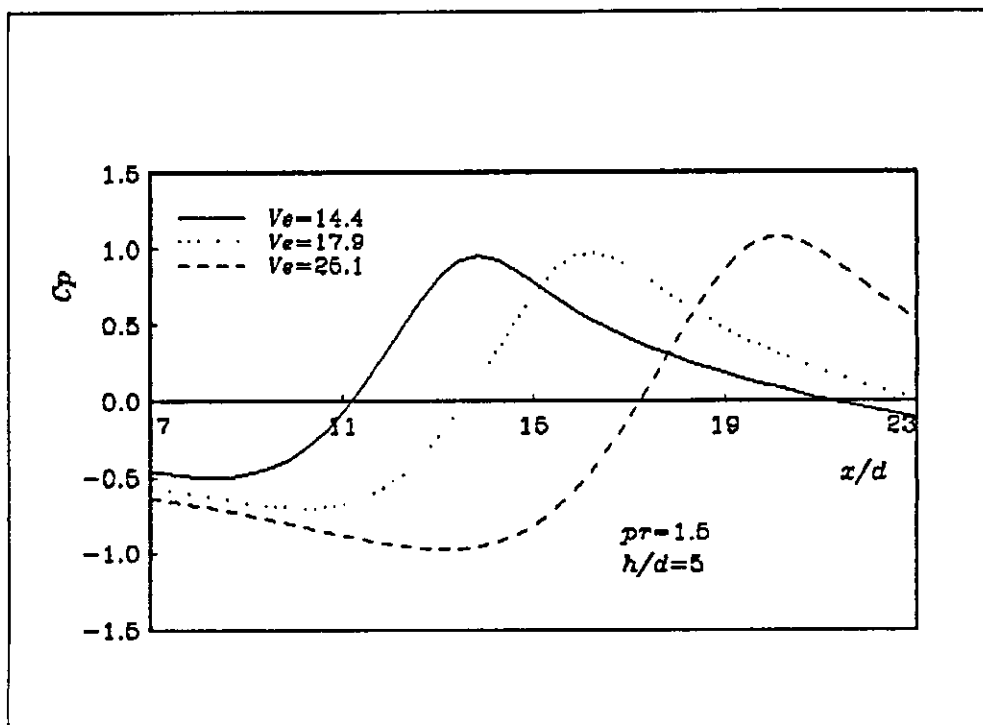


Figure 4.4: Effect of  $V_e$  on  $C_p$  distribution.

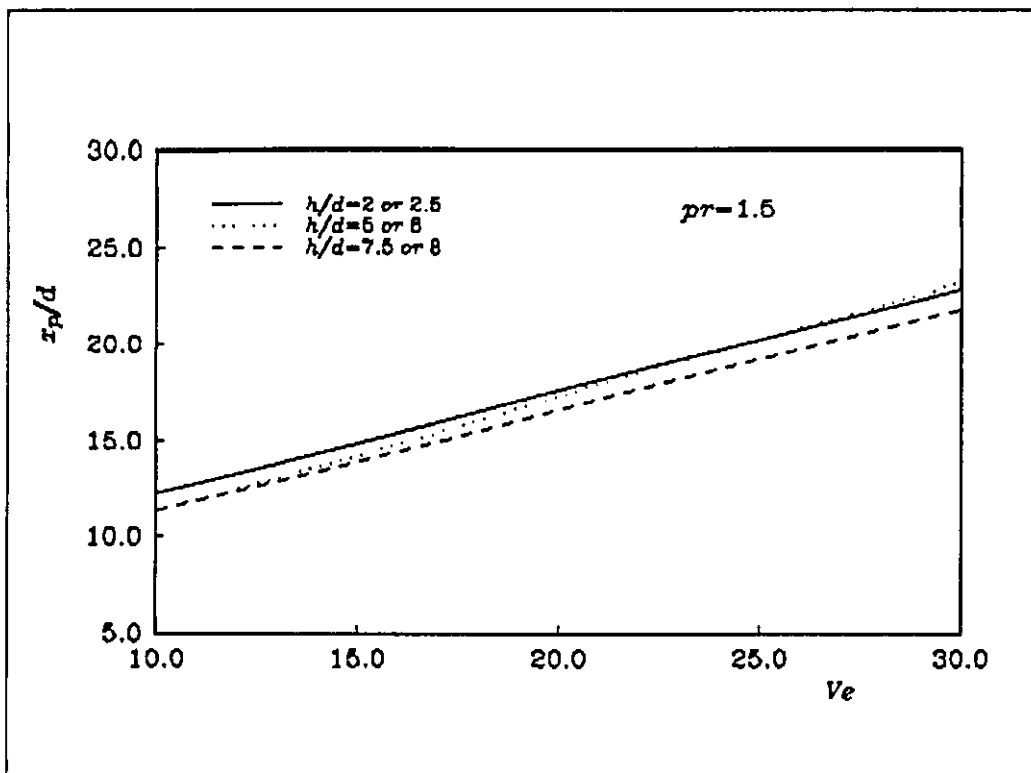


Figure 4.5: Effect of  $Ve$  on  $x_p/d$  at different values of  $h/d$ .

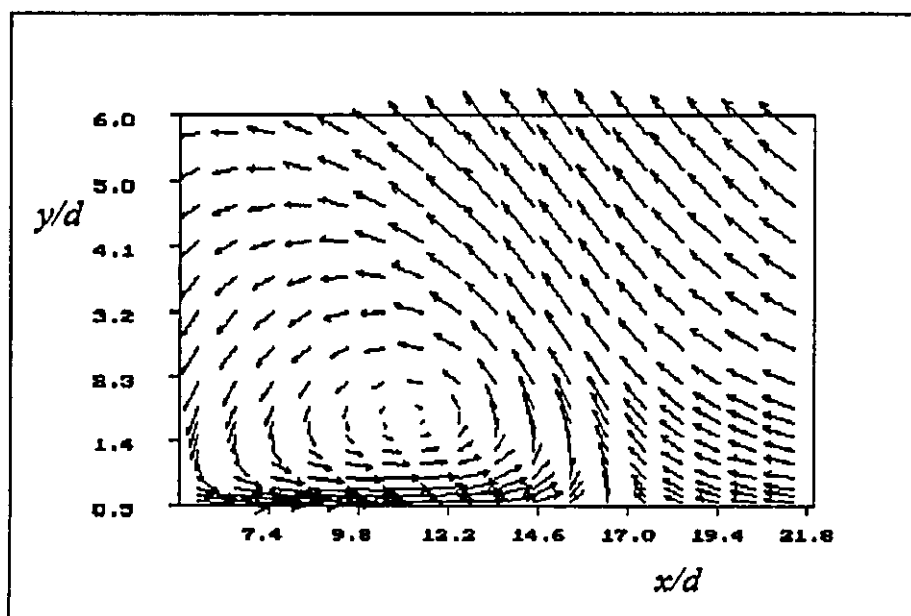


Figure 4.6: Enlarged ground vortex region (case 6).

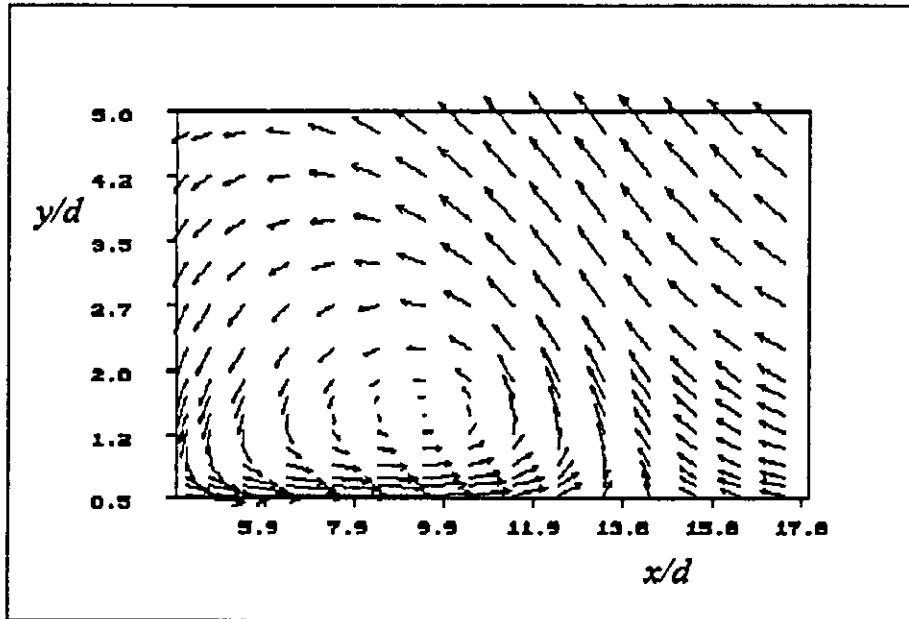


Figure 4.7: Enlarged ground vortex region (case 7).

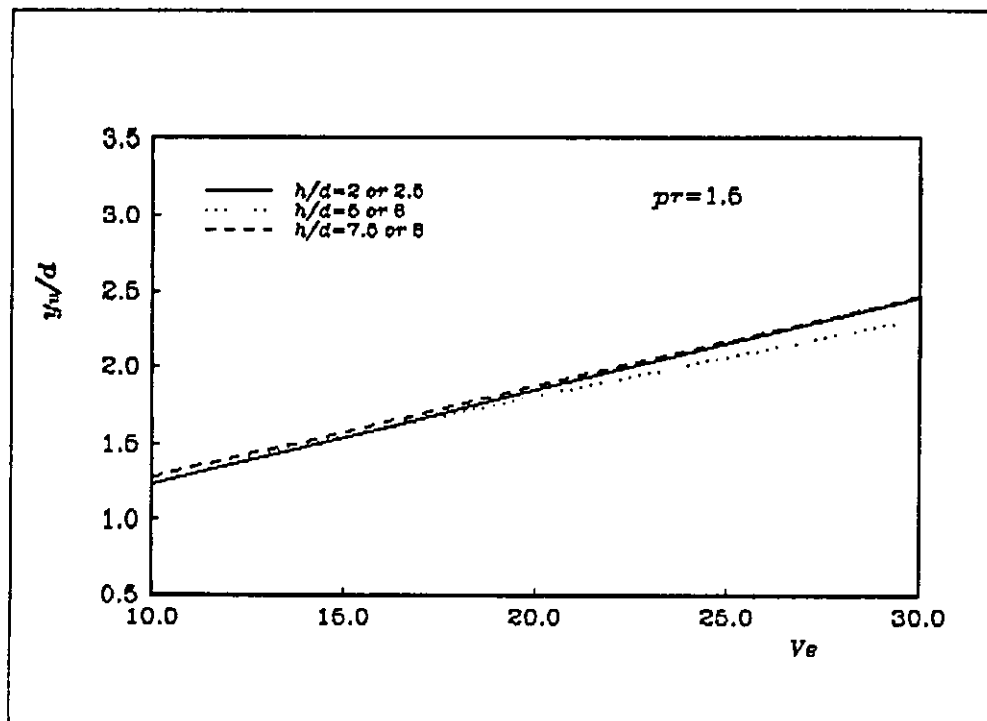


Figure 4.8: Effect of  $Ve$  on  $y_w/d$  and at different values of  $h/d$ .

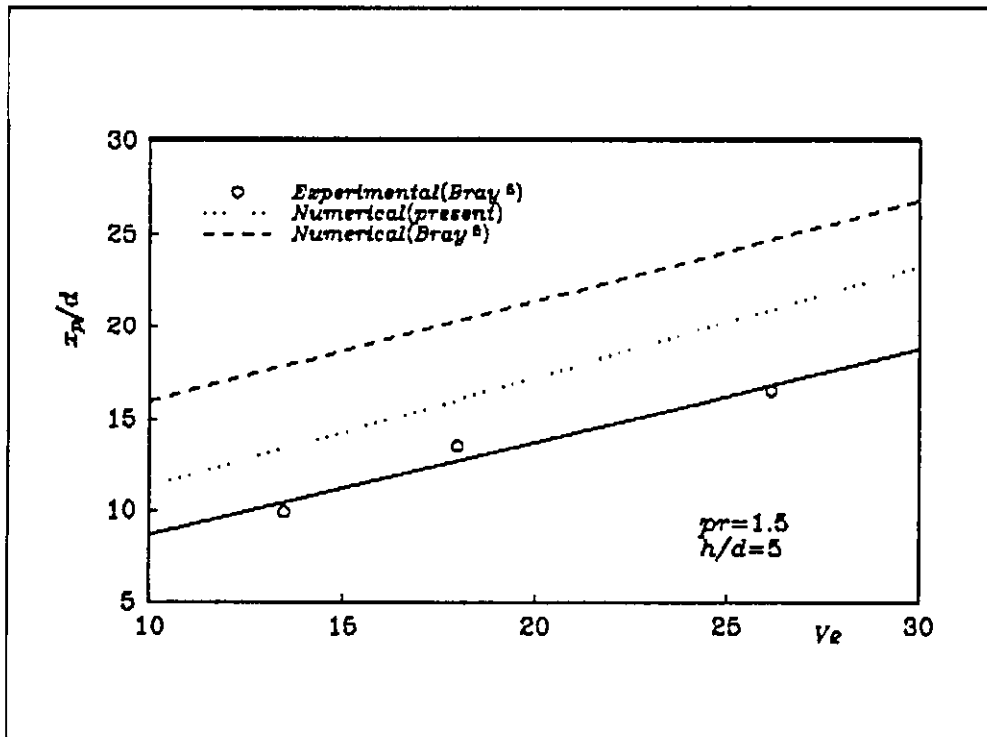


Figure 4.9: Effect of  $V_e$  on  $x_p/d$  (comparison between experimental and numerical works).

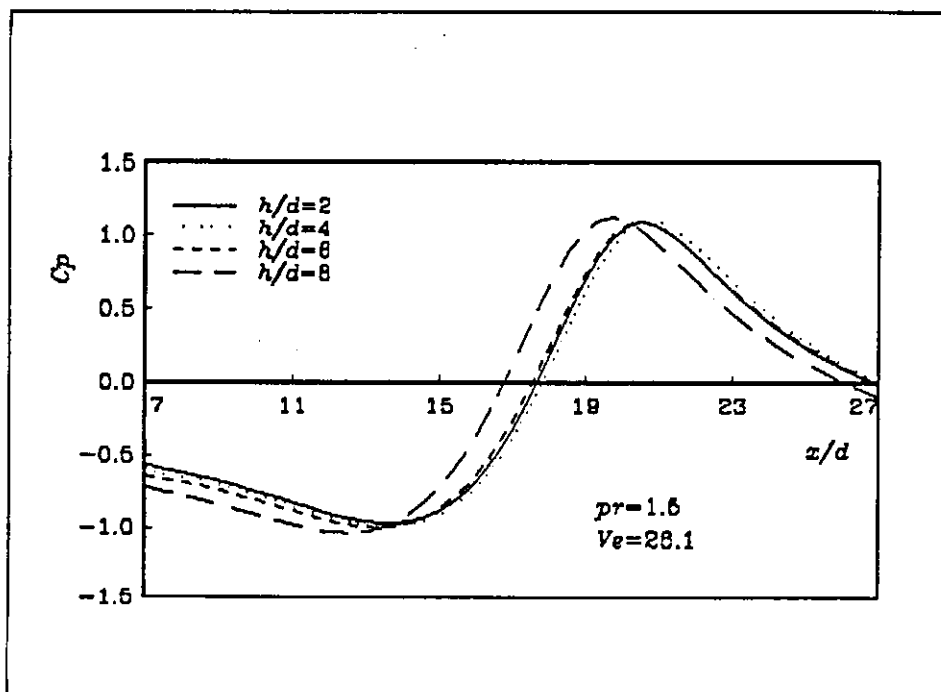


Figure 4.10: Effect of  $h/d$  on  $C_p$  distribution.

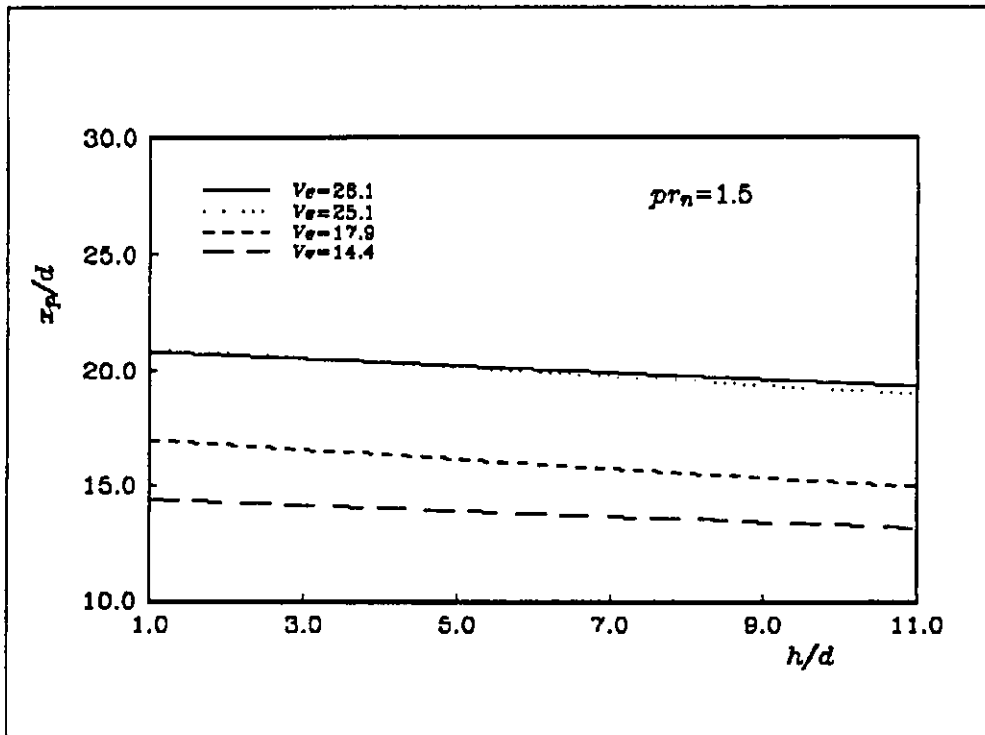


Figure 4.11: Effect of  $h/d$  on  $x_p/d$  at different values of  $Ve$ .

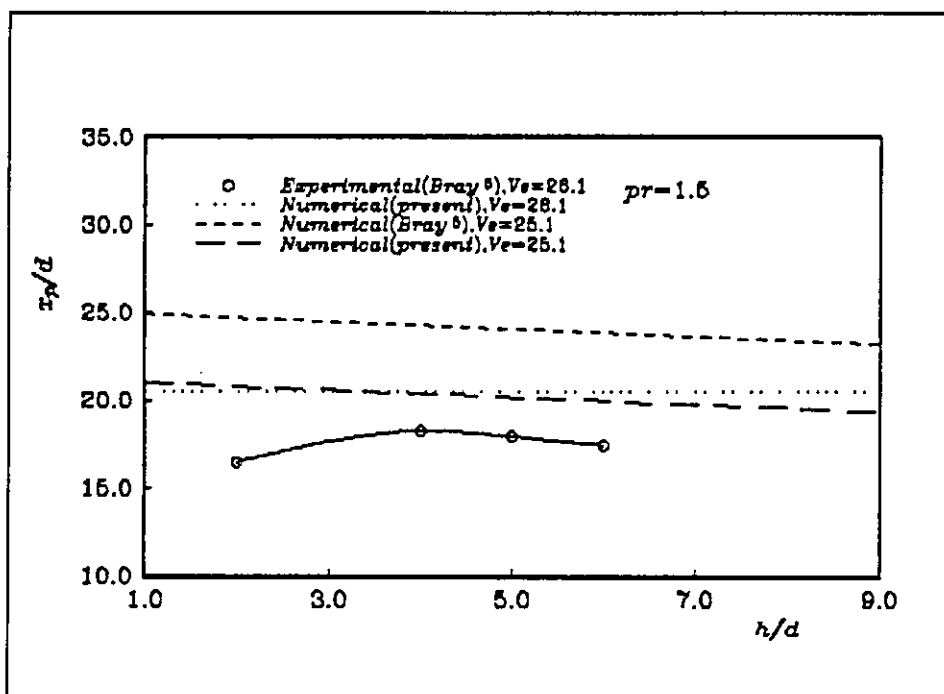


Figure 4.12: Effect of  $h/d$  on  $x_p/d$  (comparison between experimental and numerical works).

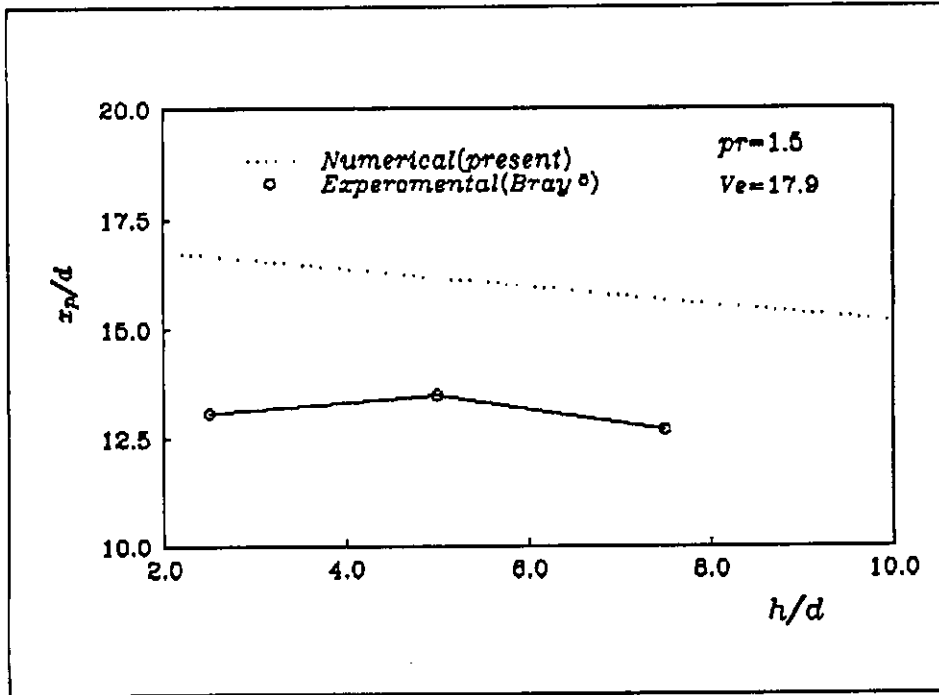


Figure 4.13: Effect of  $h/d$  on  $x_p/d$  (comparison between experimental and numerical works).

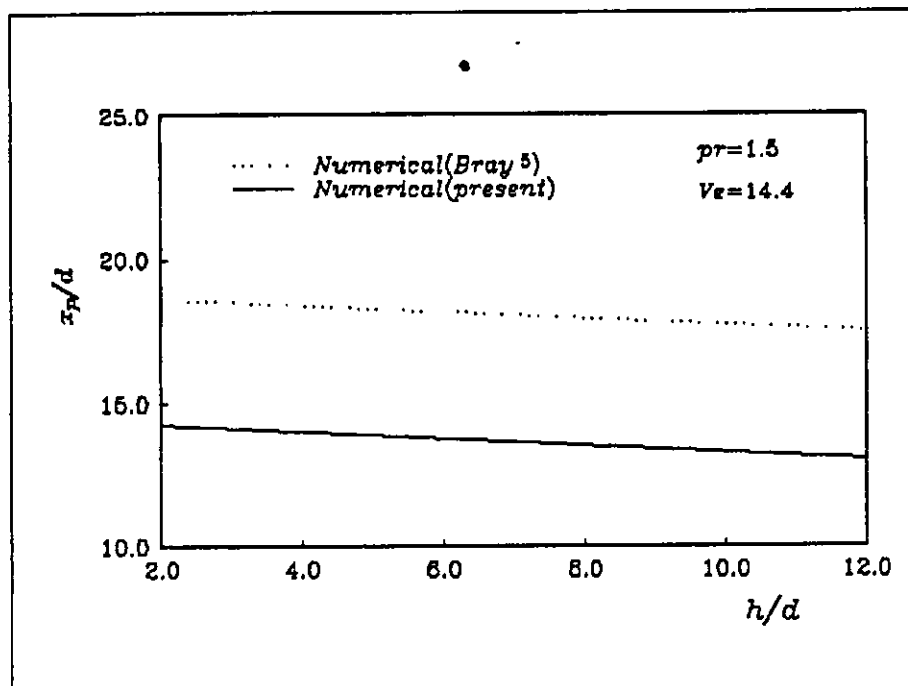


Figure 4.14: Effect of  $h/d$  on  $x_p/d$  (comparison between numerical works).



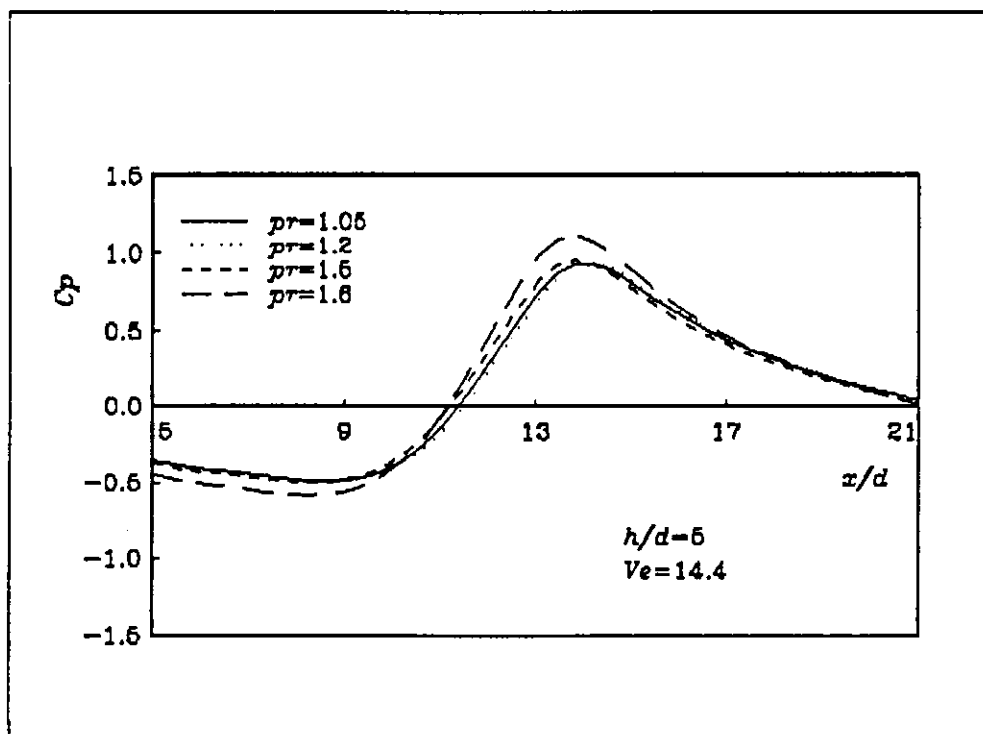


Figure 4.15: Effect of  $pr$  on  $C_p$  distribution.

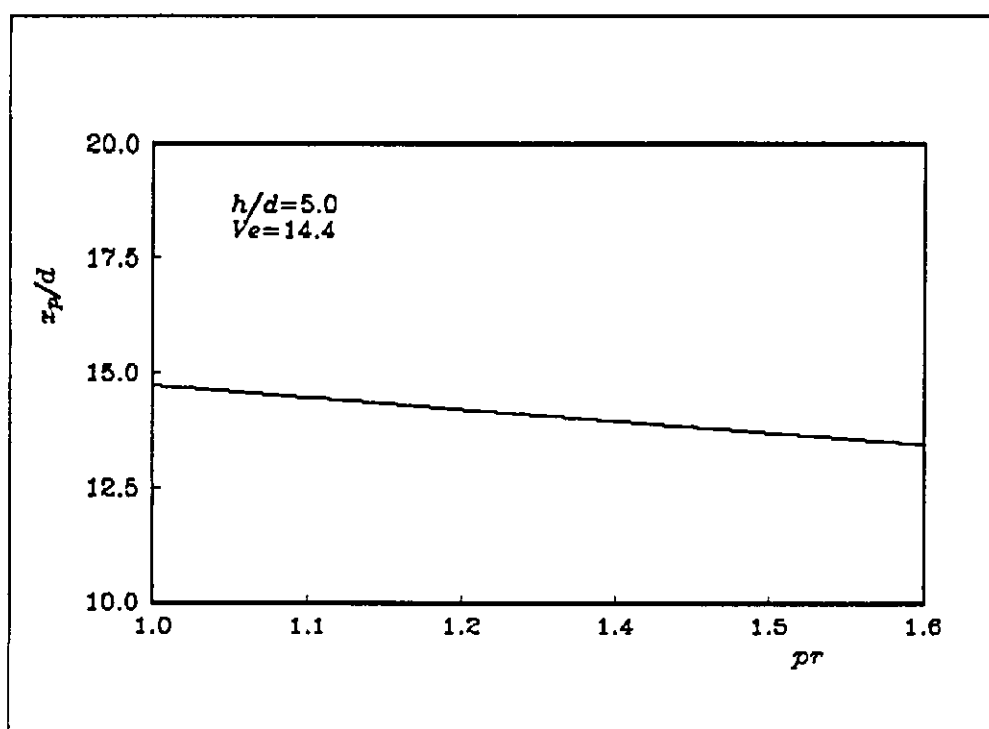


Figure 4.16: Effect of  $pr$  on  $x_p/d$ .

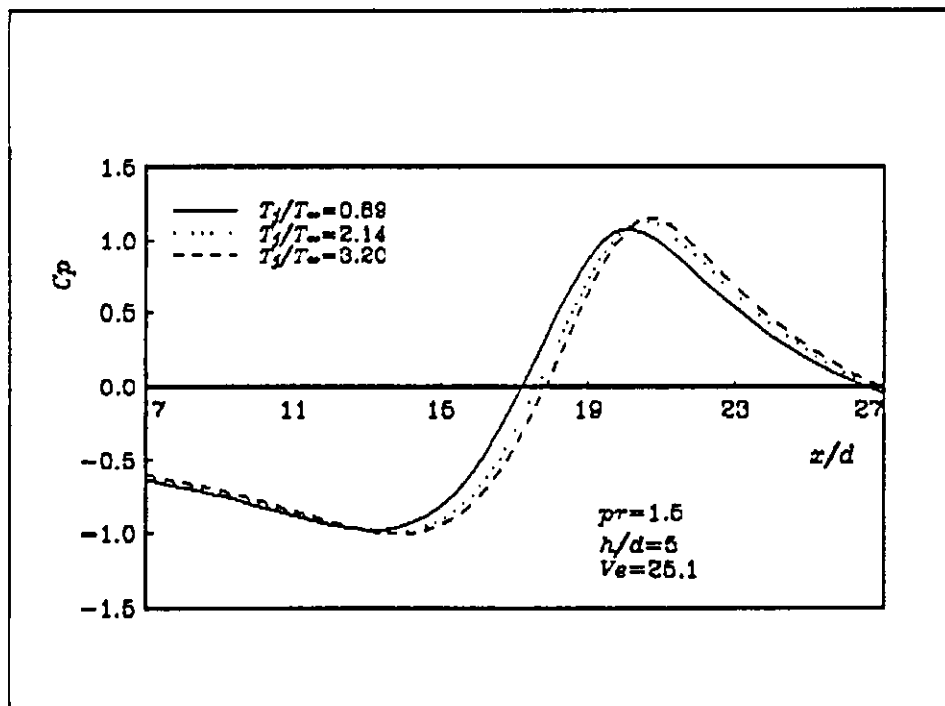


Figure 4.17: Effect of  $T_j/T_\infty$  on  $C_p$  distribution.

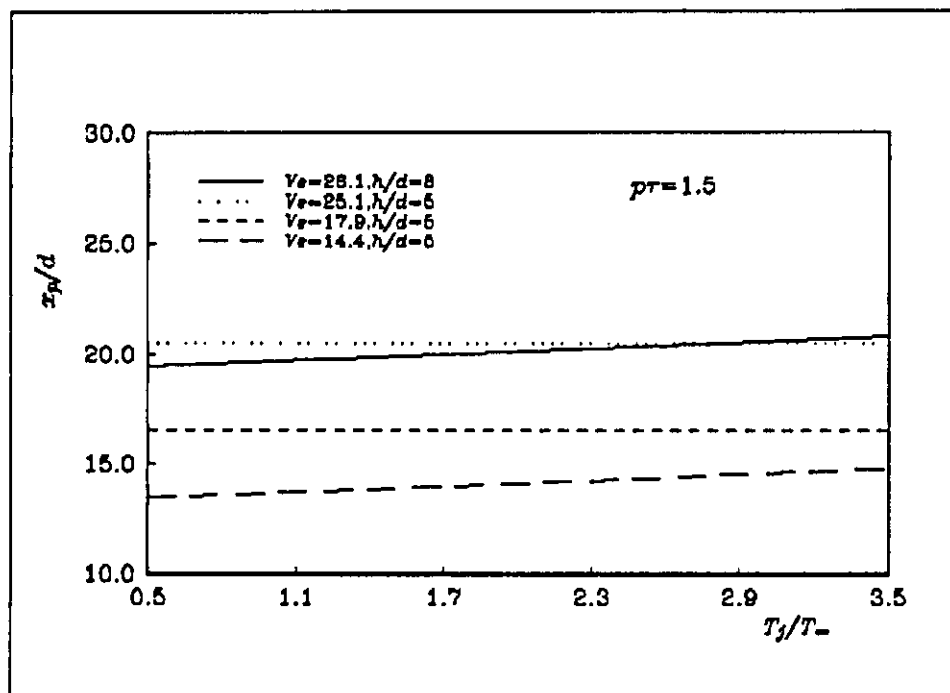


Figure 4.18: Effect of  $T_j/T_\infty$  on  $x_p/d$  at different values of  $Ve$ .

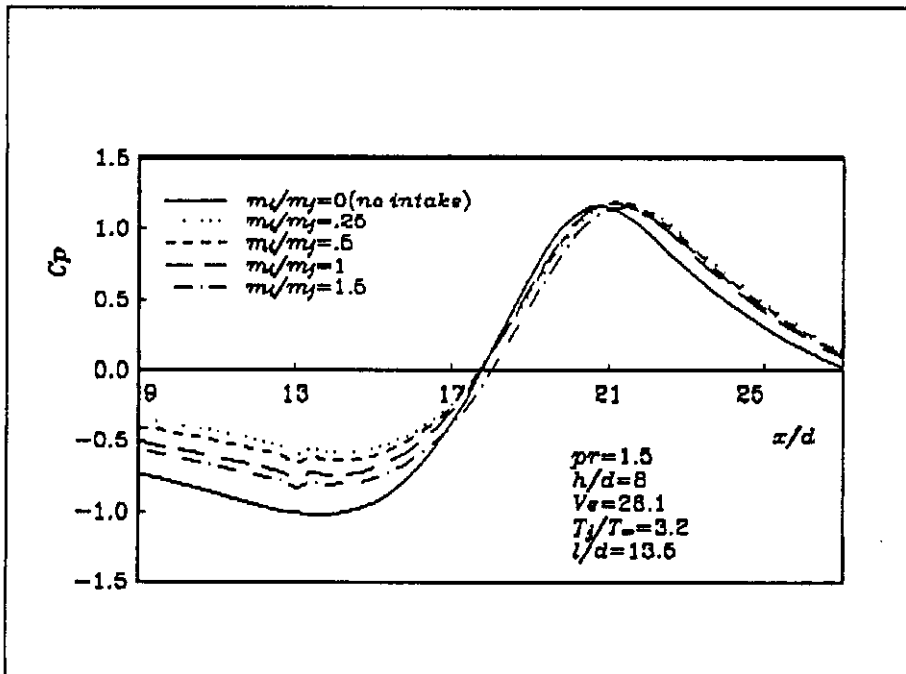


Figure 4.19: Effect of  $m_i/m_j$  on  $C_p$  distribution.

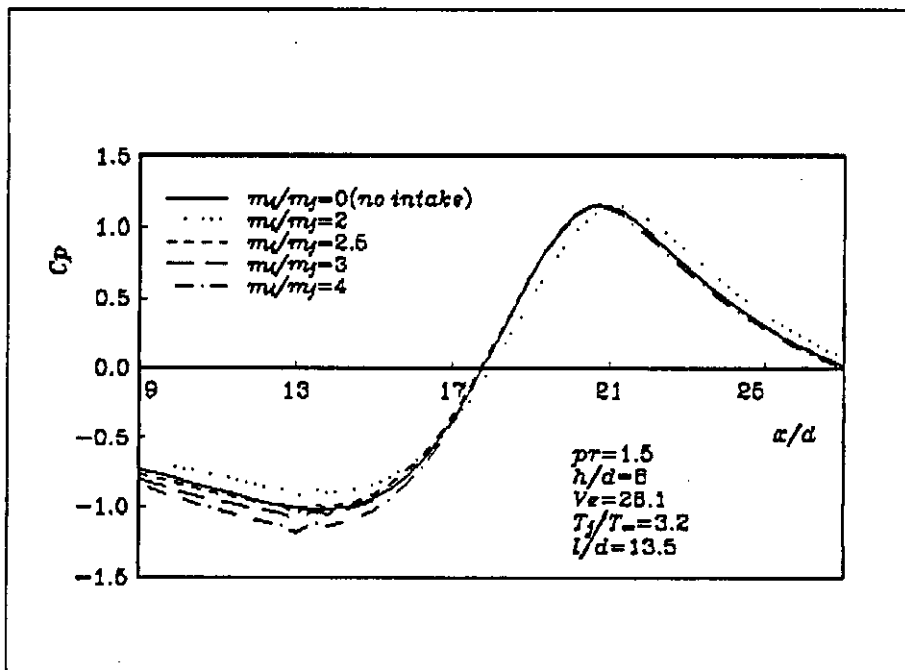


Figure 4.20: Effect of  $m_i/m_j$  on  $C_p$  distribution.

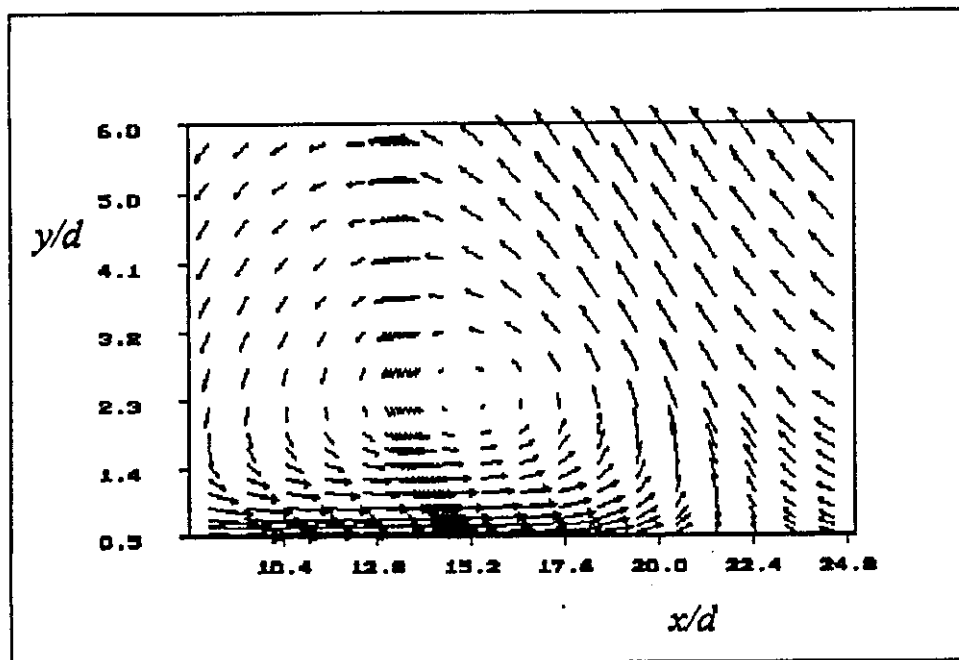


Figure 4.21: Enlarged ground vortex region (case 26).

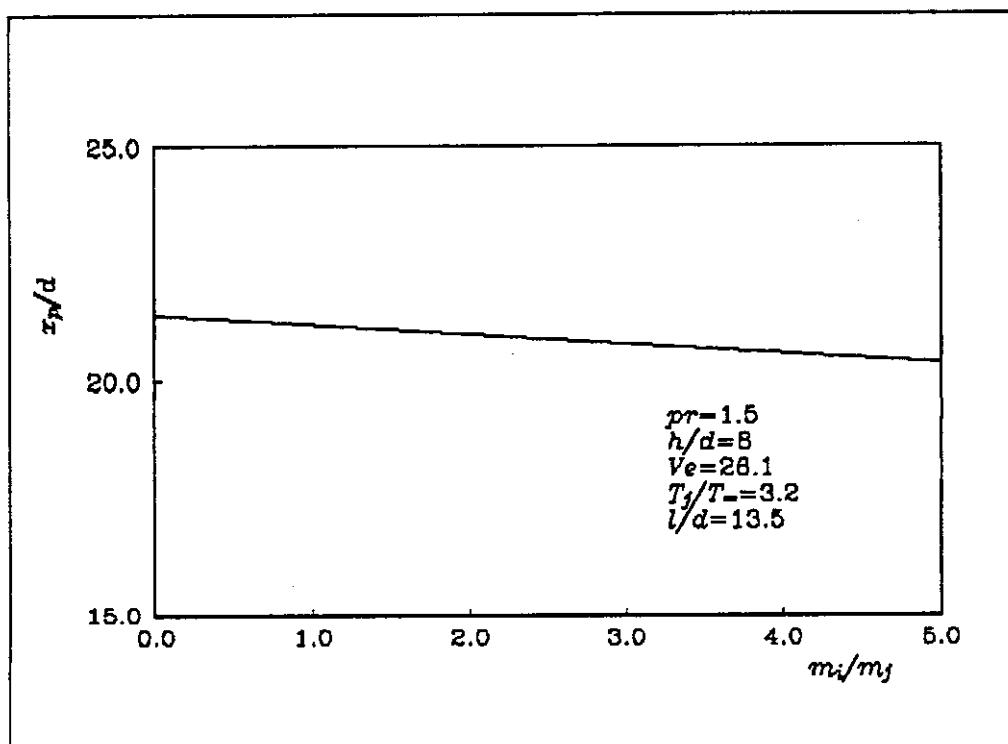


Figure 4.22: Effect of  $m_i/m_j$  on  $x_p/d$ .

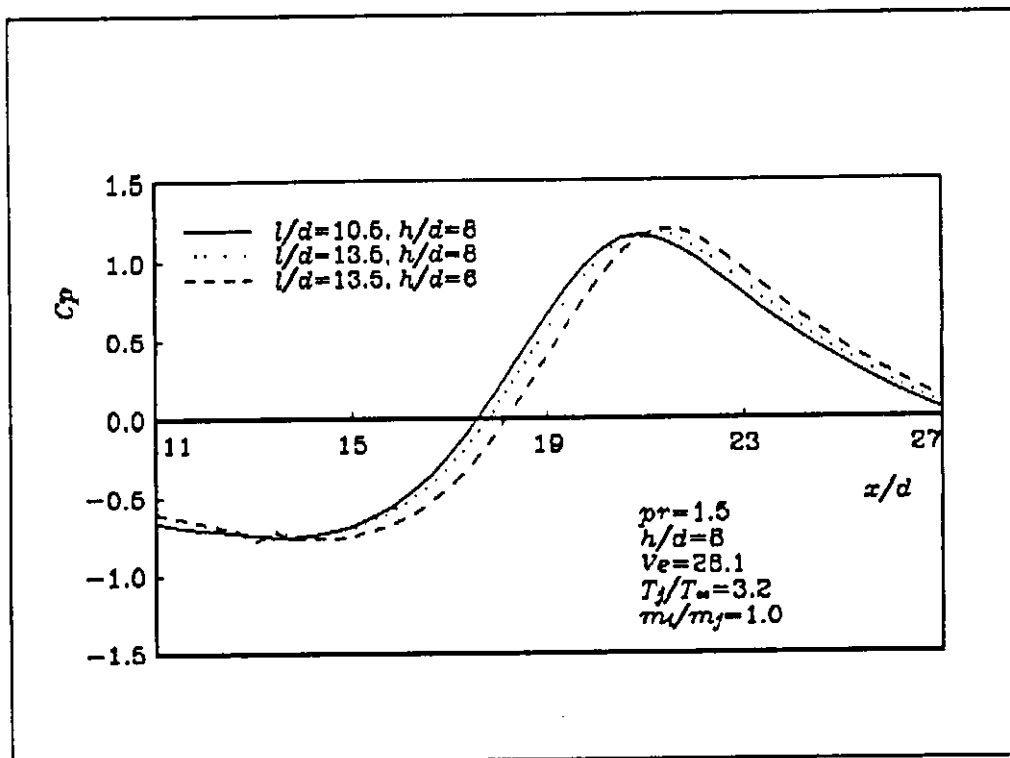


Figure 4.23: Effect of  $l/d$  on  $C_p$  distribution.

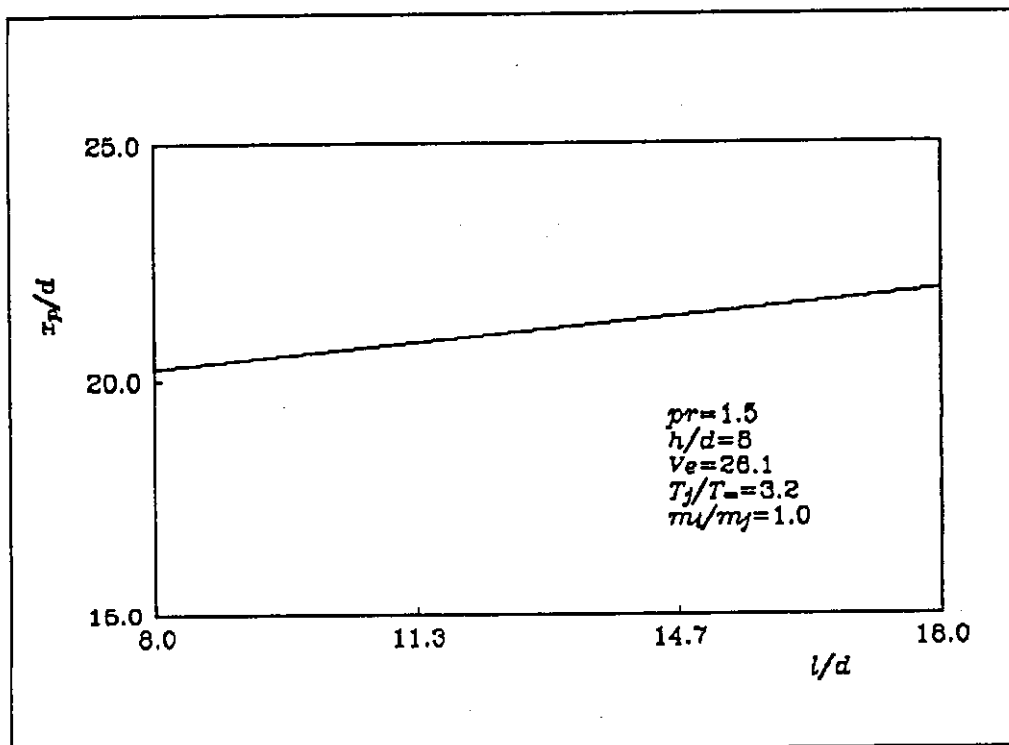


Figure 4.24: Effect of  $l/d$  on  $x_p/d$ .

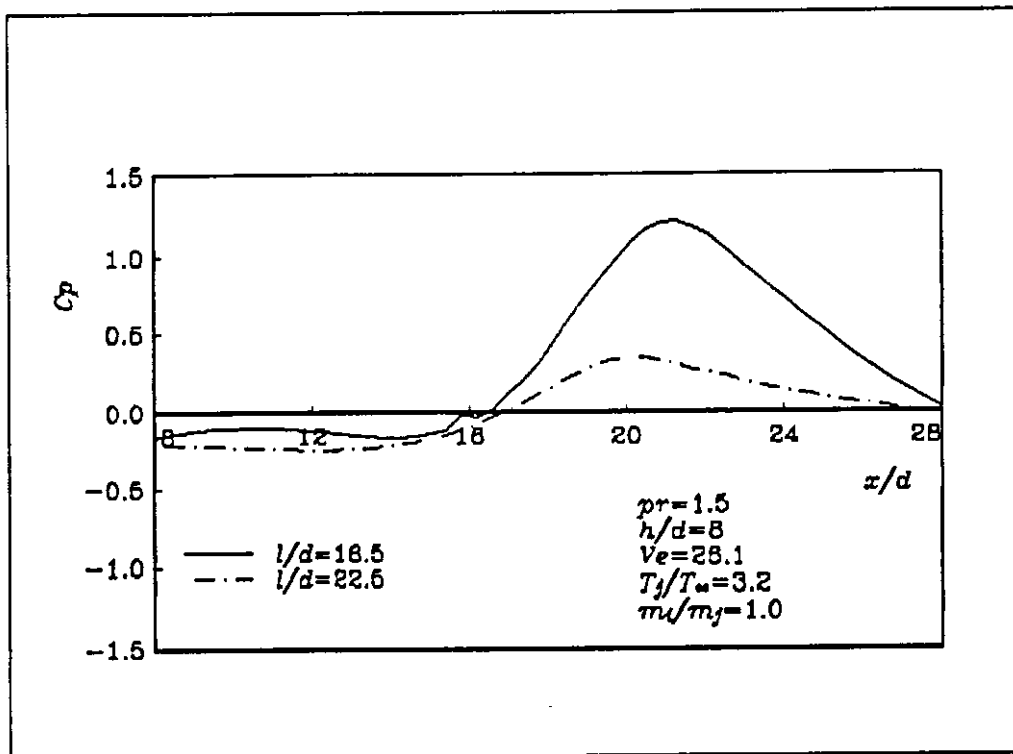


Figure 4.25: Effect of  $l/d$  on  $C_p$  distribution.

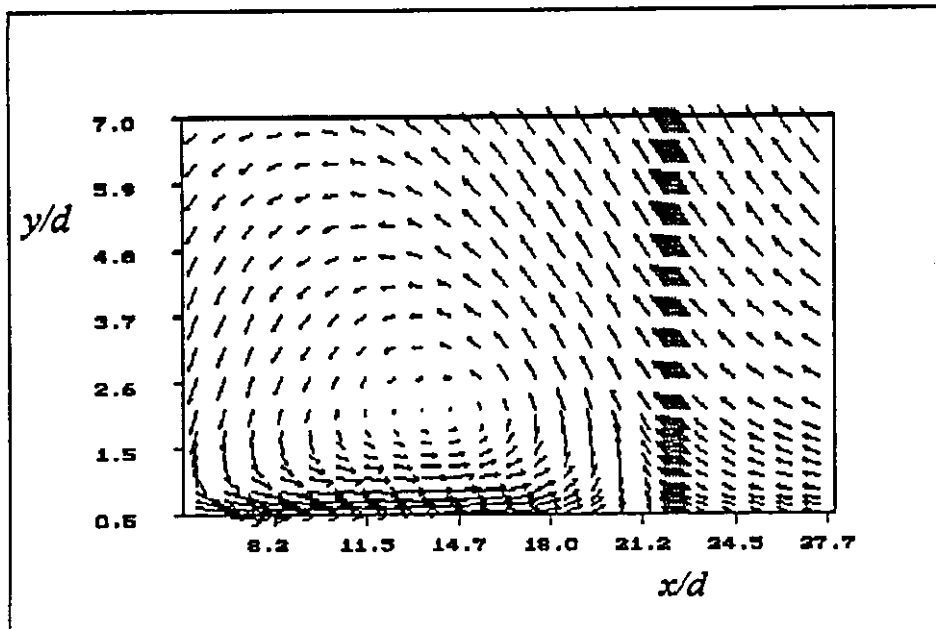


Figure 4.26: Enlarged ground vortex region (case 37).

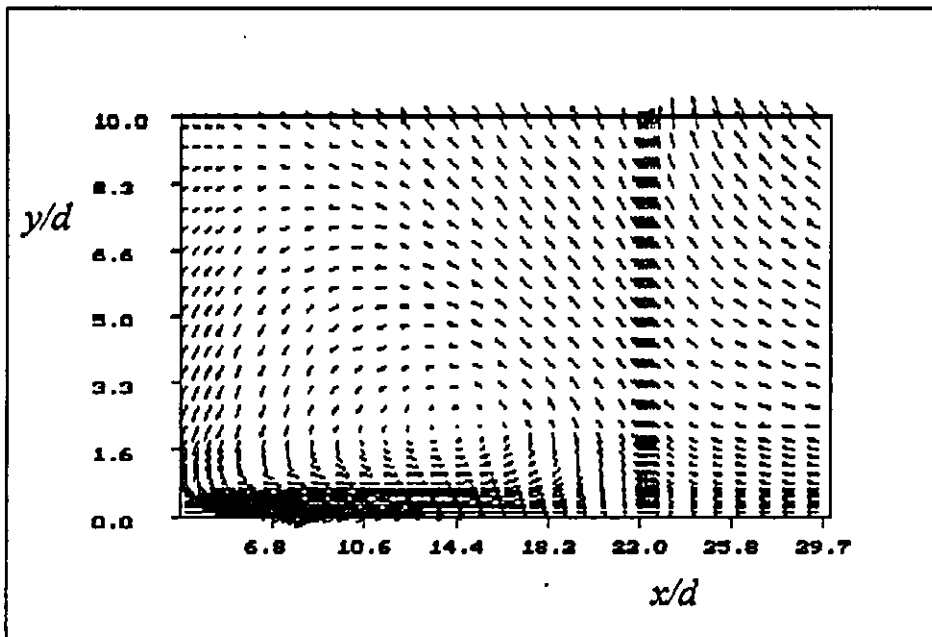


Figure 4.27: Velocity vectors (case 37).

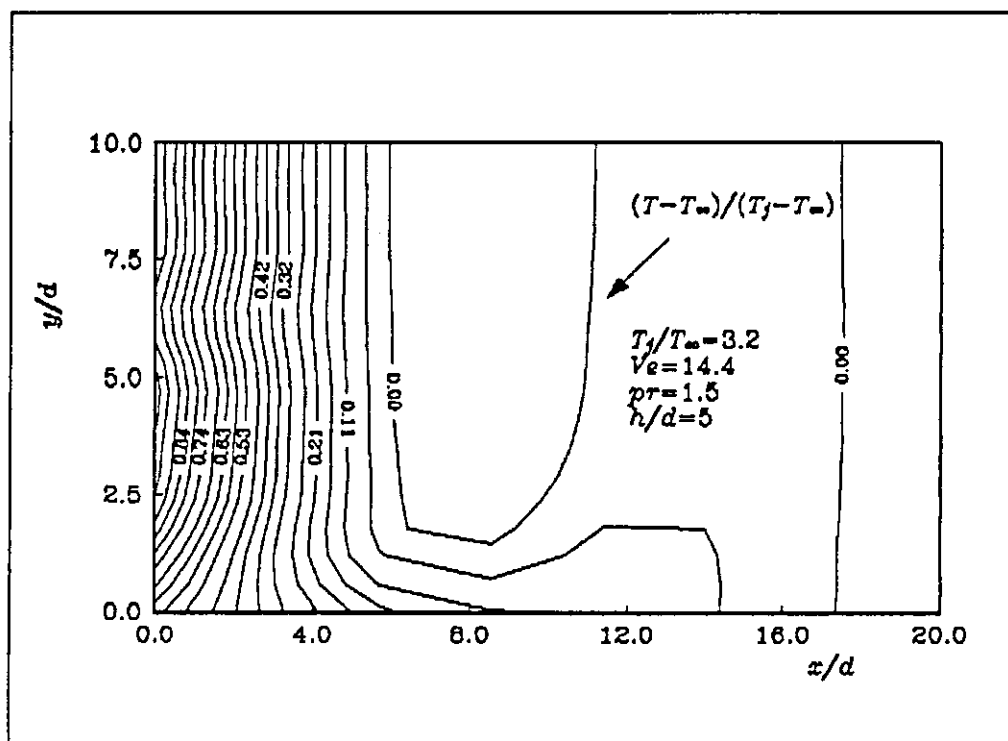


Figure 4.28: Temperature contours (case 18).

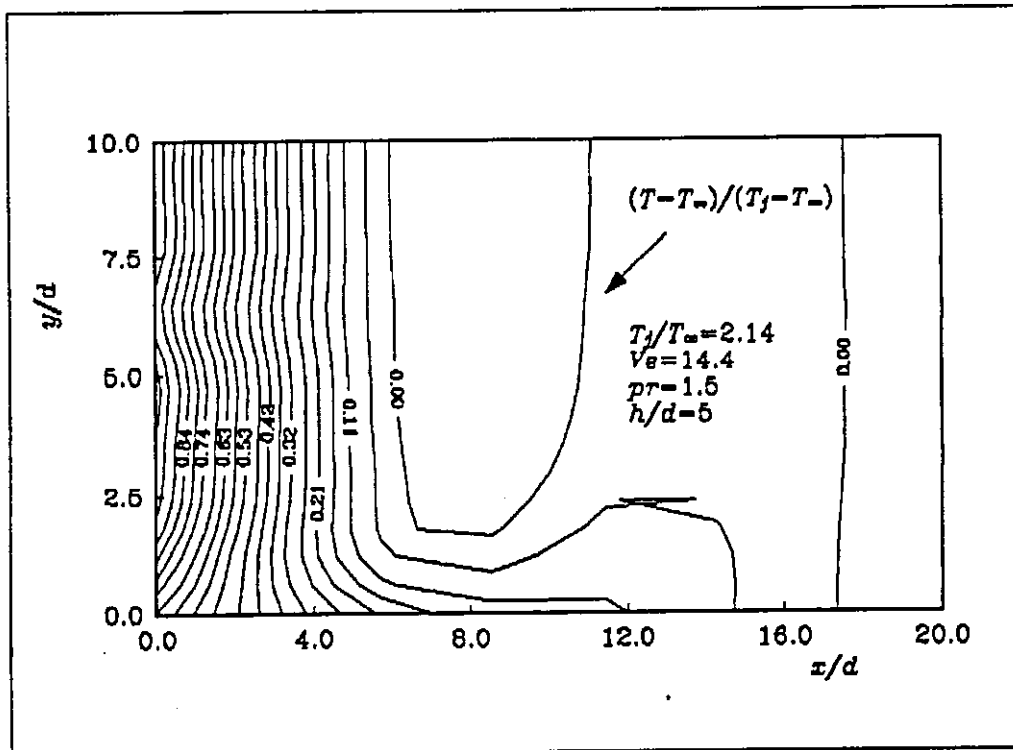


Figure 4.29: Temperature contours (case 19).

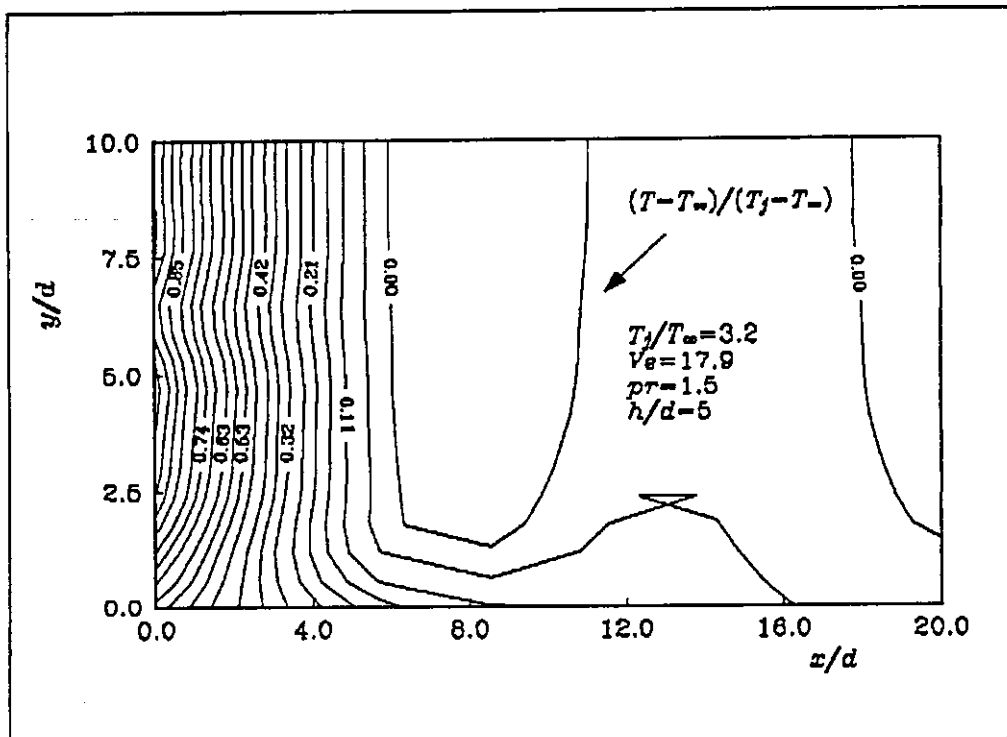


Figure 4.30: Temperature contours (case 20).



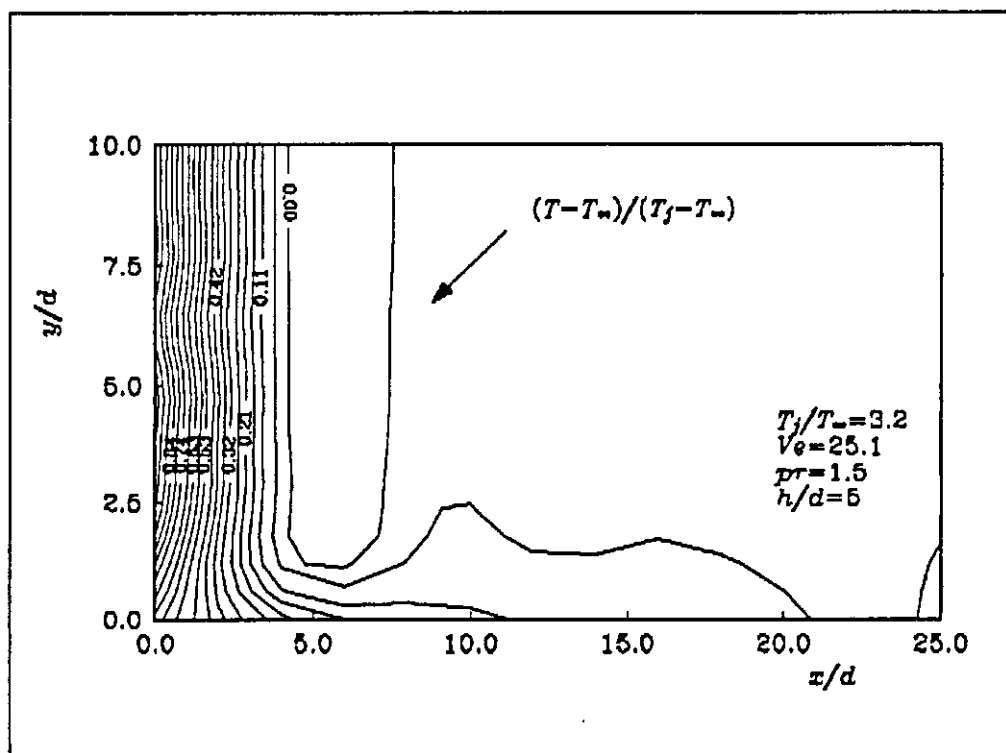


Figure 4.31: Temperature contours (case 22).

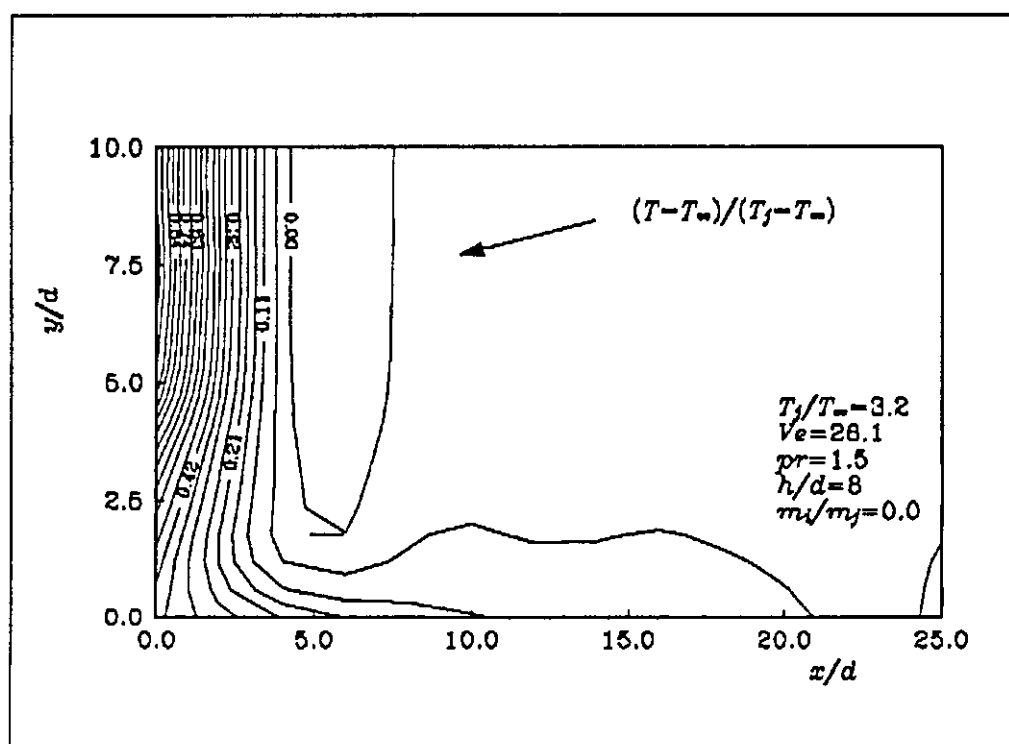


Figure 4.32: Temperature contours (case 24).

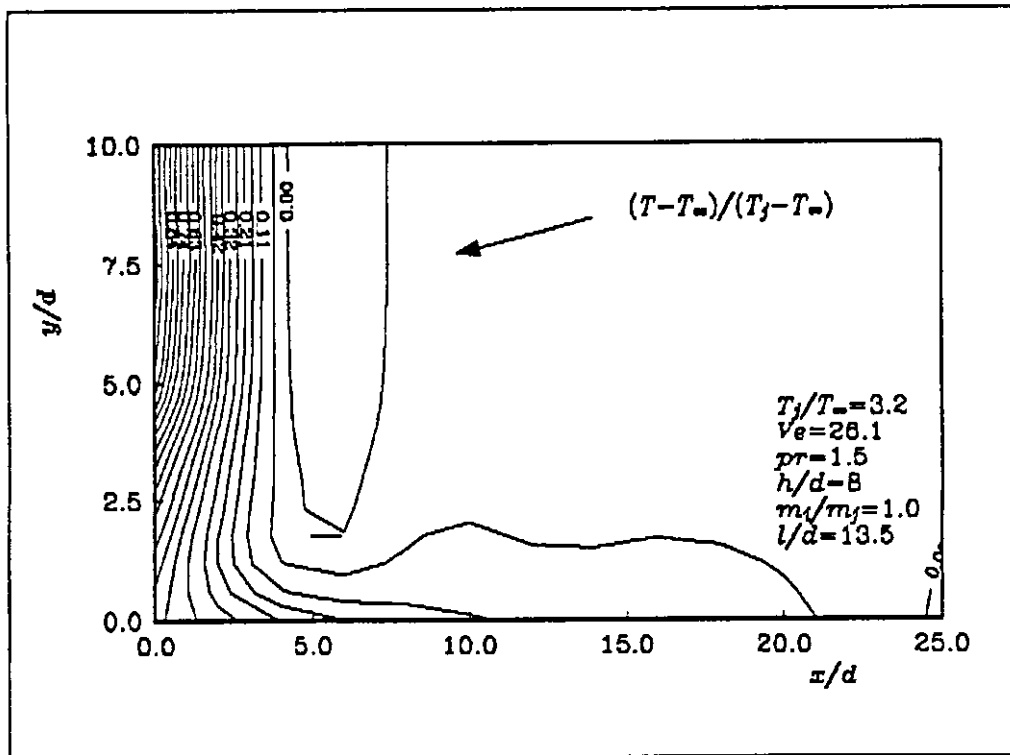


Figure 4.33: Temperature contours (case 26).

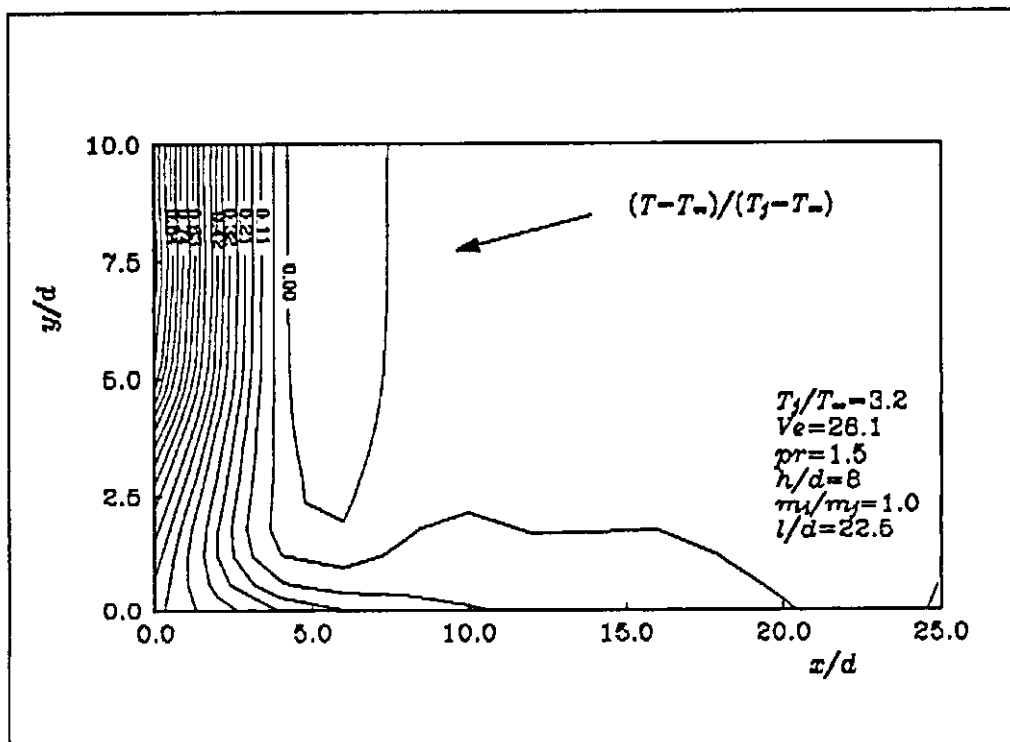


Figure 4.34: Temperature contours (case 37).

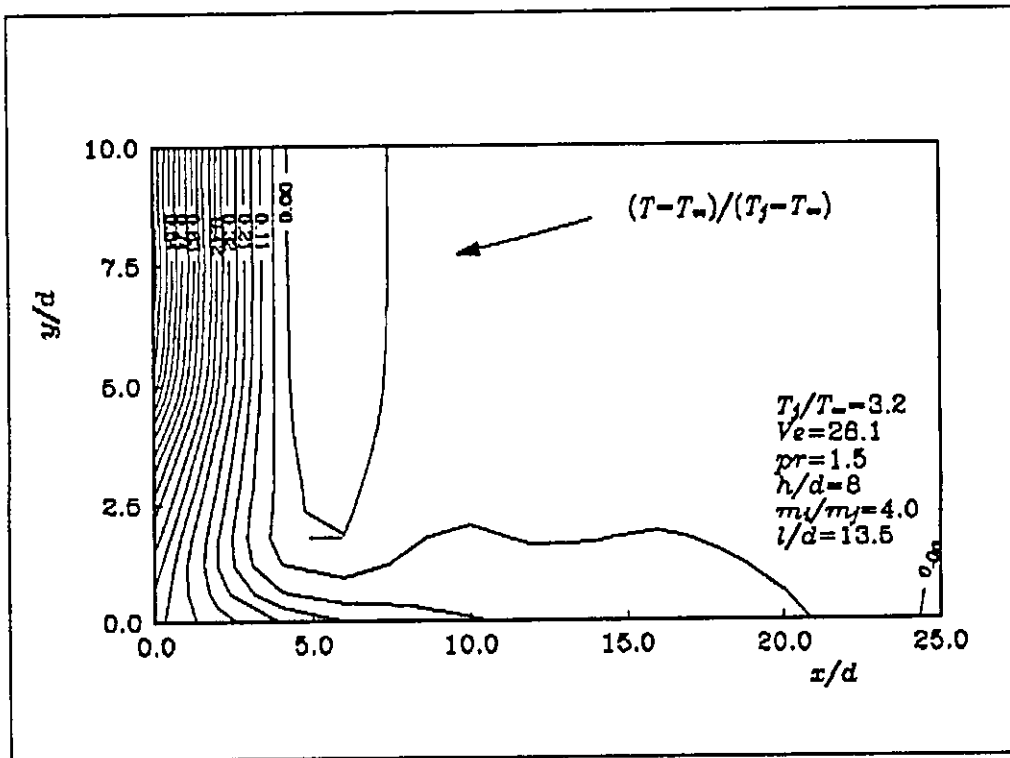


Figure 4.35: Temperature contours (case 34).

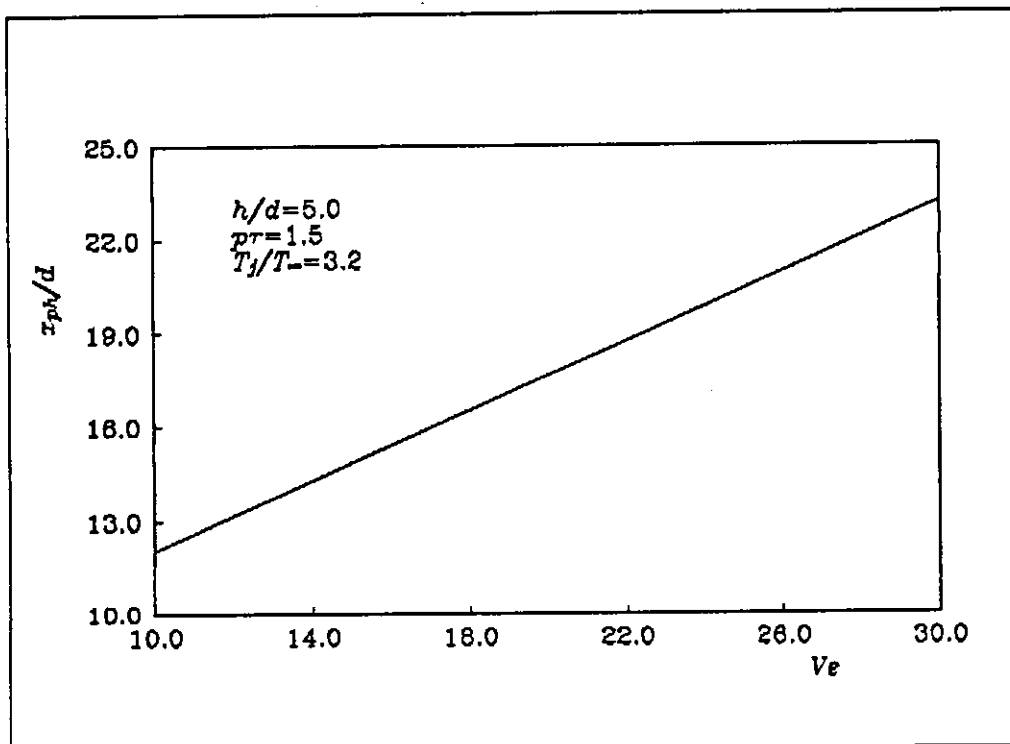


Figure 4.36: Effect of  $V_e$  on  $x_{ph}/d$ .

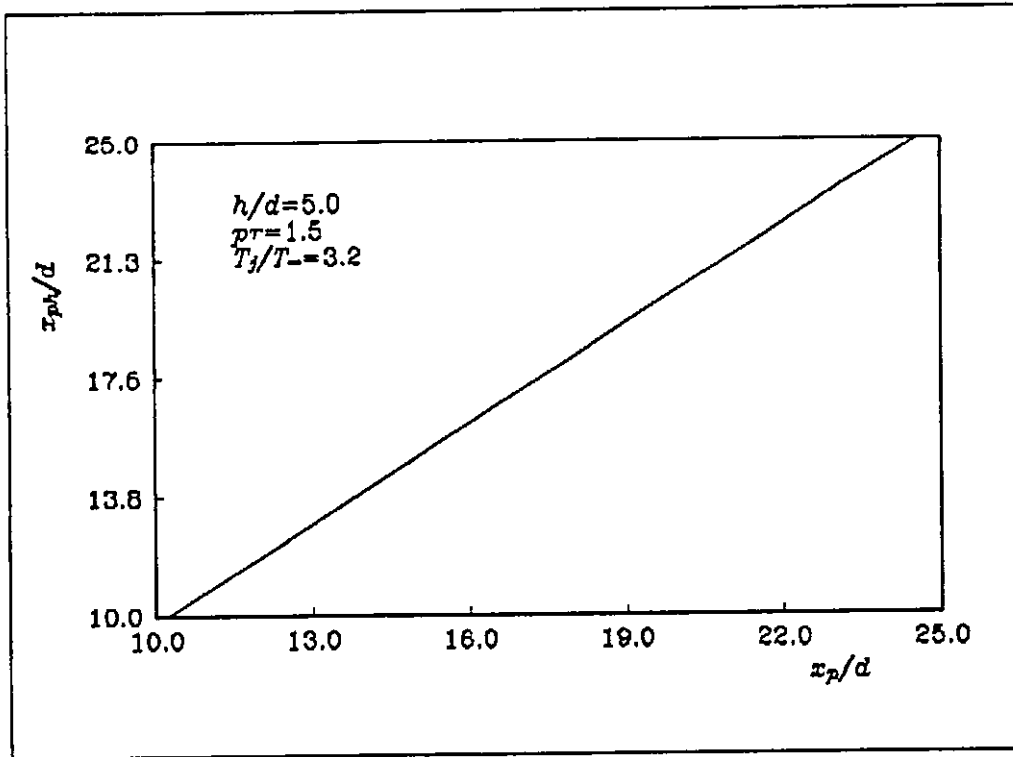


Figure 4.37: Relation between  $x_{pH}/d$  and  $x_p/d$ .

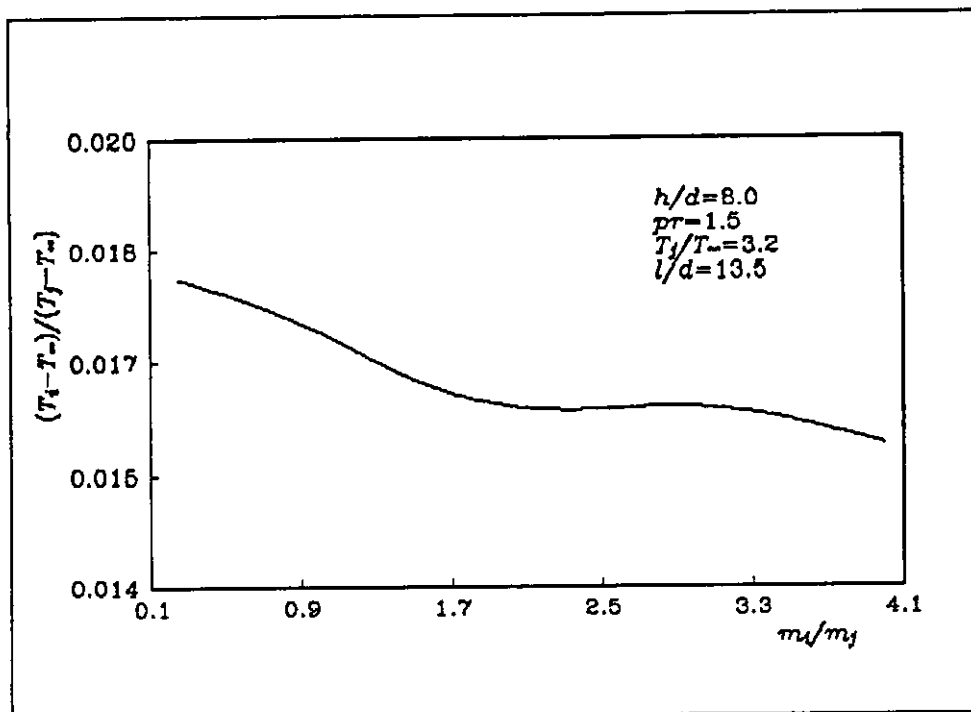


Figure 4.38: Effect of  $m_i/m_j$  on  $Tn_i$ .

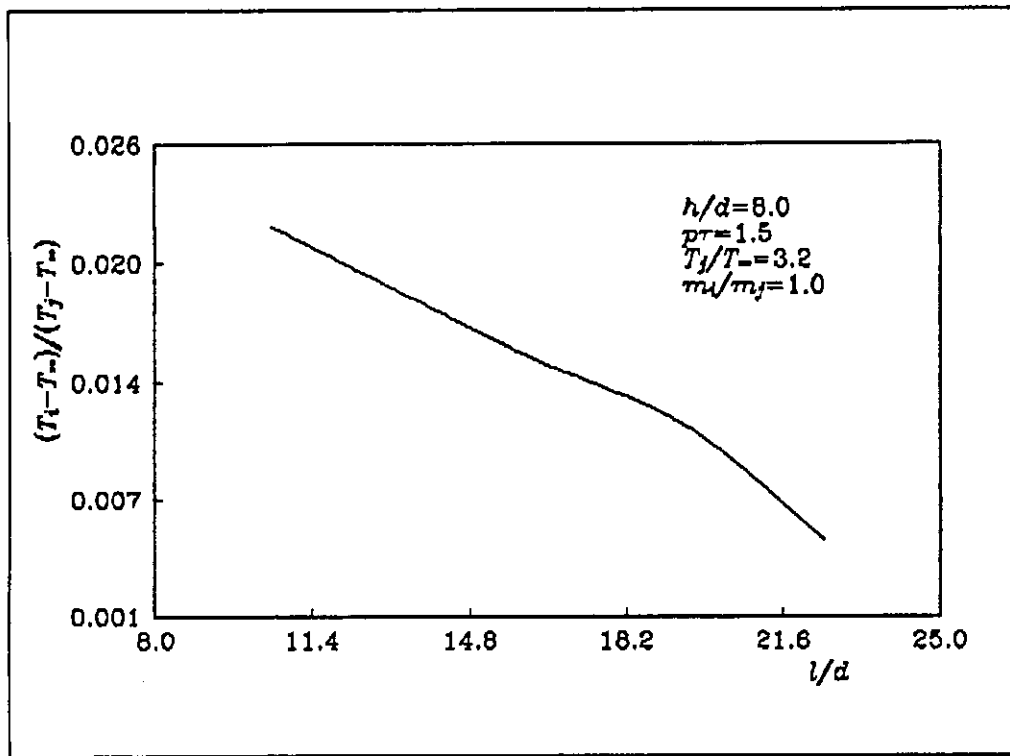


Figure 4.39: Effect of  $l/d$  on  $T_n$ .

## **Chapter 5**

# **Conclusions and Recommendations**

### **5.1 Introduction**

This chapter summarizes the work presented in the thesis, to assess the important points which have emerged from the present investigation, and to outline areas which needed further investigation.

### **5.2 Summary and Assessment of the Present Investigation**

The literature survey of chapter 2 revealed the absence of numerical modeling regarding the effects of intake conditions and their locations on the characteristics of the ground vortex. The review also shows a lack of a clear picture on the effect of certain parameters on the ground vortex penetration; such as the effect of nozzle height and nozzle pressure ratio, together with a limited number of investigations regarding the effect of the jet temperature on the ground vortex characteristics.

### 5.3 Conclusions

Several points have been emerged from the numerical modeling of impinging jet in cross-flow with particular reference to *STOVL* aircraft. These can be summarized as follows:

- 1- The effective velocity ratio is the most predominant parameter that affects the ground vortex geometry and the ground vortex strength increases with  $Ve$ .
- 2- It was possible to predict the ground vortex similarity relations with high accuracy. The predicted relation is  $x_p/x_v = 1.58$  compared with  $x_p/x_v = 1.592$  as obtained from the experimental results of [5]. Also, the relation between  $y_p$  and  $x_v$  is found to be predicted by  $y_p/x_v = 0.184$ .
- 3- The ground vortex maximum penetration point  $x_p$ , increases with  $Ve$ , the rate of increase is correctly predicted, while the absolute values of  $x_p$  are overpredicted by about 25%, compared with 40-50% for previous numerical works.
- 4- Based on previous experimental works regarding fixed impinging jet on fixed ground plane, it was found that:  $x_p/d = C_2Ve$ , where  $C_2 = 0.64-0.7$ , while based on previous numerical works, it was found that  $x_p/d = C_3Ve$ , where  $C_3 = 0.9-1.1$ . Based on the present numerical work, it was found that,  $x_p/d = 0.86Ve$ , which is closer to the experimental relation than the previous numerical works.
- 5- The ground vortex core height  $y_p$ , increases with  $Ve$ , and it was found that it could be predicted from:  $y_p/d = 0.1Ve$ .
- 6- The penetration of hot gases  $x_{ph}$ , increases with  $Ve$ . An interesting relation is found between  $x_{ph}$  and  $x_p$ , namely;  $x_{ph}/d \approx x_p/d$ , where  $x_{ph}$  is based on the penetration of the temperature contour of  $Tn = 0.05$ .
- 7- The nozzle height  $h$ , has a little effect on the ground vortex geometry, location and strength, while it has a significant effect on the temperature

at the impinging point, where the temperature significantly decreases with increasing the height due to the entrainment action. However, the penetration of the hot gases does not change significantly with increasing the height.

- 8- The nozzle pressure ratio has a little effect on the ground vortex geometry, location and strength (based on the subsonic range).
- 9- The jet temperature has a negligible effect at constant  $V_e$  and the temperature effect is included in  $V_e$ . In the meantime, the jet temperature has a negligible effect on the temperature distribution in the flow field.
- 10- The intake mass flow rate has a small effect on the ground vortex geometry and location, however, the ground vortex strength increases as the intake mass flow rate increases.
- 11- The  $HGI$  decreases as the intake mass flow rate is increased, but the intake mass flow rate has a negligible effect on the temperature distribution. However, the  $HGI$  increases as  $l/d$  is decreased.
- 12- The intake location  $l$ , has a negligible effect on the ground vortex, if it is positioned above or downstream the ground vortex core. If it is positioned upstream the ground vortex core, the strength of the ground vortex decreases. If the intake is positioned upstream the maximum penetration point, the stagnation pressure will be highly reduced.
- 13- the location of the intake has a negligible effect on the temperature distribution in the flow field.



## 5.4 Recommendations

The literature survey in chapter 2, together with the present work suggest the following points need further investigation:

- 1- The  $k-\varepsilon$  turbulence model should be either replaced by other models to test its impact on the accuracy of the predicted results.
- 2- An important step that must be taken, is to model the full 3-D case, since the 2-D modeling has many disadvantages.
- 3- A body fitted coordinate system could be used, this is necessary for modeling more complicated boundaries that include the fuselage or the wing of the aircraft.
- 4- Multi level grid techniques [28] can be used to increase the speed of convergence and decrease the number of iterations (less CPU time).
- 5- Multiple nozzle arrangement can be modeled to study the fountain flow and the associated near field ingestion.
- 6- ground vortex unsteadiness is a major area that must receive more attention in numerical works.

## References

- [1] Van Dalsem W. R., Chawla K., Smith M. H. and Abeloff P. A., "Numerical Simulation of powered-lift flows", International Powered Lift Conference, August 29-31, 1990.
- [2] Knowles K. and Bray D., "Recent Research in *ASTOVL* Aircraft Ground Environment", Private Communications, 1993.
- [3] Nosseir N. S., "Impinging Jets", Encyclopedia of Fluid Mechanics, Vol. 2, Gulf Publication Co., 1986.
- [4] Cimbala J. M., Stinebring, D. R., Treaster A. L., Billet M. L. and walters, M. M., "Experimental Investigation of a Jet Impinging on a Ground Plane in the Presence of a Cross-flow", International Powered Lift Conference, December 7-10, 1987.
- [5] Bray D., "Jets in Cross-Flow and Ground Effect", Ph.D. thesis submitted to Cranfield Institute of Technology, RMCS, England, August 1, 1991.
- [6] Kuhn R. E. "Design Concepts for Minimizing Hot-Gas Ingestion in *V/STOL* Aircraft", Journal of Aircraft, Vol. 19, No. 10, October 1982.
- [7] MacLean R., Sullivan J. and Murthy S. N. B., "Hot Gas Environment Around *STOVL* Aircraft in Ground Proximity, Part 1: Experimental Study", AIAA/SAE/ASME/ASEE 26th Joint Propulsion Conference, AIAA 90-2269, Orlando, Fl., July 16-18, 1990.

- [8] Milford , C. M., "Hot Gas Recirculation in *V/STOL*", International Powered Lift Conference, P-203, Paper no. 872306, Santa Clara, Calif., Feb. 1988.
- [9] Kuhn R. E., "The Induced Aerodynamics of Jet and Powered *V/STOL* Aircraft", International Symposium held at Stanford University, August 22-26, 1983.
- [10] Cimbala, J. M., Gaublomme D. P., Stinebring D. R. and Billet M. L. "Experiments on the Unsteady Ground Vortex", Aerospace Technology Conference and Exposition, Anaheim, California, September 25-28, 1989.
- [11] Abbott, W. A., "Studies of Flow Fields Created By Vertical and Inclined Jets when Stationary or Moving over a Horizontal Surface", Aero. Research Council, Rept. no. CP-911, October 1964.
- [12] Miller, L. S., Papadakis M. and Klausmeyer S., "Flow Visualization For A *STOVL* Aircraft In Ground Proximity", 29th Aerospace Science Meeting, AIAA 91-0769, Reno, Nevada, January 7-10, 1991.
- [13] Catalano, G. D., Chang, K. and Mathis, J. A., "Calculation and Measurement of Turbulent Jet Impingement in a Cross-flow, Part 2", 6th international conference on Numerical Methods in Laminar & Turbulent Flow. Vol. 6, pt. 2, pp. 1895-1906, Pineridge Press, 1989.
- [14] Barata, J. M. M., Durao, D. F. F., Heitor, M. V. and McGuirk J. J., "On The Validation Of 3-D Numerical Simulations Of Turbulent Impinging Jets Through A Cross-flow", private communications, 1993.

- [15] Araujo, S. R. B., Durao, D. F. G., Firmino, F. J. C., "Jets Impinging Normally and Obliquely to a Wall", Fluid Dynamics of Jets with Application to V/STOL, AGARD CP-308, 1982.
- [16] Knowles K. and Bray D., "Ground Vortex Formation With Twin Jets And Moving Ground Plane", ICAS, Stockholm, Sweden, September 1990.
- [17] Bradbury, L. J. S., "The impact of an Axisymmetric Jet onto a Normal Ground", Aeronautical quarterly, pp. 141-147, May 1972.
- [18] Knowles K. and Bray D., "The Ground Vortex Formed by Impinging Jets in Cross-Flow", 29th Aerospace Sciences Meeting, AIAA 91-0768, January 7-10, Reno, Nevada, 1991.
- [19] Knowles, K., Bray, D., Bailey, P. J. and Curtis, P., "Impinging jets in cross-flow", International Powered Lift Conference, 29-31 August 1991.
- [20] Smith, A. G., Ing D. N. and Bailey P. J., "The Experimental And Computational Study Of Jet Impingement Flow fields With Reference To VSTOL Aircraft Performance", International Powered Lift Conference, 29-31 August, 1990.
- [21] Brady, W. G. and Ludwig, G., "Theoretical And Experimental Studies Of Impinging Uniform Jets", IAS 31st Annual Meeting, IAS Paper no. 63-29, New York, January 21-23, 1963.

- [22] Catalano, G. D., Chang, K. and Mathis, J. A., "Calculation and Measurement of Turbulent Jet Impingement in a Cross-flow, Part 1", 6th international conference on Numerical Methods in Laminar & Turbulent Flow. Vol. 6, pt. 2, pp. 1895-1906, Pineridge Press, 1989.
- [23] Hwang, C. J. and Liu, J. L., "Numerical Study of Two-Dimensional Impinging Jet Flow fields", AIAA Journal, Vol. 27, No. 7, July, 1989.
- [24] Agarwal, R. K. and Bower W. W., "Navier stokes Computations of Compressible Two-Dimensional Impinging Jet Flow fields", AIAA Journal, Vol. 20, No. 5, pp. 577-584, May, 1982.
- [25] Hwang, C., Yang, S. and Liu, J., "Numerical Investigations of Airfoil / Jet / Fuselage-Undersurface Flow fields in Ground Effect", 28th Aerospace Sciences Meeting, AIAA 90-0597, Reno, Nevada, January 8-11, 1990.
- [26] Bray, D. and Knowles, K., "Numerical Modeling of Impinging Jet in Cross-Flow", AIAA/ASME/ASME/ASEE 26th Joint Propulsion Conference, AIAA 90-2246, Orlando, Fl., July 16-18, 1990.
- [27] VanOverbeke, T. J. and James, D., "A numerical Study of the Hot Gas Environment Around a *STOVL* Aircraft in Ground Proximity", AIAA/ASME /SAE/ASEE 24th Joint propulsion Conference, AIAA-88-2882, Boston, Massachusetts, July 11-13, 1988.
- [28] Tafti, D. and Vanka, S. P., "Hot Gas Environment Around *STOVL* Aircraft in Ground Proximity, Part 2: Numerical Study", AIAA/SAE/ASME/ASEE 26th Joint Propulsion Conference, AIAA 90-2270, Orlando, Fl., July 16-18, 1990.

- [29] Van Dalsem, W. R., Panaras, A. G. and Steger, J. L., "Numerical investigation of a jet in ground effect with a cross-flow", International Powered Lift Conference, P-203, Paper no. 872344, Santa Clara, Calif., February, 1988.
- [30] Childs, R. E., "Calculation of Impinging Jet Flows With Reynolds-Stress Models", 29th Aerospace Sciences Meeting, AIAA-91-0754, Reno, Nevada, January 7-10, 1991.
- [31] Corsiglia, V. R., Wardwell, D. A. and Kuhn, R. E., "Small-Scale Experiments In *STOVL* Ground Effects", International Powered Lift Conference, 29-31 August, 1990.
- [32] Huang, P. g. and Leschziner, M. A., An Introduction and Guide to the Computer code *TEAM*, University of Manchester, 1992

## Appendix A

### Calculation of jet exit conditions

The jet exit conditions are calculated using the isentropic relation and the ideal gas law. The calculation of the jet temperature, velocity, density, turbulent kinetic energy, eddy dissipation and the effective velocity ratio will be presented. The relations used in the calculations are listed as follows:

$$p_j = p_* \quad (A.1)$$

$$T_j = \frac{T_0}{pr^{1/\gamma}} \quad (A.2)$$

$$V_j = \sqrt{2c_p(T_0 - T_j)} \quad (A.3)$$

$$\rho_j = \frac{p_j}{RT_j} \quad (A.4)$$

$$k_j = (TU_j V_j)^2 \quad (A.5)$$

$$\varepsilon_j = \frac{0.15k_j^{1.5}}{0.035d} \quad (A.6)$$

$$q_j = \frac{1}{2}\rho_j V_j^2 \quad (A.7)$$

$$q_{\infty} = \frac{1}{2} \rho_{\infty} V_{\infty}^2 \quad (A.8)$$

$$v_e = \sqrt{q_j / q_{\infty}} \quad (A.9)$$

The calculations presented above are valid for the case of subsonic flow.



## Appendix B

### **Structure and Modifications of the computer code *TEAM***

The present predictions have been carried out using the computer code *TEAM*. A detailed description of the mathematical formulation and the structure of *TEAM* is given in the *TEAM* guide [32]. An outline of the structure of *TEAM* is shown in figure (B.1). The outline has been reproduced from that given by the *TEAM* guide in such a way to make it easy to understand and modify.

The available *TEAM* code is a preliminary one (*TEAM* is being under development), it has been tailored to model a specific problem, namely, impinging jets. In order to change the modeled case (by changing the initial and boundary conditions), it was necessary to modify the subroutine *USER*. The subroutine *USER* contains 14 subprograms (entries) that all had to be modified, consuming a great time and effort. The present author modified the *TEAM* code in such a way to make it easy and simple to change the boundary conditions. The structure of the modified *TEAM* code is shown in figure (B.2).

The main modification introduced to *TEAM* is that it is no more necessary to modify the *USER* subroutine. The entries of the *USER* subroutine have been changed completely, they have been re-written in such a way to call the entries of a new subroutine (*USERB*), according to the data given in a data file called the *I* file. A description of an *I* file is given in *Appendix C*. The *I* file contains only numerical and logical constants. Hence, instead of modifying the 14 entries of the *USER*

subroutine, it is only necessary to change numbers in the I file. Both the USER and USERB subroutines do not require any modifications when changing the boundary conditions, saving effort and time.

Another modification introduced to *TEAM* is the input/output and file management methods. By referring to figure (B.3), it can be seen that the subprogram *READ* reads the I file (*I.DAT*). The inputs of the I file are used by the *TEAM* code where iterations start and continue until convergence criteria is satisfied. After convergence, the subprogram *WRITE* creates five output files; *P.DAT* which contains the pressure data for all the grid points, *U.DAT* which contains the velocity data for all the grid points, *T.DAT* which contains the temperature data for all the grid points, *O.DAT* which contains the properties of the fluid, such as the density and the viscosity and *OD.DAT* which contains some information about the modeled case, such as the number of iterations and the residuals of all the variables. The file *OD.DAT* is created in a readable form, it can be read and understood by the user while the files *P.DAT*, *U.DAT*, *T.DAT* and *O.DAT*, are created to be read by the *TEAM* code. The restart capability enables the user to use previously created files as initial data for new runs as show in figure (B.3).

The files *P.DAT*, *U.DAT* and *T.DAT* can be converted to readable forms using the supplementary programs. *DRP* is a supplementary program designed to read *P.DAT* and create a readable file (*PD.DAT*) which contains  $x$ ,  $y$ ,  $p$  and  $C_p$  data in a regular sequential form, it also provides  $C_p$  plots for the points near the ground plane. *DRU* is a supplementary program designed to read *U.DAT* and create a readable file (*UD.DAT*) which contains  $x$ ,  $y$ ,  $u$  and  $v$  data in a regular sequential form, it also provides velocity vectors for the flow field. Finally, *DRT* is a supplementary program designed to read *T.DAT* and create a readable file (*TD.DAT*) which contains  $x$ ,  $y$ , and  $T$  data in a regular sequential form. The aim of creating the above readable files is not only to be understood by the user, but also

to make it possible that the available software (Graphics and Data Sheets software) import these files in order to process them and produce various plots and graphs

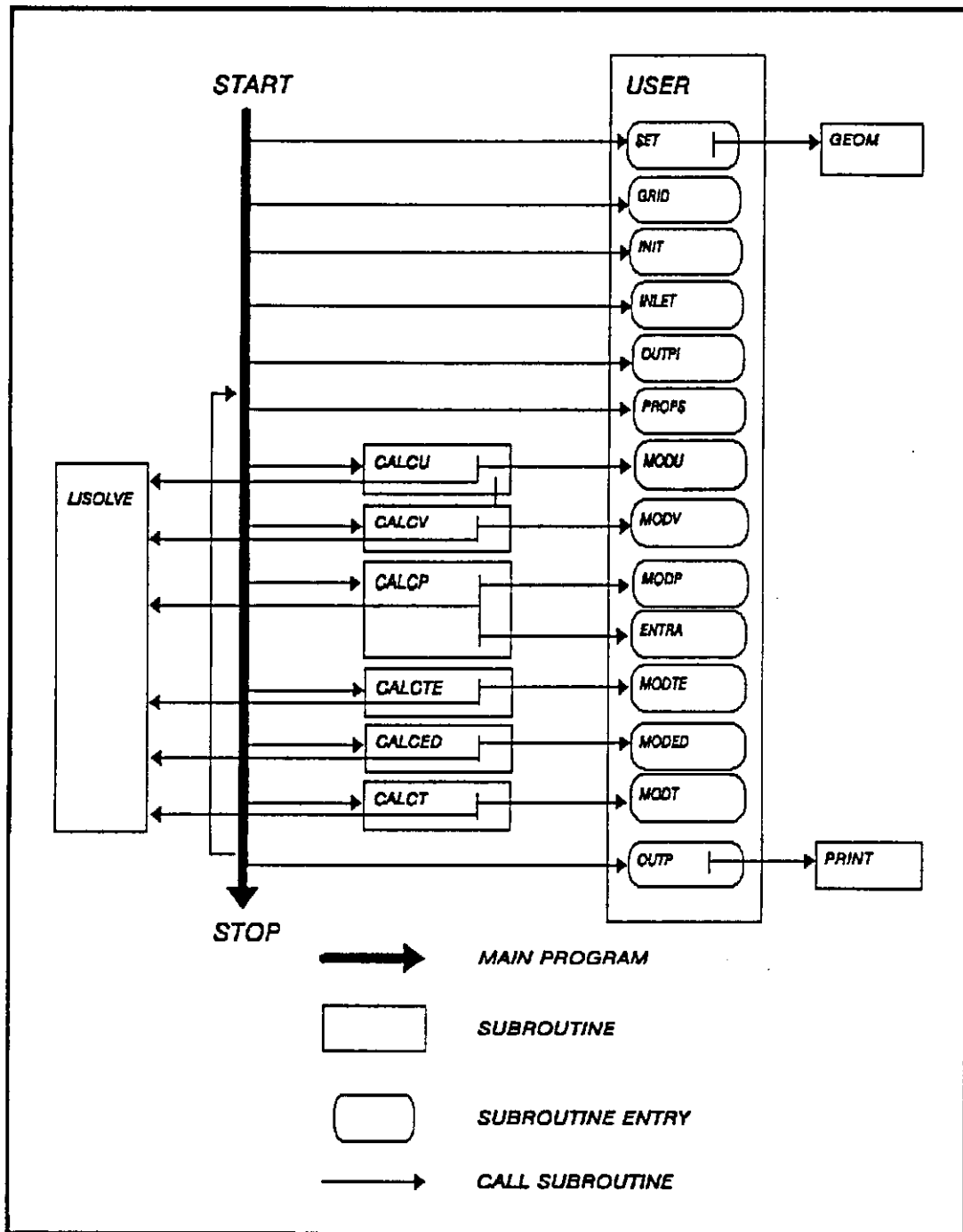


Figure B.1: Structure of the computer code *TEAM*

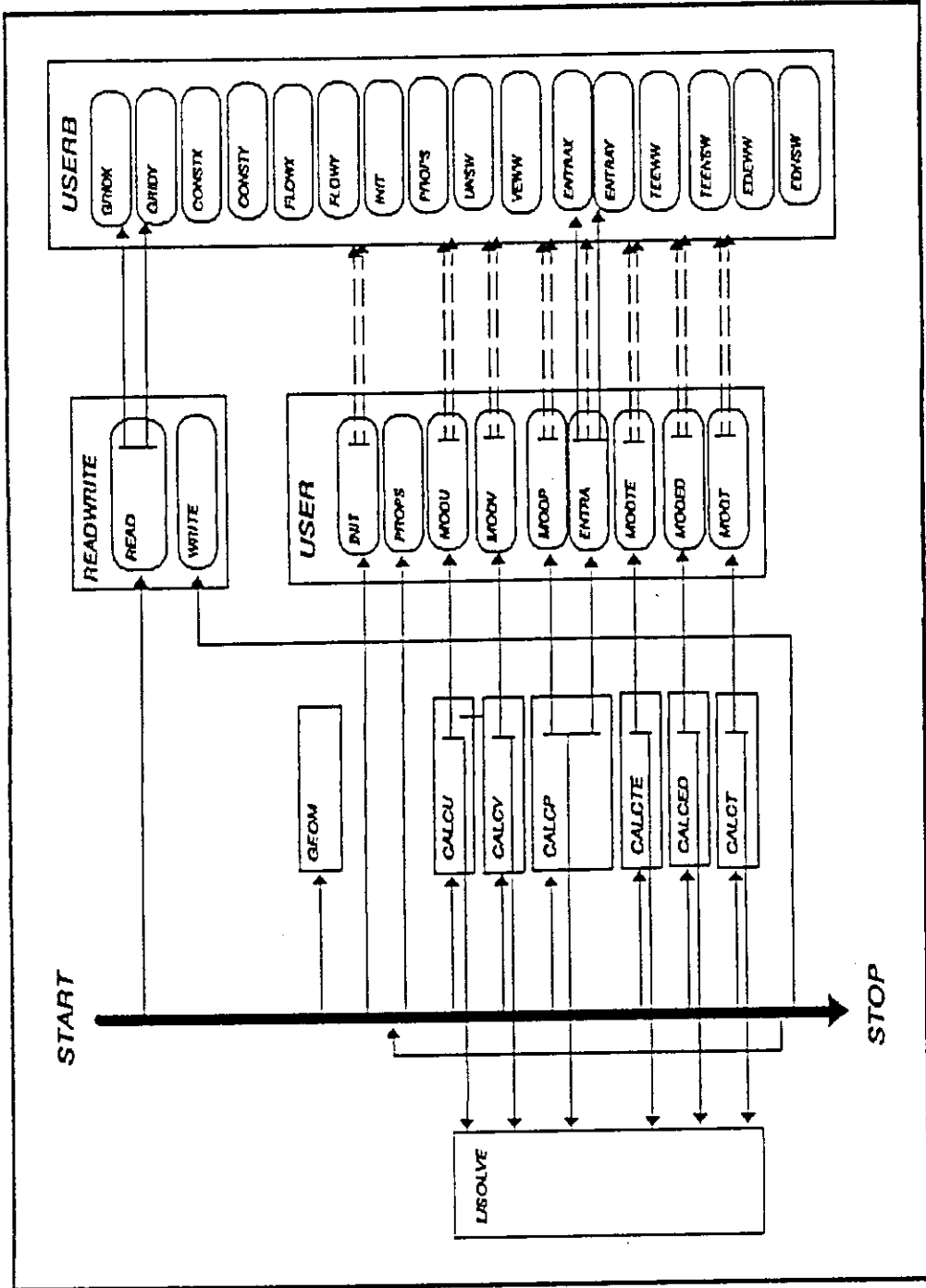


Figure B.2: Modified structure of *TEAM*

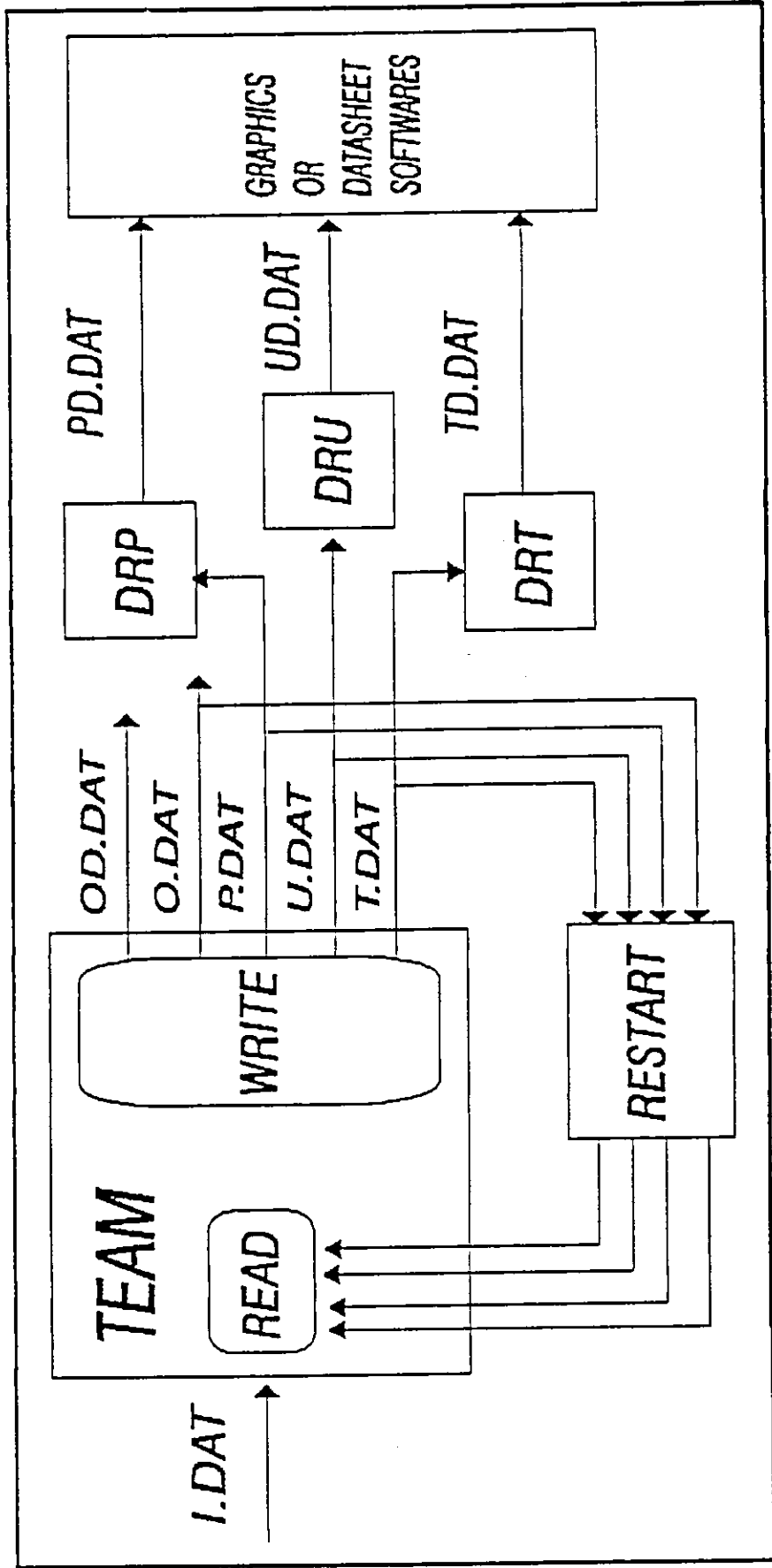


Figure B.3: File management in modified *TEAM*.

## Appendix C

### Preparing the I file

The data given in the I file (*Appendix C*) are listed in table (C.1), the table includes a description of each numerical and logical data given in the I file. Only the variables or constants that are not defined in the *TEAM* guide [32] will be discussed in the following sections.

Table (C.1): Description of the I file data (case 8).

<i>Data in I file</i>	<i>Description</i>
T,T,T	LCALKE,LCALT,LCALD
.5,.5,1,..7,1,..7,.7,.6,1.	URFU,URFV,URFP,URFK,URFGEN,URFE,URFT,URFVIS,URFDEN
1,1,2,1,1,1	NSWPU,NSWPV,NSWPP,NSWPK,NSWPE,NSWPT
.09,1.44,1.92,.4187,9.793,1,..6,-2.0	CMU,C1,C2,CAPPA,ELOG,PRTE,PRT,PFUN
2,26,3,3,0,100,1E-3,F,T, 1,0,0,1.E+30,1E-30	IPREF,JPREF,IMON,JMON,NITER,MAXIT,SORMAX,LREAD, LWRITE,NQUV,NQKE,NQT,GREAT,TINY
.000018,1.2,0,..3,.3	VISCOS,DENSIT,TEMP,TKINET,EDDYD
2,0.	IND,R(1)
33,51,.254,1.016	NIM1,NJM1,XL,YL
4	NSX
1,17,0,..2032,1.,F	I1,I2,X1,X2,RAX,FLAG

Table (C.1) (continued)

17,23,.2032,.23368,1.,F	I1,I2,X1,X2,RAX,FLAG
23,29,.23368,.24892,1.,F	I1,I2,X1,X2,RAX,FLAG
29,33,.24892,.254,1.,F	I1,I2,X1,X2,RAX,FLAG
5	NSY
1,11,0.,.03175,1.,F	J1,J2,Y1,Y2,RAY,FLAG
11,16,.03175,.0635,1.,F	J1,J2,Y1,Y2,RAY,FLAG
16,21,.0635,.127,1.,F	J1,J2,Y1,Y2,RAY,FLAG
21,46,.127,.762,1.,F	J1,J2,Y1,Y2,RAY,FLAG
46,51,.762,1.016,F	J1,J2,Y1,Y2,RAY,FLAG
2	NSS
1,11,33	IBNDS(1)....IBNDS(NSS+1)
4,4	ITYPS(1)....ITYPS(NSS)
2	NSW
1,5,51	IBNDW(1)....IBNDW(NSW+1)
1,5	ITYPW(1)....ITYPW(NSW)
1	NSN
1,33	IBNDN(1)....IBNDN(NSN+1)
1	ITYPN(1)....ITYPN(NSN)
1	NSE
1,51	IBNDE(1)....IBNDE(NSE+1)
3	ITYPE(1)....ITYPE(NSE)
253.38,0.,60.,8000.,-31.94	UINW,VINW,TEINW,EDINW
0.,-10.7,2.5,2.5,0.	UINN,VINN,TEINN,EDINN
F,0.	FIXE,TFIXE
100.,292.	PAMP,TAMP
11,10,-11	NNB,NN1,NN2



### *Flow type specification*

The are three constants used to specify the flow type namely; LCALKE, LCALT and LCALD,

if LCALKE = T then subroutines CALKE and CALED will be called (turbulent flow).

if LCALKE = F then subroutines CALKE and CALED will not be called (laminar flow).

if LCALT = T then subroutine CALT will be called (energy equation solved).

if LCALT = F then subroutine CALT will not be called (isothermal flow).

if LCALD = T then subroutine CALD will be called (compressible flow).

if LCALD = F then subroutine CALD will not be called (incompressible flow).

### *Initiallization*

The constants VISCOS, DENSIT, TEMP, TKINET and EDDYD are used as initial values of viscosity, density, temperature, turbulent kinetic energy and eddy dissipation in the flow field.

### *Grid specification*

NSX is a parameter used in generating the x-direction grid, it specifies the number of sections in the x-direction where each section has different resolution than the other sections. In the following lines, the grid points of the NSX sections are specified. For each section, the following data are to be given:

I1 and I2 which are the indices of the two end points of the section,

X1 and X2 which are the x values of the two end points,

RAX which is the expansion ratio of the grid points, the grid points are distributed between the end points in such a way that each interval length equals the proceeding interval length multiplied by RAX, i.e.  $(x_{i+1}-x_i) = RAX (x_i-x_{i-1})$ ,

and FLAG which is a logical constant, if FLAG = T, the expansion of the grid points will be done, if FLAG = F, the expansion of the grid points will be bypassed.

The same argument is applied to the  $y$ -direction where NSY, J1, J2, RAX, and FLAG in the  $y$ -direction are equivalent to NSX, I1, I2, RAX and FLAG in the  $x$ -direction.

### ***Boundary conditions specification***

NSS is a parameter used in specification of the boundary conditions, it represents the number of boundary types in the south boundary, each boundary type is associated with a section in the south boundary. Hence, we have NSS sections in the south boundary with NSS+1 end points. The indices of these NSS+1 points are specified in the next line (IBNDS(1)...IBNDS(NSS+1)). The following line specifies the types of boundaries associated with the NSS sections (ITYPS(1)...ITYPS(NSS)) where:

if ITYPS(i) = 1, then the boundary is an inlet.

if ITYPS(i) = 2, then the boundary is an exit.

if ITYPS(i) = 3, then the boundary is a wall.

if ITYPS(i) = 4, then the boundary is an axis of symmetry.

if ITYPS(i) = 5, then the boundary is an entrainment plane.

The same argument is applied to the other boundaries, namely; west, north and east boundaries.

After specifying the boundary types, more information is needed about inlets and walls. Hence, the following lines give the values of  $u$ ,  $v$ ,  $k$  and  $\epsilon$  for all the inlets in the flow field in the order that appeared when specifying the boundary types. In our case, we have two inlets, one in the west boundary and the other in the north boundary, so two lines are found in the I file giving the data of :

UINW, VINW, TEINW, EDINW and

UINN, VINN, TEINN, EDINN.

The next lines give information about the walls in the flow field in the order appeared when specifying the boundary types. In our case, we have only one wall in (east boundary), so a single line is found for the walls. The needed information are as follows; *FLXE*, which is a logical parameter that describes whether we have an adiabatic condition at the wall (*FLXE* = F) or a fixed temperature condition at the wall (*FLXE* = T). *TFLX* specifies the fixed temperature of the wall.

The next line in the I file gives the ambient pressure (*PAMB*) in and the ambient temperature (*TAMB*) in . The following line gives the parameters *NNB*, *NN1* and *NN2*, these parameters are needed when it is required to change the under-relaxation factors automatically. *NNB* represents the number of the last iterations to be considered in deciding whether the under-relaxation factor is to be increased or decreased. For example, if the *u*-velocity residual (*RESU*) decreased *NN1* times or more in the last *NNB* iterations (*u* is converging), then the *u*-velocity under-relaxation factor (*URFU*) would be increased (to speed the convergence). If *RESU* decreased *NN2* or less (increased *-NN2* times or more) in the last *NNB* iterations (*u* is diverging), then *URFU* would be decreased (to stop the divergence).

## ***Appendix D***

### ***List of Modified Subroutines and samples of Input/Output files***

The modified or added subroutines in the *TEAM* code are listed in the following pages. Also, samples of the input and output files are listed, these files correspond to case 8 (see table 4.2). The files UD.DAT and T.DAT are not listed here since they are very long. The order of the listed files are as follows:

***MAIN Program***

***READWRITE Subroutine***

***USER and USERB Subroutines***

***I.DAT File***

***OD.DAT File***

***PD.DAT File***

PARAMETER (NX=70,NY=70)

```

COMMON
+/ALL/NL,NJ,NIM1,NJM1,NIM2,NJM2,GREAT,TINY
+/GEOMX/X(NX),XU(NX),SXCV(NX),UXCV(NX),FX(NX),UCVI(NX),UCVIP(NX)
+/GEOMY/IND,Y(NY),YV(NY),SYCV(NY),VYCV(NY),FY(NY),VCVJ(NY)
+   ,VCVJP(NY),RV(NY),R(NY),RSYCV(NY),RVYCV(NY)
+/VAR1/U(NX,NY),V(NX,NY),P(NX,NY),PP(NX,NY),T(NX,NY),
+   DU(NX,NY),DV(NX,NY),DEN(NX,NY),VIS(NX,NY)
+/VAR2/DENSIT,VISCOS,PRANDL
+/UVEL/RESORU,NSWPU,URFU
+/VVEL/RESORV,NSWPV,URFV
+/PCOR/RESORM,NSWPP,URFP
+/TEMP/RESORT,NSWPT,URFT
+/HEADS/HEDU,HEDV,HEDP,HEDT,HEDK,HEDE,HEDVIS
COMMON
+/COEF/AP(NX,NY),AN(NX,NY),AS(NX,NY),AE(NX,NY),AW(NX,NY)
+   ,SU(NX,NY),SP(NX,NY)
+/COEFU/APU(NX,NY),ANU(NX,NY),ASU(NX,NY),AEU(NX,NY),AWU(NX,NY)
+   ,SUU(NX,NY),SPU(NX,NY)
+/COEFV/APV(NX,NY),ANV(NX,NY),ASV(NX,NY),AEV(NX,NY),AWV(NX,NY)
+   ,SUV(NX,NY),SPV(NX,NY)
+/OTHR1/NITER,MAXIT,URFVIS,URFDEN,IMON,JMON,IPREF,JPREF,SORMAX
+   ,FLOWIN,XMONIN,SMPW(NX)
+/TKE/TE(NX,NY),RESORK,NSWPK,URFGEN,URFK
+/TED/ED(NX,NY),RESORE,NSWPE,URFE
+/TURB1/GEN(NX,NY),CMU,C1,C2,CAPPA,ELOG,PRED,PRTE,PRT,PFUN
CHARACTER*36 HEDU,HEDV,HEDP,HEDT,HEDK,HEDE,HEDVIS

COMMON /INS/EDIN,TEIN,MOIN,TMIN

COMMON /LPAR/LCALKE,LCALT,LCALD
LOGICAL LCALKE,LCALT,LCALD
COMMON /INI/TEMP,TKINET,EDDYD
LOGICAL LREAD
LOGICAL RESLU,RESLV,RESLK,RESLE,RESLT
COMMON/RES/RESM,RESU,RESV,RESK,RESE,REST
COMMON/RESL/RESLU(15),RESLV(15),RESLK(15),RESLE(15),RESLT(15)
+ /NLESS/NLESSU,NLESSV,NLESSK,NLESSE,NLESST
+ /NMORE/NMOREU,NMOREV,NMOREK,NMOREE,NMORET
+ /RESO/RESOU,RESOV,RESOK,RESOE,RESOT
+ /NNBS/NNB,NN1,NN2,NNBO
+ /CHNGURF/CHNGURF
+/LOGIC/LREAD,LWRITE

LOGICAL CHNGURF

CALL READ

CALL INIT

IF ((.NOT.LREAD).OR.(LREAD.AND.NNB.NE.NNBO))THEN

```

NLESSU-(NNB+1)/2  
 NLESSV-(NNB+1)/2  
 NLESSK-(NNB+1)/2  
 NLESSE-(NNB+1)/2  
 NLESST-(NNB+1)/2

NMOREU-(NNB-1)/2  
 NMOREV-(NNB-1)/2  
 NMOREK-(NNB-1)/2  
 NMOREE-(NNB-1)/2  
 NMORET-(NNB-1)/2

DO 77 I=1,NNB

IF (LGT.((NNB+1)/2))THEN

RESLU(I)=.FALSE.  
 RESLV(I)=.FALSE.  
 RESLK(I)=.FALSE.  
 RESLE(I)=.FALSE.  
 RESLT(I)=.FALSE.

ELSE

RESLU(I)=.TRUE.  
 RESLV(I)=.TRUE.  
 RESLK(I)=.TRUE.  
 RESLE(I)=.TRUE.  
 RESLT(I)=.TRUE.

ENDIF

77 CONTINUE

ENDIF

C \*\*\* START ITERATION

10 NITER=NITER+1

CALL PROPS

CALL CALCU

CALL CALCV

CALL CALCP1

CALL CALCP2

IF (LCALKE)CALL CALCTE

IF (LCALKE)CALL CALCED

IF (LCALT) CALL CALCT

RESM=RESORM/FLOWIN  
 RESU=RESORU/MOIN  
 RESV=RESORV/MOIN

```

REST=RESORT/TMIN
RESE=RESORE/EDIN
RESK=RESORK/TEIN

```

```

IF(RESLU(1))THEN
NLESSU=NLESSU-1
ELSE
NMOREU=NMOREU-1
ENDIF

```

```

IF(RESLV(1))THEN
NLESSV=NLESSV-1
ELSE
NMOREV=NMOREV-1
ENDIF

```

```

IF(RESLK(1))THEN
NLESSK=NLESSK-1
ELSE
NMOREK=NMOREK-1
ENDIF

```

```

IF(RESLE(1))THEN
NLESSE=NLESSE-1
ELSE
NMOREE=NMOREE-1
ENDIF

```

```

IF(RESLT(1))THEN
NLESST=NLESST-1
ELSE
NMORET=NMORET-1
ENDIF

```

```

DO 78 I=1,NNB-1
RESLU(I)=RESLU(I+1)
RESLV(I)=RESLV(I+1)
RESLK(I)=RESLK(I+1)
RESLE(I)=RESLE(I+1)
78 RESLT(I)=RESLT(I+1)

```

```

IF (RESU.LT.RESOU)THEN
NLESSU=NLESSU+1
RESLU(NNB)=.TRUE.
ELSE
NMOREU=NMOREU+1
RESLU(NNB)=.FALSE.
ENDIF

```

```

IF (RESV.LT.RESOV)THEN
NLESSV=NLESSV+1
RESLV(NNB)=.TRUE.
ELSE
NMOREV=NMOREV+1
RESLV(NNB)=.FALSE.
ENDIF

```

***READWRITE Subroutine***



## SUBROUTINE READWRITE

LOGICAL LREAD,LWRITE,FLAG  
 LOGICAL FIXE(5),FIXW(5),FIXN(5),FIXS(5)  
 LOGICAL TFIXE(5),TFIXW(5),TFIXN(5),TFIXS(5)  
 LOGICAL CHNGKE

PARAMETER (NX=70,NY=70)

## COMMON

+ /ALL/NL,NJ,NIM1,NJM1,NIM2,NJM2,GREAT,TINY  
 + /GEOMX/X(NX),XU(NX),SXCX(NX),UXCV(NX),FX(NX),UCVI(NX),UCVIP(NX)  
 + /GEOMY/IND,Y(NY),YV(NY),SYCV(NY),VYCV(NY),FY(NY),VCVJ(NY)  
 + ,VCVJP(NY),RV(NY),R(NY),RSYCV(NY),RVYCV(NY)  
 + /VAR1/U(NX,NY),V(NX,NY),P(NX,NY),PP(NX,NY),T(NX,NY),  
 + DU(NX,NY),DV(NX,NY),DEN(NX,NY),VIS(NX,NY)  
 + /VAR2/DENSIT,VISCOS,PRANDL  
 + /UVEL/RESORU,NSWPU,URFU  
 + /VVEL/RESORV,NSWPV,URFV  
 + /PCOR/RESORM,NSWPP,URFP  
 + /TEMP/RESORT,NSWPT,URFT  
 + /QUICK/NQUICK,NQUV,NQKE,NQT,B3XS(NX),B3XU(NX),B3YS(NY),B3YV(NY)

## COMMON

+ /COEF/AP(NX,NY),AN(NX,NY),AS(NX,NY),AE(NX,NY),AW(NX,NY)  
 + ,SU(NX,NY),SP(NX,NY)  
 + /COEFU/APU(NX,NY),ANU(NX,NY),ASU(NX,NY),AEU(NX,NY),AWU(NX,NY)  
 + ,SUU(NX,NY),SPU(NX,NY)  
 + /COEFV/APV(NX,NY),ANV(NX,NY),ASV(NX,NY),AEV(NX,NY),AWV(NX,NY)  
 + ,SUV(NX,NY),SPV(NX,NY)  
 + /OTHR1/NITER,MAXIT,URFVIS,URFDEN,IMON,JMON,IPREF,JPREF,SORMAX  
 + ,FLOWIN,XMONIN,SMPW(NX)  
 + /TKE/TE(NX,NY),RESORK,NSWPK,URFGEN,URFK  
 + /TED/ED(NX,NY),RESORE,NSWPE,URFE  
 + /TURB1/GEN(NX,NY),CMU,C1,C2,CAPPA,ELOG,PRED,PRTE,PRT,PFUN

## COMMON

+ /L/XL,YL  
 + /XPTAU/XPLUSE(NY),XPLUSW(NY),YPLUSN(NX),YPLUSS(NX)  
 + ,TAUE(NY),TAUW(NY),TAUN(NX),TAUS(NX)  
 + /TURB3/CMU25,CMU75  
 + /LOGIC/LREAD,LWRITE  
 + /BND/NSS,NSW,NSN,NSE,  
 + ITYPS(5),ITYPW(5),ITYPN(5),ITYPE(5),  
 + IBNDS(6),IBNDW(6),IBNDN(6),IBNDE(6),  
 + FXKS,FXKW,FXN,FXE,TFXKS,TFXKW,TFIXN,TFIXE,  
 + UINS(5),UINW(5),UINN(5),UINE(5),  
 + VINS(5),VINW(5),VINN(5),VINE(5),  
 + TEINS(5),TEINW(5),TEINN(5),TEINE(5),  
 + EDINS(5),EDINW(5),EDINN(5),EDINE(5),  
 + TINS(5),TINW(5),TINN(5),TINE(5)  
 + /INS/EDIN,TEIN,MOIN,TMIN  
 + /FLOWJ/FLOWJ  
 + /CHNGKE/CHNGKE  
 + /AMBIENT/PAMB,TAMB

COMMON /LPAR/LCALKE,LCALT,LCALD  
 LOGICAL LCALKE,LCALT,LCALD  
 COMMON /INI/TEMP,TKINET,EDDYD

```

LOGICAL RESLU,RESLV,RESLK,RESLE,RESLT
COMMON/RES/RESM,RESU,RESV,RESK,RESE,REST
COMMON/RESL/RESLU(15),RESLV(15),RESLK(15),RESLE(15),RESLT(15)
+ /NLESS/NLESSU,NLESSV,NLESSK,NLESSE,NLESST
+ /NMORE/NMOREU,NMOREV,NMOREK,NMOREE,NMORET
+ /RESO/RESOU,RESOV,RESOK,RESOE,RESOT
+ /NNBS/NNB,NN1,NN2,NNBO
+ /CHNGURF/CHNGURF

```

```
LOGICAL CHNGURF
```

```
CHARACTER*15 INP,OUT,OUTUV,OUTPP,OUTT,FILES,FLN
```

```
ENTRY READ
```

```
PRINT*,FILES'
```

```
READ*,FILES
```

```

OPEN(UNIT=7,FILE=FILES,STATUS='OLD')
  READ(7,*)INP
OPEN(UNIT=1,FILE=INP,STATUS='OLD')
  READ(7,*)OUT
OPEN(UNIT=2,FILE=OUT,STATUS='OLD')
  READ(7,*)OUTUV
OPEN(UNIT=3,FILE=OUTUV,STATUS='OLD')
  READ(7,*)OUTPP
OPEN(UNIT=4,FILE=OUTPP,STATUS='OLD')
  READ(7,*)OUTT
OPEN(UNIT=5,FILE=OUTT,STATUS='OLD')
  READ(7,*)FLN
  READ(7,*)FLN
  READ(7,*)FLN
  READ(7,*)FLN
  READ(7,*)FLN
  READ(7,*)FLN
  READ(7,*)FLN
OPEN(UNIT=6,FILE=FLN,STATUS='NEW')

```

```
READ(1,*)LCALKE,LCALT,LCALD
```

```
PRINT*,READ'
```

```
READ(1,*)URFU,URFV,URFP,URFK,URFGEN,URFE,URFT,URFVIS,URFDEN
```

```
READ(1,*)NSWPU,NSWPFV,NSWPP,NSWPK,NSWPE,NSWPT
```

```
READ(1,*)CMU,C1,C2,CAPPA,ELOG,PRTE,PRT,PFUN
```

```

+ READ(1,*)IPREF,JPREF,IMON,JMON,NITER,MAXIT,SORMAX,
  LREAD,LWRITE,NQUV,NQKE,NQT,GREAT,TINY

```

```
READ(1,*) VISCOS,DENSIT,TEMP,TKINET,EDDYD
```

```
PRINT*,ENTER MAXIT, SORMAX
```

```
READ*,MAXIT,SORMAX
```

```
PRINT*,ENTER LREAD
```

```

READ*,LREAD
PRINT*,CHANGE URF7
READ*,CHNGURF

IF (LREAD) THEN
  READ(3,*)U,V,MOIN
  READ(4,*)P
  READ(5,*)T,TMIN
  READ(2,*)NITER,FLOWIN,FLOWJ,TE,TEIN,ED,EDIN,VIS,DEN
+ ,XPLUSE,XPLUSW,YPLUSN,YPLUSS,TAUE,TAUW,TAUN,TAUS
  MAXIT=MAXIT+NITER
  READ(2,*)URFU,URFV,URFK,URFE,URFT
  READ(2,*)RESLU,RESLV,RESLK,RESLE,RESLT
  READ(2,*)RESOU,RESOV,RESOK,RESOE,RESOT
  READ(2,*)NLESSU,NLESSV,NLESSK,NLESSE,NLESST
  READ(2,*)NMOREU,NMOREV,NMOREK,NMOREE,NMORET
  READ(2,*)NNBO
ENDIF

  READ(1,*)IND,R(1)
  READ(1,*)NIM1,NJMI,XL,YL

  READ(1,*)NSX
  DO 10 I=1,NSX
  READ(1,*)I1,I2,X1,X2,RAX,FLAG
10  CALL GRIDX(I1,I2,X1,X2,RAX,FLAG)

  READ(1,*)NSY
  DO 11 J=1,NSY
  READ(1,*)J1,J2,Y1,Y2,RAY,FLAG
11  CALL GRIDY(J1,J2,Y1,Y2,RAY,FLAG)

  READ(1,*)NSS
  READ(1,*)(IBNDS(I),I=1,NSS+1)
  READ(1,*)(ITYPS(I),I=1,NSS)
  READ(1,*)NSW
  READ(1,*)(IBNDW(I),I=1,NSW+1)
  READ(1,*)(ITYPW(I),I=1,NSW)
  READ(1,*)NSN
  READ(1,*)(IBNDN(I),I=1,NSN+1)
  READ(1,*)(ITYPN(I),I=1,NSN)
  READ(1,*)NSE
  READ(1,*)(IBNDE(I),I=1,NSE+1)
  READ(1,*)(ITYPE(I),I=1,NSE)

  DO 33 I=1,NSS
  IF(ITYPS(I).EQ.1)READ(1,*)UINS(I),VINS(I),TEINS(I),EDINS(I)
+ ,TINS(I)
  IF(ITYPS(I).EQ.3)READ(1,*)FIXS(I),TFIXS(I)
33  CONTINUE

  DO 34 I=1,NSW
  IF(ITYPW(I).EQ.1)READ(1,*)UINW(I),VINW(I),TEINW(I),EDINW(I)
+ ,TINW(I)
  IF(ITYPW(I).EQ.3)READ(1,*)FIXW(I),TFIXW(I)
34  CONTINUE

```

```

DO 35 I=1,NSN
IF(ITYPN(I).EQ.1)READ(1,*)UINN(I),VINN(I),TEINN(I),EDINN(I)
+,TINN(I)
IF(ITYPN(I).EQ.3)READ(1,*)FLXN(I),TFLXN(I)
35 CONTINUE

```

```

DO 36 I=1,NSE
IF(ITYPE(I).EQ.1)READ(1,*)UINE(I),VINE(I),TEINE(I),EDINE(I)
+,TINE(I)
IF(ITYPE(I).EQ.3)READ(1,*)FLXE(I),TFXE(I)
36 CONTINUE

```

```

C   READ(1,*)PAMB,TAMB
    PRINT*,PAMB,TAMB,PAMB,TAMB
    READ(1,*)NNB,NN1,NN2
    READ(1,*)CHNGKE

```

```

RETURN

```

```

ENTRY WRITE

```

```

REWIND 3
REWIND 4
REWIND 2
REWIND 5

```

```

WRITE(3,*)U,V,MOIN,NL,NJ,X,Y
WRITE(4,*)P,IPREF,JPREF,PAMB,NL,NJ,X,Y
WRITE(5,*)I,TMIN,IPREF,JPREF,TAMB,NL,NJ,X,Y
WRITE(2,*)NITER,FLOWIN,FLOWJ,TE,TEIN,ED,EDIN,VIS,DEN
+ ,XPLUSE,XPLUSW,YPLUSN,YPLUSS,TAUE,TAUW,TAUN,TAUS
WRITE(2,*)URFU,URFV,URFK,URFE,URFT
WRITE(2,*)RESLU,RESLV,RESLK,RESLE,RESLT
WRITE(2,*)RESOU,RESOV,RESOK,RESOE,RESOT
WRITE(2,*)NLESSU,NLESSV,NLESSK,NLESSE,NLESST
WRITE(2,*)NMOREU,NMOREV,NMOREK,NMOREE,NMORET
WRITE(2,*)NNB

```

```

WRITE(6,*)NITER,NITER,RESM-,RESM
WRITE(6,*)RESU-,RESU,URFU-,URFU,NLESSU-NMOREU-,NLESSU-NMOREU
WRITE(6,*)RESV-,RESV,URFV-,URFV,NLESSV-NMOREV-,NLESSV-NMOREV
WRITE(6,*)RESK-,RESK,URFK-,URFK,NLESSK-NMOREK-,NLESSK-NMOREK
WRITE(6,*)RESE-,RESE,URFE-,URFE,NLESSE-NMOREE-,NLESSE-NMOREE
WRITE(6,*)REST-,REST,URFT-,URFT,NLESST-NMORET-,NLESST-NMORET

```

```

RETURN

```

```

END

```

***USER and USERB Subroutines***

## SUBROUTINE USER

PARAMETER (NX=70,NY=70)

LOGICAL INLT

LOGICAL LREAD,LWRITE

LOGICAL FLAG

LOGICAL FIXE(5),FIXW(5),FIXN(5),FIXS(5)

LOGICAL TFIXE(5),TFIXW(5),TFIXN(5),TFIXS(5)

LOGICAL CHNGKE

COMMON

```

+/ALL/NL,NJ,NIM1,NJM1,NIM2,NJM2,GREAT,TINY
+/GEOMX/X(NX),XU(NX),SXCV(NX),UXCV(NX),FX(NX),UCVI(NX),UCVIP(NX)
+/GEOMY/IND,Y(NY),YV(NY),SYCV(NY),VYCV(NY),FY(NY),VCVJ(NY)
+ ,VCVJP(NY),RV(NY),R(NY),RSYCV(NY),RVYCV(NY)
+/VAR1/U(NX,NY),V(NX,NY),P(NX,NY),PP(NX,NY),T(NX,NY),
+ DU(NX,NY),DV(NX,NY),DEN(NX,NY),VIS(NX,NY)
+/VAR2/DENSIT,VISCOS,PRANDL
+/UVEL/RESORU,NSWPU,URFU
+/VVEL/RESORV,NSWPV,URFV
+/PCOR/RESORM,NSWPP,URFP
+/TEMP/RESORT,NSWPT,URFT
+/HEADS/HEDU,HEDV,HEDP,HEDT,HEDK,HEDE,HEDVIS
COMMON
+/COEF/AP(NX,NY),AN(NX,NY),AS(NX,NY),AE(NX,NY),AW(NX,NY)
+ ,SU(NX,NY),SP(NX,NY)
+/COEFU/APU(NX,NY),ANU(NX,NY),ASU(NX,NY),AEU(NX,NY),AWU(NX,NY)
+ ,SUU(NX,NY),SPU(NX,NY)
+/COEFV/APV(NX,NY),ANV(NX,NY),ASV(NX,NY),AEV(NX,NY),AWV(NX,NY)
+ ,SUV(NX,NY),SPV(NX,NY)
+/OTHR1/NITER,MAXIT,URFVIS,URFDEN,IMON,JMON,IPREF,JPREF,SORMAX
+ ,FLOWIN,XMONIN,SMPW(NX)
+/TKE/TE(NX,NY),RESORK,NSWPK,URFGEN,URFK
+/TED/ED(NX,NY),RESORE,NSWPE,URFE
+/TURB1/GEN(NX,NY),CMU,C1,C2,CAPPA,ELOG,PRED,PRTE,PRT,PFUN
+/TURB2/TKEIN,TEDIN
+/QUICK/NQUICK,NQUV,NQKE,NQT,B3XS(NX),B3XU(NX),B3YS(NY),B3YV(NY)

```

COMMON

```

+/L/XL,YL
+/XPTAU/XPLUSE(NY),XPLUSW(NY),YPLUSN(NX),YPLUSS(NX)
+ ,TAUE(NY),TAUW(NY),TAUN(NX),TAUS(NX)
+/TURB3/CMU25,CMU75
+/BND/NSS,NSW,NSN,NSE,
+ITYPS(5),ITYPW(5),ITYPN(5),ITYPE(5),
+IBNDS(6),IBNDW(6),IBNDN(6),IBNDE(6),
+FIXS,FIXW,FIXN,FIKE,TFIXS,TFIXW,TFIXN,TFIXE,
+UINS(5),UINW(5),UINN(5),UINE(5),
+VINS(5),VINW(5),VINN(5),VINE(5),
+TEINS(5),TEINW(5),TEINN(5),TEINE(5),
+EDINS(5),EDINW(5),EDINN(5),EDINE(5),
+TINS(5),TINW(5),TINN(5),TINE(5)
+/LOGIC/LREAD,LWRITE
+/INS/EDIN,TEIN,MOIN,TMIN
+/FLOWJ/FLOWJ,RATIO
+/CHNGKE/CHNGKE

```

+/AMBIENT/PAMB,TAMB

COMMON /LPAR/LCALKE,LCALT,LCALD  
 LOGICAL LCALKE,LCALT,LCALD  
 COMMON /INI/TEMP,TKINET,EDDYD

ENTRY INIT

PRED=CAPPA\*\*2/(C2-C1)/SQRT(CMU)  
 CMU25=CMU\*\*0.25  
 CMU75=CMU\*\*0.75

DO 951 I=1,N1  
 DO 951 J=1,NJ  
 DU(L,J)=0.0  
 DV(L,J)=0.0  
 SU(L,J)=0.0  
 SP(L,J)=0.0  
 GEN(L,J)=0.0  
 AE(L,J)=0.0  
 AW(L,J)=0.0  
 AN(L,J)=0.0  
 AEU(L,J)=0.  
 AWU(L,J)=0.  
 ANU(L,J)=0.  
 ASU(L,J)=0.  
 SUU(L,J)=0.  
 SPU(L,J)=0.  
 AEV(L,J)=0.  
 AWV(L,J)=0.  
 ANV(L,J)=0.  
 ASV(L,J)=0.  
 SUV(L,J)=0.  
 SPV(L,J)=0.  
 AS(L,J)=0.0  
 SMPW(J)=0.0  
 951 CONTINUE

IF(LREAD) RETURN

FLOWIN=0.0  
 MOIN=0.0  
 TMIN=0.0  
 EDIN=0.0  
 TEIN=0.0

DO 950 J=1,NJ

CALL CONSTX(1,NL,J,TE,TKINET)  
 CALL CONSTX(1,NL,J,ED,EDDYD)  
 CALL CONSTX(1,NL,J,T,TEMP)  
 CALL CONSTX(1,NIM1,J,U,0.0)  
 IF(J.NE.NJ) CALL CONSTX(1,NL,J,V,0.0)  
 CALL CONSTX(1,NL,J,DEN,DENSIT)  
 CALL CONSTX(1,NL,J,VIS,VISCOS)

```

      CALL CONSTX(1,NL,J,P,0.0)
      CALL CONSTX(1,NL,J,PP,0.0)

950  CONTINUE

      IF (LCALKE) THEN

      DO 851 I=1,NL
      DO 851 J=1,NJ
851  VIS(L,J)=CMU*DEN(L,J)*TE(L,J)**2/(ED(L,J)+TINY)+VISCOS

      DO 302 J=1,NJ
      TAUE(J)=0.0
      TAUW(J)=0.0
      XPLUSW(J)=40.
302  XPLUSE(J)=40.

      DO 1302 I=1,NL
      TAUN(I)=0.0
      TAUS(I)=0.0
      YPLUSN(I)=40.
1302 YPLUSS(I)=40.

      ENDIF

      DO 15 I=1,NSS

      IF (ITYPS(I).EQ.1) THEN
      CALL CONSTX(IBNDS(I)+1,IBNDS(I+1)-1,1,U,UINS(I))
      CALL CONSTX(IBNDS(I)+1,IBNDS(I+1),1,V,VINS(I))
      CALL CONSTX(IBNDS(I)+1,IBNDS(I+1),1,TE,TEINS(I))
      CALL CONSTX(IBNDS(I)+1,IBNDS(I+1),1,ED,EDINS(I))
      CALL CONSTX(IBNDS(I)+1,IBNDS(I+1),1,T,TINS(I))
      CALL FLOWX(IBNDS(I)+1,IBNDS(I+1),FLOW,AREADENT,,FALSE.)
      FLOWIN=FLOWIN+FLOW
      EDIN=EDIN+ABS(FLOW*EDINS(I))
      TEIN=TEIN+ABS(FLOW*TEINS(I))
      UV=SQRT(UINS(I)**2+VINS(I)**2)
      MOIN=MOIN+ABS(FLOW*UV)
      TMIN=TMIN+ABS(FLOW*TINS(I))
      ENDIF

      IF (ITYPS(I).EQ.3) THEN
      CALL CONSTX(IBNDS(I),IBNDS(I+1),1,U,0.0)
      CALL CONSTX(IBNDS(I)+1,IBNDS(I+1),1,V,0.0)
      CALL CONSTX(IBNDS(I)+1,IBNDS(I+1),1,TE,0.0)
      CALL CONSTX(IBNDS(I)+1,IBNDS(I+1),1,ED,0.0)
      IF (FIXS(I)) CALL CONSTX(IBNDS(I)+1,IBNDS(I+1),1,T,TFIXS(I))
      ENDIF

15  CONTINUE

      DO 17 I=1,NSW

      IF (ITYPW(I).EQ.1) THEN

```



```

CALL CONSTY(IBNDW(I)+1,IBNDW(I+1)-1,1,V,VINW(I))
CALL CONSTY(IBNDW(I)+1,IBNDW(I+1),1,U,UIW(I))
CALL CONSTY(IBNDW(I)+1,IBNDW(I+1),1,TE,TEINW(I))
CALL CONSTY(IBNDW(I)+1,IBNDW(I+1),1,ED,EDINW(I))
CALL CONSTY(IBNDW(I)+1,IBNDW(I+1),1,T,TINW(I))
CALL FLOWY(IBNDW(I)+1,IBNDW(I+1),FLOW,AREADENT,,FALSE.)

```

C ONLY FOR INLET CASE

```
FLOWJ=FLOW
```

C ONLY FOR INLET CASE

```

FLOWIN=FLOWIN+FLOW
EDIN=EDIN+ABS(FLOW*EDINW(I))
TEIN=TEIN+ABS(FLOW*TEINW(I))
UV=SQRT(UIW(I)**2+VINW(I)**2)
MOIN=MOIN+ABS(FLOW*UV)
TMIN=TMIN+ABS(FLOW*TINW(I))
ENDIF

```

```
IF (ITYPW(I).EQ.3) THEN
```

```

CALL CONSTY(IBNDW(I),IBNDW(I+1),1,V,0.0)
CALL CONSTY(IBNDW(I)+1,IBNDW(I+1),1,U,0.0)
CALL CONSTY(IBNDW(I)+1,IBNDW(I+1),1,TE,0.0)
CALL CONSTY(IBNDW(I)+1,IBNDW(I+1),1,ED,0.0)
IF(FIXW(I)) CALL CONSTY(IBNDW(I)+1,IBNDW(I+1),1,T,TFIXW(I))
ENDIF

```

17 CONTINUE

```
DO 16 I=1,NSN
```

```
IF (ITYPN(I).EQ.1) THEN
```

```

CALL CONSTX(IBNDN(I)+1,IBNDN(I+1)-1,NJ,U,UIIN(I))
CALL CONSTX(IBNDN(I)+1,IBNDN(I+1),NJM1,V,VINN(I))
CALL CONSTX(IBNDN(I)+1,IBNDN(I+1),NJ,TE,TEINN(I))
CALL CONSTX(IBNDN(I)+1,IBNDN(I+1),NJ,ED,EDINN(I))
CALL CONSTX(IBNDN(I)+1,IBNDN(I+1),NJ,T,TINN(I))
CALL FLOWX(IBNDN(I)+1,IBNDN(I+1),FLOW,AREADENT,,TRUE.)
FLOWIN=FLOWIN-FLOW
EDIN=EDIN+ABS(FLOW*EDINN(I))
TEIN=TEIN+ABS(FLOW*TEINN(I))
UV=SQRT(UIIN(I)**2+VINN(I)**2)
MOIN=MOIN+ABS(FLOW*UV)
TMIN=TMIN+ABS(FLOW*TINN(I))
ENDIF

```

```
IF (ITYPN(I).EQ.3) THEN
```

```

CALL CONSTX(IBNDN(I),IBNDN(I+1),NJ,U,0.0)
CALL CONSTX(IBNDN(I)+1,IBNDN(I+1),NJM1,V,0.0)
CALL CONSTX(IBNDN(I)+1,IBNDN(I+1),NJ,TE,0.0)
CALL CONSTX(IBNDN(I)+1,IBNDN(I+1),NJ,ED,0.0)
IF(FIXN(I)) CALL CONSTX(IBNDN(I)+1,IBNDN(I+1),NJ,T,TFIXN(I))
ENDIF

```

16 CONTINUE

```
DO 18 I=1,NSE
```

```

IF (ITYPE(I).EQ.1) THEN
CALL CONSTY(IBNDE(I)+1,IBNDE(I+1)-1,NL,V,VINE(I))
CALL CONSTY(IBNDE(I)+1,IBNDE(I+1),NIM1,U,UTNE(I))
CALL CONSTY(IBNDE(I)+1,IBNDE(I+1),NL,TE,TEINE(I))
CALL CONSTY(IBNDE(I)+1,IBNDE(I+1),NL,ED,EDINE(I))
CALL CONSTY(IBNDE(I)+1,IBNDE(I+1),NL,T,TINE(I))
CALL FLOWY(IBNDE(I)+1,IBNDE(I+1),FLOW,AREADENT,TRUE.)
FLOWIN=FLOWIN-FLOW
EDIN=EDIN+ABS(FLOW*EDINE(I))
TEIN=TEIN+ABS(FLOW*TEINE(I))
UV=SQRT(UTNE(I)**2+VINE(I)**2)
MOIN=MOIN+ABS(FLOW*UV)
TMIN=TMIN+ABS(FLOW*TINE(I))
ENDIF

IF (ITYPE(I).EQ.3) THEN
CALL CONSTY(IBNDE(I),IBNDE(I+1),NL,V,0.0)
CALL CONSTY(IBNDE(I)+1,IBNDE(I+1),NIM1,U,0.0)
CALL CONSTY(IBNDE(I)+1,IBNDE(I+1),NL,TE,0.0)
CALL CONSTY(IBNDE(I)+1,IBNDE(I+1),NL,ED,0.0)
IF(FIXE(I)) CALL CONSTY(IBNDE(I)+1,IBNDE(I+1),NL,T,TFIXE(I))

ENDIF

18 CONTINUE

RETURN

ENTRY PROPS

PREF=P(IPREF,JPREF)
TREF=T(IPREF,JPREF)

DO 900 I=1,NI
DO 900 J=1,NJ

IF(LCALD) THEN

PREAL=P(L,J)+(PAMB*1000.-PREF)
TREAL=T(L,J)+(TAMB-TREF)
DENNEW=(PREAL/1000.)/(.287*TREAL)
DEN(L,J)=DEN(L,J)+URFDEN*(DENNEW-DEN(L,J))
ENDIF

IF(LCALKE) THEN
VISNEW=DEN(L,J)*TE(L,J)**2*CMU/(ABS(ED(L,J))+TINY)+VISCOS
VIS(L,J)=VIS(L,J)+URFVIS*(VISNEW-VIS(L,J))
ENDIF

900 CONTINUE

RETURN

ENTRY MODU

```

```

DO 30 I=1,NSS
  IF (ITYPS(I).EQ.4.OR.ITYPS(I).EQ.5)
+ CALL SYMX(IBNDS(I)+1,IBNDS(I+1)-1,U,ASU,.FALSE.,1)
  IF (ITYPS(I).EQ.2)
+ CALL CONSTX(IBNDS(I)+1,IBNDS(I+1)-1,1,U,0.0)
  IF (ITYPS(I).EQ.3)
+ CALL UNSW(IBNDS(I)+1,IBNDS(I+1)-1,.FALSE.)
30 CONTINUE

```

```

DO 31 I=1,NSN
  IF (ITYPN(I).EQ.4.OR.ITYPN(I).EQ.5)
+ CALL SYMX(IBNDN(I)+1,IBNDN(I+1)-1,U,ANU,.TRUE.,NJ)
  IF (ITYPN(I).EQ.2)
+ CALL CONSTX(IBNDN(I)+1,IBNDN(I+1)-1,NJ,U,0.0)
  IF (ITYPN(I).EQ.3)
+ CALL UNSW(IBNDN(I)+1,IBNDN(I+1)-1,.TRUE.)
31 CONTINUE

```

```

DO 32 I=1,NSW
  IF (ITYPW(I).EQ.4)
+ CALL CONSTY(IBNDW(I)+1,IBNDW(I+1),1,U,0.0)
32 CONTINUE

```

```

DO 34 I=1,NSE
  IF (ITYPE(I).EQ.4)
+ CALL CONSTY(IBNDE(I)+1,IBNDE(I+1),NIM1,U,0.0)
34 CONTINUE

```

C ONLY FOR NOZZLE CASE

```

CALL CONSTX(IBNDS(1)+1,IBNDS(2),IBNDW(2)+1,SUU,0.0)
CALL CONSTX(IBNDS(1)+1,IBNDS(2),IBNDW(2)+1,SPU,-GREAT)

CALL CONSTY(IBNDW(1)+1,IBNDW(2),IBNDS(2),SUU,UIW(1)*GREAT)
CALL CONSTY(IBNDW(1)+1,IBNDW(2),IBNDS(2),SPU,-GREAT)

CALL UNSW(IBNDS(1)+1,IBNDS(2)-1,.FALSE.)

```

C ONLY FOR NOZZLE CASE

C VERTEX NODES

C SOUTH WEST NODE

```

IF (ITYPS(1).EQ.3.OR.ITYPW(1).EQ.3.OR.ITYPW(1).EQ.4) THEN
  U(1,1)=0.0
ELSEIF (ITYPS(1).EQ.4.OR.ITYPS(1).EQ.5) THEN
  U(1,1)=U(1,2)
ENDIF

```

C SOUTH EAST

```

IF (ITYPS(NSS).EQ.3.OR.ITYPE(1).EQ.3.OR.ITYPE(1).EQ.4) THEN
  U(NIM1,1)=0.0
ELSEIF (ITYPS(NSS).EQ.4.OR.ITYPS(NSS).EQ.5) THEN
  U(NIM1,1)=U(NIM1,2)
ENDIF

```

## C NORTH EAST

```

IF (ITYPN(NSN).EQ.3.OR.ITYPE(NSE).EQ.3.OR.ITYPE(NSE).EQ.4) THEN
  U(NIM1,NJ)=0.0
ELSEIF (ITYPN(NSN).EQ.4.OR.ITYPN(NSN).EQ.5) THEN
  U(NIM1,NJ)=U(NIM1,NJM1)
ENDIF

```

## C NORTH WEST

```

IF (ITYPN(1).EQ.3.OR.ITYPW(NSW).EQ.3.OR.ITYPW(NSW).EQ.4) THEN
  U(1,NJ)=0.0
ELSEIF (ITYPN(1).EQ.4.OR.ITYPN(1).EQ.5) THEN
  U(1,NJ)=U(1,NJM1)
ENDIF

```

RETURN

## ENTRY MODV

```

DO 36 I=1,NSW
  IF (ITYPW(I).EQ.4.OR.ITYPW(I).EQ.5)
+ CALL SYMY(IBNDW(I)+1,IBNDW(I+1)-1,V,AWV,FALSE,1)
  IF (ITYPW(I).EQ.2)
+ CALL CONSTY(IBNDW(I)+1,IBNDW(I+1)-1,1,V,0.0)
  IF (ITYPW(I).EQ.3)
+ CALL VEWW(IBNDW(I)+1,IBNDW(I+1)-1,FALSE.)
36 CONTINUE

```

```

DO 37 I=1,NSE
  IF (ITYPE(I).EQ.4.OR.ITYPE(I).EQ.5)
+ CALL SYMY(IBNDE(I)+1,IBNDE(I+1)-1,V,AEV,TRUE,NI)
  IF (ITYPE(I).EQ.2)
+ CALL CONSTY(IBNDE(I)+1,IBNDE(I+1)-1,NI,V,0.0)
  IF (ITYPE(I).EQ.3)
+ CALL VEWW(IBNDE(I)+1,IBNDE(I+1)-1,TRUE.)
37 CONTINUE

```

```

DO 38 I=1,NSS
  IF (ITYPS(I).EQ.4)
+ CALL CONSTX(IBNDS(I)+1,IBNDS(I+1),1,V,0.0)
38 CONTINUE

```

```

DO 40 I=1,NSN
  IF (ITYPN(I).EQ.4)
+ CALL CONSTX(IBNDN(I)+1,IBNDN(I+1),NJM1,V,0.0)
40 CONTINUE

```

## C ONLY FOR NOZZLE CASE

```

CALL CONSTX(IBNDS(1)+1,IBNDS(2),IBNDW(2),SUV,0.0)

```

```

CALL CONSTX(IBNDS(1)+1,IBNDS(2),IBNDW(2),SPV,-GREAT)

CALL CONSTY(IBNDW(1)+1,IBNDW(2)-1,IBNDS(2),SUV,VINW(1)*GREAT)
CALL CONSTY(IBNDW(1)+1,IBNDW(2)-1,IBNDS(2),SPV,-GREAT)

C ONLY FOR NOZZLE CASE

C VERTX NODES

C SOUTH WEST NODE

IF (ITYPS(1).EQ.3.OR.ITYPW(1).EQ.3.OR.ITYPS(1).EQ.4) THEN
  V(1,1)=0.0
ELSEIF (ITYPW(1).EQ.4.OR.ITYPW(1).EQ.5) THEN
  V(1,1)=V(2,1)
ENDIF

C SOUTH EAST

IF (ITYPS(NSS).EQ.3.OR.ITYPE(1).EQ.3.OR.ITYPS(NSS).EQ.4) THEN
  V(NI,1)=0.0
ELSEIF (ITYPE(1).EQ.4.OR.ITYPE(1).EQ.5) THEN
  V(NI,1)=V(NIM1,1)
ENDIF

C NORTH EAST

IF (ITYPN(NSN).EQ.3.OR.ITYPE(NSE).EQ.3.OR.ITYPN(NSN).EQ.4) THEN
  V(NI,NJM1)=0.0
ELSEIF (ITYPE(NSE).EQ.4.OR.ITYPE(NSE).EQ.5) THEN
  V(NI,NJM1)=V(NIM1,NJM1)
ENDIF

C NORTH WEST

IF (ITYPN(1).EQ.3.OR.ITYPW(NSW).EQ.3.OR.ITYPN(1).EQ.4) THEN
  V(1,NJM1)=0.0
ELSEIF (ITYPW(NSW).EQ.4.OR.ITYPW(NSW).EQ.5) THEN
  V(1,NJM1)=V(2,NJM1)
ENDIF

RETURN

ENTRY MODF

DO 42 I=1,NSS
  IF (ITYPS(I).EQ.5.OR.ITYPS(I).EQ.2) THEN
    CALL CONSTX(IBNDS(I)+1,IBNDS(I+1),2,SU,0.0)
    CALL CONSTX(IBNDS(I)+1,IBNDS(I+1),2,SP,-GREAT)
  ENDIF
42 CONTINUE

DO 43 I=1,NSN
  IF (ITYPN(I).EQ.5.OR.ITYPN(I).EQ.2) THEN
    CALL CONSTX(IBNDN(I)+1,IBNDN(I+1),NJM1,SU,0.0)
    CALL CONSTX(IBNDN(I)+1,IBNDN(I+1),NJM1,SP,-GREAT)
  ENDIF
43 CONTINUE

```

```

      ENDIF
43  CONTINUE

      DO 44 I=1,NSW
      IF (ITYPW(I).EQ.5.OR.ITYPW(I).EQ.1) THEN
      CALL CONSTY(IBNDW(I)+1,IBNDW(I+1),2,SU,0.0)
      CALL CONSTY(IBNDW(I)+1,IBNDW(I+1),2,SP,-GREAT)
      ENDIF
44  CONTINUE

      DO 45 I=1,NSE
      IF (ITYPE(I).EQ.5.OR.ITYPE(I).EQ.2) THEN
      CALL CONSTY(IBNDE(I)+1,IBNDE(I+1),NIM1,SU,0.0)
      CALL CONSTY(IBNDE(I)+1,IBNDE(I+1),NIM1,SP,-GREAT)
      ENDIF
45  CONTINUE

C ONLY FOR NOZZLE CASE

      CALL CONSTY(IBNDW(1)+1,IBNDW(2),IBNDS(2),SU,0.0)
      CALL CONSTY(IBNDW(1)+1,IBNDW(2),IBNDS(2),SP,-GREAT)

C ONLY FOR NOZZLE CASE

      RETURN

      ENTRY ENTRA

      DO 150 I=1,NSS
150  IF (ITYPS(I).EQ.5)
      + CALL ENTRAX(IBNDS(I)+1,IBNDS(I+1),.FALSE.)

      DO 151 I=1,NSN
151  IF (ITYPN(I).EQ.5)
      + CALL ENTRAX(IBNDN(I)+1,IBNDN(I+1),.TRUE.)

      DO 152 I=1,NSW
152  IF (ITYPW(I).EQ.5)
      + CALL ENTRAY(IBNDW(I)+1,IBNDW(I+1),.FALSE.)

      DO 153 I=1,NSE
153  IF (ITYPE(I).EQ.5)
      + CALL ENTRAY(IBNDE(I)+1,IBNDE(I+1),.TRUE.)

      ENTRY EXIT

      FLOWOUT=0.0
      AREADENTOUT=0.0
      VINC=0.0

      INLT=.FALSE.

      DO 132 I=1,NSW

```

```
IF (ITYPW(I).EQ.2.OR.ITYPW(I).EQ.5) THEN
```

```
CALL FLOWY(IBNDW(I)+1,IBNDW(I+1),FLOW,AREADENT,,FALSE.)
```

```
C ONLY FOR INLET CASE
```

```
IF(ITYPW(I).EQ.2)THEN
```

```
FLOWE~FLOW
```

```
AREADENTE=AREADENT
```

```
INLT=.TRUE.
```

```
ENDIF
```

```
C ONLY FOR INLET CASE
```

```
FLOWOUT=FLOWOUT-FLOW
```

```
AREADENTOUT=AREADENTOUT+AREADENT
```

```
ENDIF
```

```
132 CONTINUE
```

```
DO 134 I=1,NSE
```

```
IF (ITYPE(I).EQ.2.OR.ITYPE(I).EQ.5) THEN
```

```
CALL FLOWY(IBNDE(I)+1,IBNDE(I+1),FLOW,AREADENT,,TRUE.)
```

```
FLOWOUT=FLOWOUT+FLOW
```

```
AREADENTOUT=AREADENTOUT+AREADENT
```

```
ENDIF
```

```
134 CONTINUE
```

```
C ONLY FOR CROSS FLOW
```

```
IF (CHNGKE) THEN
```

```
CALL FLOWX(IBNDN(I)+1,IBNDN(I+1),FLOW,AREADENT,,TRUE.)
```

```
EDIN=EDIN+ABS(FLOW*ED(INT(NI/2),NJ))
```

```
TEIN=TEIN+ABS(FLOW*TE(INT(NI/2),NJ))
```

```
ENDIF
```

```
C ONLY FOR CROSS FLOW
```

```
DO 140 I=1,NSN
```

```
IF (ITYPN(I).EQ.2.OR.ITYPN(I).EQ.5) THEN
```

```
CALL FLOWX(IBNDN(I)+1,IBNDN(I+1),FLOW,AREADENT,,TRUE.)
```

```
FLOWOUT=FLOWOUT+FLOW
```

```
AREADENTOUT=AREADENTOUT+AREADENT
```

```
ENDIF
```

```
140 CONTINUE
```

```
DO 138 I=1,NSS
```

```
IF (ITYPS(I).EQ.2.OR.ITYPS(I).EQ.5) THEN
```

```
CALL FLOWX(IBNDS(I)+1,IBNDS(I+1),FLOW,AREADENT,,FALSE.)
```

```
FLOWOUT=FLOWOUT-FLOW
```

```
AREADENTOUT=AREADENTOUT+AREADENT
```

```
ENDIF
```

```
138 CONTINUE
```

```
C ONLY FOR INLET CASE
```

```
IF (INLT)THEN
```

```
VINCE=(FLOWJ-RATIO*FLOWE)/AREADENTE
```

```
ENDIF
```

```
C ONLY FOR INLET CASE
```

```

VINC=(FLOWIN-FLOWOUT)/AREADENTOUT

A=REAL(NITER)/5.
B=INT(A)
C=A-REAL(B)
IF(C.LE.1E-5) THEN
PRINT*,*****
PRINT*,FLOWIN-',FLOWIN,' FLOWOUT-',FLOWOUT
PRINT*,FLOWJ-',FLOWJ,' FLOWE',FLOWE
ENDIF

C ONLY FOR INLET CASE
DO 1144 I=1,NSW
IF (ITYPW(I).EQ.2) THEN
DO 1145 J=IBNDW(I)+1,IBNDW(I+1)
1145 U(1,J)=U(1,J)-VINCE
ENDIF
1144 CONTINUE
C ONLY FOR INLET CASE

RETURN

ENTRY MODTE

DO 46 I=1,NSS
IF (ITYPS(I).EQ.2.OR.ITYPS(I).EQ.4.OR.ITYPS(I).EQ.5)
+ CALL SYMX(IBNDS(I)+1,IBNDS(I+1),TE,AS,.FALSE.,1)
IF (ITYPS(I).EQ.3)
+ CALL TENSXW(IBNDS(I)+1,IBNDS(I+1),.FALSE.)
46 CONTINUE

DO 47 I=1,NSN
IF (ITYPN(I).EQ.2.OR.ITYPN(I).EQ.4.OR.ITYPN(I).EQ.5)
+ CALL SYMX(IBNDN(I)+1,IBNDN(I+1),TE,AN,.TRUE.,NJ)
C ONLY FOR CROSS FLOW
IF (CHNGKE)
+ CALL SYMX(IBNDN(I)+1,IBNDN(I+1),TE,AN,.TRUE.,NJ)
C ONLY FOR CROSS FLOW
IF (ITYPN(I).EQ.3)
+ CALL TENSXW(IBNDN(I)+1,IBNDN(I+1),.TRUE.)
47 CONTINUE

C TE(1,NJ)=0.5*(TE(1,NJM1)+TE(2,NJ))

DO 48 I=1,NSW
IF (ITYPW(I).EQ.2.OR.ITYPW(I).EQ.4.OR.ITYPW(I).EQ.5)
+ CALL SYMY(IBNDW(I)+1,IBNDW(I+1),TE,AW,.FALSE.,1)
IF (ITYPW(I).EQ.3)
+ CALL TEEWW(IBNDW(I)+1,IBNDW(I+1),.FALSE.)
48 CONTINUE

DO 49 I=1,NSE
IF (ITYPE(I).EQ.2.OR.ITYPE(I).EQ.4.OR.ITYPE(I).EQ.5)
+ CALL SYMY(IBNDE(I)+1,IBNDE(I+1),TE,AE,.TRUE.,NI)
IF (ITYPE(I).EQ.3)
+ CALL TEEWW(IBNDE(I)+1,IBNDE(I+1),.TRUE.)

```



49 CONTINUE

C XPLUSE(NJ)-XPLUSE(NJM1)  
C XPLUSE(1)-XPLUSE(2)

C ONLY FOR NOZZLE CASE

```
CALL CONSTX(IBNDS(1)+1,IBNDS(2),IBNDW(2)+1,SU,0.0)
CALL CONSTX(IBNDS(1)+1,IBNDS(2),IBNDW(2)+1,SP,-GREAT)

CALL CONSTY(IBNDW(1)+1,IBNDW(2),IBNDS(2),SU,TEINW(1)*GREAT)
CALL CONSTY(IBNDW(1)+1,IBNDW(2),IBNDS(2),SP,-GREAT)

CALL TENSXW(IBNDS(1)+1,IBNDS(2)-1,.FALSE.)
```

C ONLY FOR NOZZLE CASE

C VERTX NODES

C SOUTH WEST NODE

```
IF (ITYPS(1).EQ.3.OR.ITYPW(1).EQ.3) THEN
  TE(1,1)-0.0
ELSEIF ( (ITYPS(1).EQ.4.OR.ITYPS(1).EQ.5)
+ .OR. (ITYPW(1).EQ.4.OR.ITYPW(1).EQ.5) ) THEN
  TE(1,1)-0.5*(TE(1,2)+TE(2,1))
  IF (ITYPW(1).NE.4.AND.ITYPW(1).NE.5) TE(1,1)-TE(1,2)
  IF (ITYPS(1).NE.4.AND.ITYPS(1).NE.5) TE(1,1)-TE(2,1)
ENDIF
```

C SOUTH EAST

```
IF (ITYPS(NSS).EQ.3.OR.ITYPE(1).EQ.3) THEN
  TE(NL,1)-0.0
ELSEIF ( (ITYPS(NSS).EQ.4.OR.ITYPS(NSS).EQ.5)
+ .OR. (ITYPE(1).EQ.4.OR.ITYPE(1).EQ.5) ) THEN
  TE(NL,1)-0.5*(TE(NL,2)+TE(NIM1,1))
  IF (ITYPE(1).NE.4.AND.ITYPE(1).NE.5) TE(NL,1)-TE(NL,2)
  IF (ITYPS(NSS).NE.4.AND.ITYPS(NSS).NE.5) TE(NL,1)-TE(NIM1,1)
ENDIF
```

C NORTH EAST

```
IF (ITYPN(NSN).EQ.3.OR.ITYPE(NSE).EQ.3) THEN
  TE(NL,NJ)-0.0
ELSEIF ( (ITYPN(NSN).EQ.4.OR.ITYPN(NSN).EQ.5)
+ .OR. (ITYPE(NSE).EQ.4.OR.ITYPE(NSE).EQ.5) ) THEN
  TE(NL,NJ)-0.5*(TE(NL,NJM1)+TE(NIM1,NJ))
  IF (ITYPE(NSE).NE.4.AND.ITYPE(NSE).NE.5) TE(NL,NJ)-TE(NL,NJM1)
  IF (ITYPN(NSN).NE.4.AND.ITYPN(NSN).NE.5) TE(NL,NJ)-TE(NIM1,NJ)
ENDIF
```

C NORTH WEST

```
IF (ITYPN(1).EQ.3.OR.ITYPW(NSW).EQ.3) THEN
  TE(1,NJ)-0.0
ELSEIF ( (ITYPN(1).EQ.4.OR.ITYPN(1).EQ.5)
```

```

+ .OR. (ITYPW(NSW).EQ.4.OR.ITYPW(NSW).EQ.5) THEN
  TE(1,NJ)-0.5*(TE(1,NJM1)+TE(2,NJ))
  IF (ITYPW(NSW).NE.4.AND.ITYPW(NSW).NE.5)TE(1,NJ)-TE(1,NJM1)
  IF (ITYPN(1).NE.4.AND.ITYPN(1).NE.5)TE(1,NJ)-TE(2,NJ)
ENDIF

```

```

RETURN

```

```

ENTRY MODED

```

```

  DO 50 I=1,NSS
    IF (ITYPS(I).EQ.2.OR.ITYPS(I).EQ.4.OR.ITYPS(I).EQ.5)
+ CALL SYMX(IBNDS(I)+1,IBNDS(I+1),ED,AS,.FALSE.,1)
    IF (ITYPS(I).EQ.3)
+ CALL EDNSW(IBNDS(I)+1,IBNDS(I+1),.FALSE.)
50 CONTINUE

```

```

  DO 51 I=1,NSN
    IF (ITYPN(I).EQ.2.OR.ITYPN(I).EQ.4.OR.ITYPN(I).EQ.5)
+ CALL SYMX(IBNDN(I)+1,IBNDN(I+1),ED,AN,.TRUE.,NJ)
C ONLY FOR CROSS FLOW
    IF (CHNGKE)
+ CALL SYMX(IBNDN(I)+1,IBNDN(I+1),ED,AN,.TRUE.,NJ)
C ONLY FOR CROSS FLOW
    IF (ITYPN(I).EQ.3)
+ CALL EDNSW(IBNDN(I)+1,IBNDN(I+1),.TRUE.)
51 CONTINUE

```

```

  DO 52 I=1,NSW
    IF (ITYPW(I).EQ.2.OR.ITYPW(I).EQ.4.OR.ITYPW(I).EQ.5)
+ CALL SYMY(IBNDW(I)+1,IBNDW(I+1),ED,AW,.FALSE.,1)
    IF (ITYPW(I).EQ.3)
+ CALL EDEWW(IBNDW(I)+1,IBNDW(I+1),.FALSE.)
52 CONTINUE

```

```

  DO 53 I=1,NSE
    IF (ITYPE(I).EQ.2.OR.ITYPE(I).EQ.4.OR.ITYPE(I).EQ.5)
+ CALL SYMY(IBNDE(I)+1,IBNDE(I+1),ED,AE,.TRUE.,NI)
    IF (ITYPE(I).EQ.3)
+ CALL EDEWW(IBNDE(I)+1,IBNDE(I+1),.TRUE.)
53 CONTINUE

```

```

C ONLY FOR NOZZLE CASE

```

```

  CALL CONSTX(IBNDS(1)+1,IBNDS(2),IBNDW(2)+1,SU,0.0)
  CALL CONSTX(IBNDS(1)+1,IBNDS(2),IBNDW(2)+1,SP,-GREAT)

```

```

  CALL CONSTY(IBNDW(1)+1,IBNDW(2),IBNDS(2),SU,EDINW(1)*GREAT)
  CALL CONSTY(IBNDW(1)+1,IBNDW(2),IBNDS(2),SP,-GREAT)

```

```

  CALL EDNSW(IBNDS(1)+1,IBNDS(2)-1,.FALSE.)

```

```

C ONLY FOR NOZZLE CASE

```

```

C VERTEX NODES

```

## C SOUTH WEST NODE

```

IF (ITYPS(1).EQ.3.OR.ITYPW(1).EQ.3) THEN
  ED(1,1)=0.0
ELSEIF ( (ITYPS(1).EQ.4.OR.ITYPS(1).EQ.5)
+ .OR. (ITYPW(1).EQ.4.OR.ITYPW(1).EQ.5) ) THEN
  ED(1,1)=0.5*(ED(1,2)+ED(2,1))
  IF (ITYPW(1).NE.4.AND.ITYPW(1).NE.5) ED(1,1)=ED(1,2)
  IF (ITYPS(1).NE.4.AND.ITYPS(1).NE.5) ED(1,1)=ED(2,1)
ENDIF

```

## C SOUTH EAST

```

IF (ITYPS(NSS).EQ.3.OR.ITYPE(1).EQ.3) THEN
  TE(NL,1)=0.0
ELSEIF ( (ITYPS(NSS).EQ.4.OR.ITYPS(NSS).EQ.5)
+ .OR. (ITYPE(1).EQ.4.OR.ITYPE(1).EQ.5) ) THEN
  ED(NL,1)=0.5*(ED(NL,2)+ED(NIM1,1))
  IF (ITYPE(1).NE.4.AND.ITYPE(1).NE.5) ED(NL,1)=ED(NL,2)
  IF (ITYPS(NSS).NE.4.AND.ITYPS(NSS).NE.5) ED(NL,1)=ED(NIM1,1)
ENDIF

```

## C NORTH EAST

```

IF (ITYPN(NSN).EQ.3.OR.ITYPE(NSE).EQ.3) THEN
  ED(NL,NJ)=0.0
ELSEIF ( (ITYPN(NSN).EQ.4.OR.ITYPN(NSN).EQ.5)
+ .OR. (ITYPE(NSE).EQ.4.OR.ITYPE(NSE).EQ.5) ) THEN
  ED(NL,NJ)=0.5*(ED(NL,NJM1)+ED(NIM1,NJ))
  IF (ITYPE(NSE).NE.4.AND.ITYPE(NSE).NE.5) ED(NL,NJ)=ED(NL,NJM1)
  IF (ITYPN(NSN).NE.4.AND.ITYPN(NSN).NE.5) ED(NL,NJ)=ED(NIM1,NJ)
ENDIF

```

## C NORTH WEST

```

IF (ITYPN(1).EQ.3.OR.ITYPW(NSW).EQ.3) THEN
  ED(1,NJ)=0.0
ELSEIF ( (ITYPN(1).EQ.4.OR.ITYPN(1).EQ.5)
+ .OR. (ITYPW(NSW).EQ.4.OR.ITYPW(NSW).EQ.5) ) THEN
  ED(1,NJ)=0.5*(ED(1,NJM1)+ED(2,NJ))
  IF (ITYPW(NSW).NE.4.AND.ITYPW(NSW).NE.5) ED(1,NJ)=ED(1,NJM1)
  IF (ITYPN(1).NE.4.AND.ITYPN(1).NE.5) ED(1,NJ)=ED(2,NJ)
ENDIF

```

RETURN

## ENTRY MODT

```

K=0
DO 54 I=1,NSS
  IF (ITYPS(I).EQ.2.OR.ITYPS(I).EQ.4.OR.ITYPS(I).EQ.5)
+ CALL SYMX(IBNDS(I)+1,IBNDS(I+1),T,AS,FALSE,1)
  IF (ITYPS(I).EQ.3) THEN
    K=K+1
  IF (.NOT.FIXS(K))

```

```

+ CALL SYMX(IBNDS(I)+1,IBNDS(I+1),T,AS,,FALSE.,1)
  ENDF
54 CONTINUE

  K=0
  DO 55 I=1,NSN
    IF (ITYPN(I).EQ.2.OR.ITYPN(I).EQ.4.OR.ITYPN(I).EQ.5)
+ CALL SYMX(IBNDN(I)+1,IBNDN(I+1),T,AN,,TRUE.,NJ)
    IF (ITYPN(I).EQ.3) THEN
      K=K+1
      IF (.NOT.FIXN(K))
+ CALL SYMX(IBNDN(I)+1,IBNDN(I+1),T,AN,,TRUE.,NJ)
    ENDF
55 CONTINUE

  K=0
  DO 56 I=1,NSW
    IF (ITYPW(I).EQ.2.OR.ITYPW(I).EQ.4.OR.ITYPW(I).EQ.5)
+ CALL SYMY(IBNDW(I)+1,IBNDW(I+1),T,AW,,FALSE.,1)
    IF (ITYPW(I).EQ.3) THEN
      K=K+1
      IF (.NOT.FIXW(K))
+ CALL SYMY(IBNDW(I)+1,IBNDW(I+1),T,AW,,FALSE.,1)
    ENDF
56 CONTINUE

  K=0
  DO 57 I=1,NSE
    IF (ITYPE(I).EQ.2.OR.ITYPE(I).EQ.4.OR.ITYPE(I).EQ.5)
+ CALL SYMY(IBNDE(I)+1,IBNDE(I+1),T,AE,,TRUE.,NI)
    IF (ITYPE(I).EQ.3) THEN
      K=K+1
      IF (.NOT.FIXE(K))
+ CALL SYMY(IBNDE(I)+1,IBNDE(I+1),T,AE,,TRUE.,NI)
    ENDF
57 CONTINUE

C ONLY FOR NOZZLE CASE

  CALL SYMX(IBNDS(1)+1,IBNDS(2),T,AS,,FALSE.,IBNDW(2)+1)

  CALL CONSTY(IBNDW(1)+1,IBNDW(2),IBNDS(2),SU,TINW(1)*GREAT)
  CALL CONSTY(IBNDW(1)+1,IBNDW(2),IBNDS(2),SP,-GREAT)

C ONLY FOR NOZZLE CASE

C VERTIX NODES

C SOUTH WEST NODE

  IF (ITYPS(1).EQ.3.OR.ITYPW(1).EQ.3) THEN
    T(1,1)=0.5*(T(1,2)+T(2,1))
    IF (ITYPW(1).NE.3) THEN
      T(1,1)=T(1,2)
      IF (FIXS(1))T(1,1)=TFIXS(1)
    ELSEIF (ITYPS(1).NE.3) THEN
      T(1,1)=T(2,1)
      IF (FIXW(1))T(1,1)=TFIXW(1)

```

```

      ENDIF
      ELSEIF ( (ITYPS(1).EQ.4.OR.ITYPS(1).EQ.5)
+ .OR. (ITYPW(1).EQ.4.OR.ITYPW(1).EQ.5) ) THEN
      T(1,1)=0.5*(T(1,2)+T(2,1))
      IF (ITYPW(1).NE.4.AND.ITYPW(1).NE.5) T(1,1)=T(1,2)
      IF (ITYPS(1).NE.4.AND.ITYPS(1).NE.5) T(1,1)=T(2,1)
      ENDIF

```

#### C SOUTH EAST

```

      IF (ITYPS(NSS).EQ.3.OR.ITYPE(1).EQ.3) THEN
      T(NL,1)=0.5*(T(NL,2)+T(NIM1,1))
      IF (ITYPE(1).NE.3) THEN
      T(NL,1)=T(NL,2)
      IF (FLXS(NSS))T(NL,1)=TFLXS(NSS)
      ELSEIF (ITYPS(NSS).NE.3) THEN
      T(NL,1)=T(NIM1,1)
      IF (FLXE(1))T(NL,1)=TFLXE(1)
      ENDIF
      ELSEIF ( (ITYPS(NSS).EQ.4.OR.ITYPS(NSS).EQ.5)
+ .OR. (ITYPE(1).EQ.4.OR.ITYPE(1).EQ.5) ) THEN
      T(NL,1)=0.5*(T(NL,2)+T(NIM1,1))
      IF (ITYPE(1).NE.4.AND.ITYPE(1).NE.5)T(NL,1)=T(NL,2)
      IF (ITYPS(NSS).NE.4.AND.ITYPS(NSS).NE.5)T(NL,1)=T(NIM1,1)
      ENDIF

```

#### C NORTH EAST

```

      IF (ITYPN(NSN).EQ.3.OR.ITYPE(NSE).EQ.3) THEN
      T(NL,NJ)=0.5*(T(NL,NJM1)+T(NIM1,NJ))
      IF (ITYPE(NSE).NE.3) THEN
      T(NL,NJ)=T(NL,NJM1)
      IF (FIXN(NSN))T(NL,NJ)=TFIXN(NSN)
      ELSEIF (ITYPN(NSN).NE.3) THEN
      T(NL,NJ)=T(NIM1,NJ)
      IF (FIXE(NSE))T(NL,NJ)=TFIXE(NSE)
      ENDIF
      ELSEIF ( (ITYPN(NSN).EQ.4.OR.ITYPN(NSN).EQ.5)
+ .OR. (ITYPE(NSE).EQ.4.OR.ITYPE(NSE).EQ.5) ) THEN
      T(NL,NJ)=0.5*(T(NL,NJM1)+T(NIM1,NJ))
      IF (ITYPE(NSE).NE.4.AND.ITYPE(NSE).NE.5)T(NL,NJ)=T(NL,NJM1)
      IF (ITYPN(NSN).NE.4.AND.ITYPN(NSN).NE.5)T(NL,NJ)=T(NIM1,NJ)
      ENDIF

```

#### C NORTH WEST

```

      IF (ITYPN(1).EQ.3.OR.ITYPW(NSW).EQ.3) THEN
      T(1,NJ)=0.5*(T(1,NJM1)+T(2,NJ))
      IF (ITYPW(NSW).NE.3) THEN
      T(1,NJ)=T(1,NJM1)
      IF (FIXN(1))T(1,NJ)=TFIXN(1)
      ELSEIF (ITYPN(1).NE.3) THEN
      T(1,NJ)=T(2,NJ)
      IF (FIXW(NSW))T(1,NJ)=TFIXW(NSW)
      ENDIF
      ELSEIF ( (ITYPN(1).EQ.4.OR.ITYPN(1).EQ.5)
+ .OR. (ITYPW(NSW).EQ.4.OR.ITYPW(NSW).EQ.5) ) THEN

```

```

T(1,NJ)=0.5*(T(1,NJM1)+T(2,NJ))
  IF (ITYPW(NSW).NE.4.AND.ITYPW(NSW).NE.5)T(1,NJ)=T(1,NJM1)
  IF (ITYPN(1).NE.4.AND.ITYPN(1).NE.5)T(1,NJ)=T(2,NJ)
ENDIF

```

```

RETURN

```

```

END

```

```

SUBROUTINE USERB

```

```

PARAMETER (NX=70,NY=70)
LOGICAL LREAD,LWRITE
COMMON
+/ALL/NL,NJ,NM1,NJM1,NM2,NJM2,GREAT,TINY
+/GEOMX/X(NX),XU(NX),SXC(NX),UXCV(NX),FX(NX),UCVI(NX),UCVIP(NX)
+/GEOMY/IND,Y(NY),YV(NY),SYCV(NY),VYCV(NY),FY(NY),VCVJ(NY)
+ ,VCVJP(NY),RV(NY),R(NY),RSYCV(NY),RVYCV(NY)
+/VARI/U(NX,NY),V(NX,NY),P(NX,NY),PP(NX,NY),T(NX,NY),
+ DU(NX,NY),DV(NX,NY),DEN(NX,NY),VIS(NX,NY)
+/VAR2/DENSIT,VISCOS,PRANDL
+/VEL/RESORU,NSWPU,URFU
+/VVEL/RESORV,NSWPV,URFV
+/PCOR/RESORM,NSWPP,URFP
+/TEMP/RESORT,NSWPT,URFT
+/HEADS/HEDU,HEDV,HEDP,HEDT,HEDK,HEDE,HEDVIS
COMMON
+/COEF/AP(NX,NY),AN(NX,NY),AS(NX,NY),AE(NX,NY),AW(NX,NY)
+ ,SU(NX,NY),SP(NX,NY)
+/COEFU/APU(NX,NY),ANU(NX,NY),ASU(NX,NY),AEU(NX,NY),AWU(NX,NY)
+ ,SUU(NX,NY),SPU(NX,NY)
+/COEFV/APV(NX,NY),ANV(NX,NY),ASV(NX,NY),AEV(NX,NY),AWV(NX,NY)
+ ,SUV(NX,NY),SPV(NX,NY)
+/OTHR1/NITER,MAXIT,URFVIS,URFDEN,IMON,JMON,IPREF,JPREF,SORMAX
+ ,FLOWIN,XMONIN,SMPW(NX)
+/TKE/TE(NX,NY),RESORK,NSWPK,URFGEN,URFK
+/TED/ED(NX,NY),RESORE,NSWPE,URFE
+/TURB1/GEN(NX,NY),CMU,C1,C2,CAPPA,ELOG,PRED,PRTE,PRT,PFUN
+/TURB2/TKEIN,TEDIN
+/QUICK/NQUICK,NQUV,NQKE,NQT,B3XS(NX),B3XU(NX),B3YS(NY),B3YV(NY)
+/BND/NSS,NSW,NSN,NSE,
+ITYPE(5),ITYPW(5),ITYPN(5),ITYPE(5),
+IBNDS(6),IBNDW(6),IBNDN(6),IBNDE(6),
+FIXS,FIXW,FXN,FXE,TFXS,TFXW,TFXN,TFXE,
+UINS(5),UINW(5),UINN(5),UINE(5),
+VINS(5),VINW(5),VINN(5),VINE(5),
+TEINS(5),TEINW(5),TEINN(5),TEINE(5),
+EDINS(5),EDINW(5),EDINN(5),EDINE(5),
+TINS(5),TINW(5),TINN(5),TINE(5)

C THIS IS THE ADDED VARIABLES
COMMON
+/XPTAU/XPLUSE(NY),XPLUSW(NY),YPLUSN(NX),YPLUSS(NX)
+ ,TAUE(NY),TAUW(NY),TAUN(NX),TAUS(NX)

```

+/TURB3/CMU25,CMU75

DIMENSION PHI(NX,NY),APHI(NX,NY),UA(NX,NY),VA(NX,NY)

LOGICAL EAST, WEST, NORTH, SOUTH

COMMON /LPAR/LCALKE,LCALT,LCALD  
 LOGICAL LCALKE,LCALT,LCALD  
 COMMON /INI/TEMP,TKINET,EDDYD

ENTRY GRIDX(IW,IE,XW,XE,RAX,EAST)

WEST=.NOT.EAST

XU(IW)-XW  
 XU(IE)-XE

N=IE-IW  
 TOX=0.0

DO 107 I=1,N  
 107 TOX=TOX+RAX\*\*(I-1)  
 DX=(XE-XW)/TOX

DO 108 I=1,N-1

IF (EAST)XU(IE-I)-XU(IE-I+1)-DX\*RAX\*\*(I-1)  
 108 IF (WEST)XU(IW+I)-XU(IW+I-1)+DX\*RAX\*\*(I-1)

RETURN

ENTRY GRIDY(JS,JN,YS,YN,RAY,NORTH)

SOUTH=.NOT.NORTH

YV(JS)-YS  
 YV(JN)-YN

N=JN-JS  
 TOY=0.0

DO 1107 J=1,N  
 1107 TOY=TOY+RAY\*\*(J-1)  
 DY=(YN-YS)/TOY

DO 1108 J=1,N-1

IF(NORTH) YV(JN-J)-YV(JN-J+1)-DY\*RAY\*\*(J-1)  
 1108 IF(SOUTH) YV(JS+J)-YV(JS+J-1)+DY\*RAY\*\*(J-1)

RETURN

ENTRY CONSTX(IW,IE,JI,PHI,CONST)

DO 375 I=IW,IE

```

PHI(L,J)-CONST
375 CONTINUE

RETURN

ENTRY CONSTY(JS,JN,IL,PHI,CONST)

DO 376 J=JS,JN
PHI(IL,J)-CONST
376 CONTINUE

RETURN

ENTRY FLOWX(IW,IE,FLOW,AREADENT,NORTH)

SOUTH=.NOT.NORTH
FLOW=0.0
AREADENT=0.0

IF(SOUTH) THEN
DO 5300 I=IW,IE
AREADEN=RV(1)*SXCVC(I)*DEN(L,1)
FLOW=FLOW+AREADEN*V(L,1)
AREADENT=AREADENT+AREADEN
5300 CONTINUE
ELSE
DO 5301 I=IW,IE
AREADEN=RV(NJM1)*SXCVC(I)*DEN(L,NJ)
FLOW=FLOW+AREADEN*V(L,NJM1)
AREADENT=AREADENT+AREADEN
5301 CONTINUE
ENDIF

RETURN

ENTRY FLOWY(JS,JN,FLOW,AREADENT,EAST)

WEST=.NOT.EAST
FLOW=0.0
AREADENT=0.0

IF(WEST) THEN
DO 6300 J=JS,JN
AREADEN=RSYCV(J)*DEN(1,J)
FLOW=FLOW+AREADEN*U(1,J)
AREADENT=AREADENT+AREADEN
6300 CONTINUE
ELSE
DO 6301 J=JS,JN
AREADEN=RSYCV(J)*DEN(NI,J)
FLOW=FLOW+AREADEN*U(NIM1,J)
AREADENT=AREADENT+AREADEN
6301 CONTINUE
ENDIF

RETURN

```



```

ENTRY SYMX(IW,IE,PHI,APHI,NORTH,JJ)

DO 400 I=IW,IE

SOUTH=.NOT.NORTH

IF(SOUTH)THEN
  APHI(L,JJ+1)=0.0
  PHI(L,JJ)=PHI(L,JJ+1)
ELSE
  APHI(L,JJ-1)=0.0
  PHI(L,JJ)=PHI(L,JJ-1)
ENDIF

400 CONTINUE

RETURN

ENTRY SYMY(JS,JN,PHI,APHI,EAST,I)

WEST=.NOT.EAST

DO 1400 J=JS,JN

IF(WEST)THEN
  APHI(I+1,J)=0.0
  PHI(I,J)=PHI(I+1,J)
ELSE
  APHI(I-1,J)=0.0
  PHI(I,J)=PHI(I-1,J)
ENDIF

1400 CONTINUE

RETURN

ENTRY TEEWW(JS,JN,EAST)

WEST=.NOT.EAST

XP=UXCV(1)
IF(EAST)XP=UXCV(NIM1)
I=2
IF (EAST)I=NIM1

DO 715 J=JS,JN

IF (WEST) THEN

SQRTK=SQRT(ABS(TE(L,J)))
XPLUSW(J)=DEN(L,J)*SQRTK*CMU25*XP/VISCOS
AW(L,J)=0.0
VOL=RSYCV(J)*SXCV(I)
TVIS=VIS(L,J)-VISCOS+TINY
SU(L,J)=SU(L,J)-GEN(L,J)*VOL
SP(L,J)=SP(L,J)-CMU*DEN(L,J)**2*ABS(TE(L,J))/TVIS*VOL
GENCOU=0.5*(ABS(TAUW(J)*V(L,J))+ABS(TAUW(J-1)*V(L,J-1)))/XP

```

```

VE=0.5*(V(L,J)+V(L,J-1)+FX(I)*(V(I+1,J)-V(I+1,J-1)-V(L,J)-V(L,J-1)
+))
VW=0.5*(V(I-1,J)+V(I-1,J-1)+FX(I-1)*(V(L,J)+V(L,J-1)-V(I-1,J)
+ -V(I-1,J-1)))
DVDX=(VE-VW)/SXCVC(I)
UN=0.5*(U(L,J)+U(I-1,J)+FY(J)*(U(L,J+1)+U(I-1,J+1)-U(L,J)-U(I-1,J)
+))
US=0.5*(U(L,J-1)+U(I-1,J-1)+FY(J-1)*(U(L,J)+U(I-1,J)-U(L,J-1)
+ -U(I-1,J-1)))
DUDY=(UN-US)/SYCV(J)
GENRES=GEN(L,J)-URFGEN*TVIS*(DVDX+DUDY)**2
GEN(L,J)=URFGEN*GENCOU+GENRES
DITERM=DEN(L,J)*CMU75*SQRK*XPLUSW(J)/XP
IF(XPLUSW(J).GT.11.63)DITERM=DITERM*ALOG(ELOG*XPLUSW(J)
+/XPLUSW(J)/CAPPA
SU(L,J)=GEN(L,J)*VOL+SU(L,J)
SP(L,J)=SP(L,J)-DITERM*VOL

```

ELSE

```

SQRK=SQRT(ABS(TE(L,J)))
XPLUSE(J)=DEN(L,J)*SQRK*CMU25*XP/VISCOS
AE(L,J)=0.0
VOL=RSYCV(J)*SXCVC(I)
TVIS=VIS(L,J)-VISCOS+TINY
SU(L,J)=SU(L,J)-GEN(L,J)*VOL
SP(L,J)=SP(L,J)+CMU*DEN(L,J)**2*ABS(TE(L,J))/TVIS*VOL
GENCOU=0.5*(ABS(TAUE(J)*V(L,J)+ABS(TAUE(J-1)*V(L,J-1)))/XP
VE=0.5*(V(L,J)+V(L,J-1)+FX(I)*(V(I+1,J)+V(I+1,J-1)-V(L,J)-V(L,J-1)
+))
VW=0.5*(V(I-1,J)+V(I-1,J-1)+FX(I-1)*(V(L,J)+V(L,J-1)-V(I-1,J)
+ -V(I-1,J-1)))
DVDX=(VE-VW)/SXCVC(I)
UN=0.5*(U(L,J)+U(I-1,J)+FY(J)*(U(L,J+1)+U(I-1,J+1)-U(L,J)-U(I-1,J)
+))
US=0.5*(U(L,J-1)+U(I-1,J-1)+FY(J-1)*(U(L,J)+U(I-1,J)-U(L,J-1)
+ -U(I-1,J-1)))
DUDY=(UN-US)/SYCV(J)
GENRES=GEN(L,J)-URFGEN*TVIS*(DVDX+DUDY)**2
GEN(L,J)=URFGEN*GENCOU+GENRES
DITERM=DEN(L,J)*CMU75*SQRK*XPLUSE(J)/XP
IF(XPLUSE(J).GT.11.63)DITERM=DITERM*ALOG(ELOG*XPLUSE(J)
+/XPLUSE(J)/CAPPA
SU(L,J)=GEN(L,J)*VOL+SU(L,J)
SP(L,J)=SP(L,J)-DITERM*VOL

```

ENDIF

715 CONTINUE

RETURN

ENTRY VEWV(JS,JN,EAST)

IF (.NOT.LCALKE) RETURN

```

WEST=.NOT.EAST

IF(WEST) THEN

I=2
XP=UXCV(1)

DO 5505 J=JS,JN

AREA=RVYCV(J)
AWV(L,J)=0.0
SQRTK=SQRT(ABS(TE(L,J)+FY(J)*(TE(L,J+1)-TE(L,J))))
DENV=DEN(L,J)+FY(J)*(DEN(L,J+1)-DEN(L,J))
XPLUSV=XPLUSW(J)+FY(J)*(XPLUSW(J+1)-XPLUSW(J))
TMULT=VISCOS/XP
IF(XPLUSV.GT.11.63)TMULT=DENV*CMU25*SQRTK*CAPPA/ALOG(ELOG*XPLUSV)
TAUW(J)=TMULT*V(L,J)
5505 SPV(L,J)=SPV(L,J)-TMULT*AREA

      TAUW(JS-1)=TAUW(JS)
      TAUW(JN+1)=TAUW(JN)

ELSE

      I=NIM1
      XP=UXCV(NIM1)

      DO 6505 J=JS,JN

AREA=RVYCV(J)
AEV(L,J)=0.0
SQRTK=SQRT(ABS(TE(L,J)+FY(J)*(TE(L,J+1)-TE(L,J))))
DENV=DEN(L,J)+FY(J)*(DEN(L,J+1)-DEN(L,J))
XPLUSV=XPLUSE(J)+FY(J)*(XPLUSE(J+1)-XPLUSE(J))
TMULT=VISCOS/XP
IF(XPLUSV.GT.11.63)TMULT=DENV*CMU25*SQRTK*CAPPA/ALOG(ELOG*XPLUSV)
TAUE(J)=TMULT*V(L,J)
6505 SPV(L,J)=SPV(L,J)-TMULT*AREA

      TAUE(JS-1)=TAUE(JS)
      TAUE(JN+1)=TAUE(JN)

ENDIF

RETURN

ENTRY EDEWW(JS,JN,EAST)

WEST=.NOT.EAST

XP=UXCV(1)
IF(EAST)XP=UXCV(NIM1)
I=2
IF (EAST)I=NIM1

```

```

TERM=CMU75/CAPPA/XP
DO 5815 J=JS,JN
  SU(L,J)=GREAT*TERM*ABS(TE(L,J))**1.5
5815 SP(L,J)=GREAT
  RETURN

  ENTRY UNSW(IW,IE,NORTH)
  IF (.NOT.LCALKE) RETURN

SOUTH=.NOT.NORTH
IF(SOUTH) THEN
  J=2
  YP=VYCV(1)
C ONLY FOR NOZZLE CASE
  J=IBNDW(2)+2
  YP=VYCV(IBNDW(2)+1)
C ONLY FOR NOZZLE CASE
  DO 1505 I=IW,IE
    AREA=UXCV(I)
    ASU(L,J)=0.0
    SQRTK=SQRT(ABS(TE(L,J)+FX(I)*(TE(I+1,J)-TE(L,J))))
    DENV=DEN(L,J)+FX(I)*(DEN(I+1,J)-DEN(L,J))
    YPLUSU=YPLUSS(I)+FX(I)*(YPLUSS(I+1)-YPLUSS(I))
    TMULT=VISCOS/YP
    IF(YPLUSU.GT.11.63)TMULT=DENV*CMU25*SQRTK*CAPPA/ALOG(ELOG*YPLUSU)
    TAUS(I)=TMULT*U(L,J)
1505 SPU(L,J)=SPU(L,J)-TMULT*AREA

    TAUS(IW-1)=TAUS(IW)
    TAUS(IE+1)=TAUS(IE)

  ELSE
    J=NJMI
    YP=VYCV(NJMI)

    DO 2505 I=IW,IE
      AREA=UXCV(I)
      ANU(L,J)=0.0
      SQRTK=SQRT(ABS(TE(L,J)+FX(I)*(TE(I+1,J)-TE(L,J))))
      DENV=DEN(L,J)+FX(I)*(DEN(I+1,J)-DEN(L,J))
      YPLUSU=YPLUSN(I)+FX(I)*(YPLUSN(I+1)-YPLUSN(I))
      TMULT=VISCOS/YP
      IF(YPLUSU.GT.11.63)TMULT=DENV*CMU25*SQRTK*CAPPA/ALOG(ELOG*YPLUSU)
      TAUN(I)=TMULT*U(L,J)

```

```

2505 SPU(L,J)-SPU(L,J)-TMULT*AREA

      TAUS(IW-1)-TAUS(IW)
      TAUS(IE+1)-TAUS(IE)

ENDIF

      RETURN

      ENTRY TENSW(IW,IE,NORTH)

      SOUTH=.NOT.NORTH

      YP-VYCV(1)
      IF(NORTH)YP-VYCV(NJM1)
      J-2
      IF (NORTH)J-NJM1

C ONLY FOR NOZZLE CASE
      J-IBNDW(2)+2
      YP-VYCV(1BNDW(2)+1)
C ONLY FOR NOZZLE CASE

      DO 1715 I=IW,IE

      IF (SOUTH) THEN

      SQRTK=SQRT(ABS(TE(L,J)))
      YPLUSS(I)-DEN(L,J)*SQRTK*CMU25*YP/VISCOS
      AS(L,J)=0.0
      VOL=RSYCV(J)*SXCVC(I)
      TVIS=VIS(L,J)-VISCOS+TINY
      SU(L,J)=SU(L,J)-GEN(L,J)*VOL
      SP(L,J)=SP(L,J)-CMU*DEN(L,J)**2*ABS(TE(L,J))/TVIS*VOL
      GENCOU=0.5*(ABS(TAUS(I)*U(L,J))+ABS(TAUS(I-1)*U(I-1,J)))/YP
      VE=0.5*(V(L,J)+V(L,J-1)+FX(I)*(V(I+1,J)+V(I+1,J-1)-V(L,J)-V(L,J-1)
      +))
      VW=0.5*(V(I-1,J)+V(I-1,J-1)+FX(I-1)*(V(L,J)+V(L,J-1)-V(I-1,J)
      + -V(I-1,J-1)))
      DVDX=(VE-VW)/SXCVC(I)
      UN=0.5*(U(L,J)+U(I-1,J)+FY(J)*(U(L,J+1)+U(I-1,J+1)-U(L,J)-U(I-1,J)
      +))
      US=0.5*(U(L,J-1)+U(I-1,J-1)+FY(J-1)*(U(L,J)+U(I-1,J)-U(L,J-1)
      + -U(I-1,J-1)))
      DUDY=(UN-US)/SYCV(J)
      GENRES=GEN(L,J)-URFGEN*TVIS*(DVDX+DUDY)**2
      GEN(L,J)=URFGEN*GENCOU+GENRES
      DITERM=DEN(L,J)*CMU75*SQRTK*YPLUSS(I)*YP
      IF(YPLUSS(I).GT.11.63)DITERM=DITERM*ALOG(ELOG*YPLUSS(I)
      +/YPLUSS(I)/CAPPA
      SU(L,J)=GEN(L,J)*VOL+SU(L,J)
      SP(L,J)=SP(L,J)-DITERM*VOL

      ELSE

```

```

SQRTK=SQRT(ABS(TE(L,J)))
YPLUSN(I)-DEN(L,J)*SQRTK*CMU25*YP/VISCOS
AN(L,J)=0.0
VOL=RSYCV(J)*SXCVC(I)
TVIS=VIS(L,J)-VISCOS+TINY
SU(L,J)=SU(L,J)-GEN(L,J)*VOL
SP(L,J)=SP(L,J)+CMU*DEN(L,J)**2*ABS(TE(L,J))/TVIS*VOL
GENCOU=0.5*(ABS(TAUN(I)*U(L,J))+ABS(TAUN(I-1)*U(I-1,J)))/YP
VE=0.5*(V(L,J)+V(L,J-1)+FX(I)*(V(I+1,J)+V(I+1,J-1)-V(L,J)-V(L,J-1)
+))
VW=0.5*(V(I-1,J)+V(I-1,J-1)+FX(I-1)*(V(L,J)+V(L,J-1)-V(I-1,J)
+ -V(I-1,J-1)))
DVDX=(VE-VW)/SXCVC(I)
UN=0.5*(U(L,J)+U(I-1,J)+FY(J)*(U(L,J+1)+U(I-1,J+1)-U(L,J)-U(I-1,J)
+))
US=0.5*(U(L,J-1)+U(I-1,J-1)+FY(J-1)*(U(L,J)+U(I-1,J)-U(L,J-1)
+ -U(I-1,J-1)))
DUDY=(UN-US)/SYCV(J)
GENRES=GEN(L,J)-URFGEN*TVIS*(DVDX+DUDY)**2
GEN(L,J)=URFGEN*GENCOU+GENRES
DITERM=DEN(L,J)*CMU75*SQRTK*YPLUSN(I)/YP
IF(YPLUSN(I).GT.11.63)DITERM=DITERM*ALOG(ELOG*YPLUSN(I))
+/YPLUSN(I)/CAPPA
SU(L,J)=GEN(L,J)*VOL+SU(L,J)
SP(L,J)=SP(L,J)-DITERM*VOL

      ENDIF

1715 CONTINUE

      RETURN

      ENTRY EDNSW(IW,IE,NORTH)

      SOUTH=.NOT.NORTH

      YP=VYCV(1)
      IF(NORTH)YP=VYCV(NJM1)
      J=2
      IF (NORTH)J=NJM1

C ONLY FOR NOZZLE CASE
      J=IBNDW(2)+2
      YP=VYCV(1)
C ONLY FOR NOZZLE CASE

      TERM=CMU75/CAPPA/YP

      DO 2815 I=IW,IE

      SU(L,J)=GREAT*TERM*ABS(TE(L,J))**1.5
2815 SP(L,J)=GREAT

```

RETURN

ENTRY ENTRAY(JS,JN,EAST)

WEST-.NOT.EAST

IF (WEST) THEN  
DO 1000 J=JS,JN

DENW=DEN(1,J)  
DENE=DEN(2,J)+FX(2)\*(DEN(3,J)-DEN(2,J))  
DENS=DEN(2,J-1)+FY(J-1)\*(DEN(2,J)-DEN(2,J-1))  
DENN=DEN(2,J)+FY(J)\*(DEN(2,J+1)-DEN(2,J))

1000 U(1,J)=DENE/DENW\*U(2,J)+(DENN/DENW\*V(2,J)\*RV(J)  
+DENS/DENW\*V(2,J-1)\*RV(J-1))\*SXCVC(2)/RSYCV(J)

ELSE

DO 1001 J=JS,JN

DENW=DEN(NIM2,J)+FX(NIM2)\*(DEN(NIM1,J)-DEN(NIM2,J))  
DENE=DEN(NL,J)  
DENS=DEN(NIM1,J-1)+FY(J-1)\*(DEN(NIM1,J)-DEN(NIM1,J-1))  
DENN=DEN(NIM1,J)+FY(J)\*(DEN(NIM1,J+1)-DEN(NIM1,J))

1001 U(NIM1,J)=DENW/DENE\*U(NIM2,J)-(DENN/DENE\*V(NIM1,J)\*RV(J)  
+DENS/DENE\*V(NIM1,J-1)\*RV(J-1))\*SXCVC(NIM1)/RSYCV(J)  
ENDIF

RETURN

ENTRY ENTRAX(IW,IE,NORTH)

SOUTH-.NOT.NORTH

IF (NORTH) THEN

DENS=DEN(L,NJM2)+FY(NJM2)\*(DEN(L,NJM1)-DEN(L,NJM2))  
DENN=DEN(L,NJ)  
DENW=DEN(I-1,NJM1)+FX(I-1)\*(DEN(L,NJM1)-DEN(I-1,NJM1))  
DENE=DEN(L,NJM1)+FX(I)\*(DEN(I+1,NJM1)-DEN(L,NJM1))

DO 1050 I=IW,IE  
1050 V(L,NJM1)=DENS/DENN\*V(L,NJM2)\*RV(NJM2)/RV(NJM1)-  
(DENE/DENN\*U(L,NJM1)-DENW/DENN\*U(I-1,NJM1))  
+\*RSYCV(NJM1)/RV(NJM1)/SXCVC(I)

ELSE

DO 1051 I=IW,IE

```
DENS=DEN(L,1)
DENN=DEN(I,2)+FY(2)*(DEN(L,3)-DEN(L,2))
DENW=DEN(I-1,2)+FX(I-1)*(DEN(L,2)-DEN(I-1,2))
DENE=DEN(L,2)+FX(I)*(DEN(I+1,2)-DEN(L,2))

1051 V(L,1)=DENN/DENS*V(L,2)*RV(2)/RV(1)+(DENE/DENS*U(L,2)
  +DENW/DENS*U(I-1,2))*RSYCV(2)/RV(1)/SXCVC(I)
ENDIF

RETURN

END
```



T,T,T  
 .5,.5,1.,7,1.,7.,7.,6,1.  
 1,1,2,1,1,1  
 .09,1.44,1.92,,4187,9.793,1.0,,6,-2.0  
 2,26,3,3,0,100,1.E-3,F,T,1,0,0,1.E+30,1.E-30  
 .000018,1.20,0.0,,3,,3  
 2,0.0  
 33,51,,254,1.016  
 4  
 1,17,0.0,,2032,1.0,F  
 17,23,,2032,,23368,1.0,F  
 23,29,,23368,,24892,1.0,F  
 29,33,,24892,,254,1.0,F  
 5  
 1,11,0.0,,03175,1.0,F  
 11,16,,03175,,0635,1.0,F  
 16,21,,0635,,127,1.0,F  
 21,46,,127,,762,1.0,F  
 46,51,,762,1.016,1.0,F  
 2  
 1,11,33  
 4,4  
 2  
 1,5,51  
 1,5  
 1  
 1,33  
 1  
 1  
 1,51  
 3  
 253.38,0.0,60,8000,-31.94  
 0.0,-10.7,2.5,2.5,0.0  
 .FALSE,,0.0  
 100.,292.  
 11,10,-11

NITER	10005RESM-	1.8700654E-06			
RESU-	2.2209924E-05URFU-	0.5000000	NLESSU-NMOREU-	-1	
RESV-	4.8095309E-05URFV-	0.5000000	NLESSV-NMOREV-	1	
RESK-	1.6558509E-03URFK-	0.7000000	NLESSK-NMOREK-	3	
RESE-	1.3021533E-02URFE-	0.7000000	NLESSE-NMOREE-	3	
REST-	0.5193840	URFT-	0.7000000	NLESST-NMORET-	3

THERE IS A MAXIMA AT X/D= 6.2500007E-02  
 THERE IS A MINIMA AT X/D= 4.250000  
 THERE IS A MAXIMA AT X/D= 4.750000  
 THERE IS A MINIMA AT X/D= 5.500000  
 THERE IS A MAXIMA AT X/D= 6.500000  
 THERE IS A MINIMA AT X/D= 13.50000  
 THERE IS A MAXIMA AT X/D= 20.50001  
 THERE IS A MINIMA AT X/D= 37.00000  
 1 6.2500007E-02 58807.57 856.0801  
 2 0.1875000 51763.53 753.5379  
 3 0.3125001 41487.68 603.9491  
 4 0.4375001 31108.48 452.8559  
 5 0.5625001 22363.07 325.5462  
 6 0.6875001 15616.95 227.3408  
 7 0.8125001 10664.99 155.2536  
 8 0.9375001 7153.679 104.1383  
 9 1.062500 4733.145 68.90187  
 10 1.187500 3106.164 45.21740  
 11 1.375000 1625.128 23.65750  
 12 1.625000 707.0870 10.29329  
 13 1.875000 317.0058 4.614752  
 14 2.125000 137.9754 2.008551  
 15 2.375000 54.04762 0.7867880  
 16 2.750000 -17.95087 -0.2613164  
 17 3.250000 -38.93819 -0.5668354  
 18 3.750000 -45.44477 -0.6615537  
 19 4.250000 -46.05913 -0.6704972  
 20 4.750000 -43.13604 -0.6279448  
 21 5.500000 -44.71581 -0.6509420  
 22 6.500000 -43.10809 -0.6275379  
 23 7.500000 -45.23174 -0.6584526  
 24 8.500000 -48.62434 -0.7078397  
 25 9.500000 -52.93623 -0.7706092  
 26 10.50000 -57.81883 -0.8416867  
 27 11.50000 -62.61879 -0.9115613  
 28 12.50000 -66.20579 -0.9637783  
 29 13.50000 -66.73439 -0.9714733  
 30 14.50000 -61.58271 -0.8964787  
 31 15.50000 -47.81384 -0.6960410  
 32 16.50000 -23.54695 -0.3427803  
 33 17.50000 9.782115 0.1424013  
 34 18.50000 45.08093 0.6562572  
 35 19.50000 70.13243 1.020940  
 36 20.50001 72.76170 1.059215  
 37 21.50000 59.89608 0.8719260  
 38 22.50001 43.79871 0.6375915  
 39 23.50000 29.68646 0.4321551  
 40 24.50000 18.04466 0.2626818  
 41 25.50000 8.404816 0.1223515  
 42 26.50001 0.3102114 4.5158439E-03  
 43 27.50000 -6.571120 -9.5657840E-02  
 44 28.50000 -12.46882 -0.1815125  
 45 29.50000 -17.53617 -0.2552795  
 46 31.00001 -23.79216 -0.3463499  
 47 33.00000 -30.01360 -0.4369173  
 48 35.00000 -34.10120 -0.4964218  
 49 37.00000 -35.96248 -0.5235170  
 50 39.00000 -32.39230 -0.4715448

***Abstract in Arabic***

## ملخص

دراسة عددية للنفثات المرتبطة في جريان معترض والمتعلقة بطائرات قصيرة الاقلاع وعودية الهبوط

اعداد: بهاء محمود سليمان

اشراف: د. بسام علي جبران

في هذه الدراسة، قد اجري بحث عددي على مجال الجريان الناتج عن نفث مرتطم واحد في جريان معترض، باستعمال نموذج عددي محوري التناظر (ثنائي الأبعاد)، المتغيرات التي تمت دراستها هي: نسبة السرعة الفعالة ( $Ve = 14.4-26.1$ ) وارتفاع المنفث ( $h/d = 2.0-10.0$ ) ونسبة الاضغاط في المنفث ( $pr = 1.05-1.6$ ) وموقع مدخل المحرك ( $l/d = 10.5-22.5$ ) ومعدل الدفع الكتلي للمدخل ( $m/m_j = .25-4$ ) ودرجة حرارة النفث ( $T/T_\infty = 0.89-3.2$ )، لقد تم بحث تأثير المتغيرات المذكورة سابقا على موقع وحجم وقوة الدوامة الأرضية (*ground vortex*) وعلى توزيع درجات الحرارة في مجال الجريان.

على الرغم من محدودية استخدام النموذج العددي الثنائي الأبعاد، فإن النموذج قد أوجد مجالات جريان شبيهة لتلك التي تم إيجادها عمليا، بالنسبة لمتجهات السرعة وتوزيع معاملات الضغط على مستوى الأرض. ان علاقات التشابه الذاتي للدوامة الأرضية قد تم التنبؤ بها بشكل دقيق.

لقد وجد ان نسبة السرعة الفعالة ( $Ve$ ) هي أهم متغير له تأثير على مجال الجريان، ان نقطة الاختراق القصوى للدوامة الأرضية ( $x_p$ ) تزداد باضطراد مع زيادة  $Ve$ . لقد وجد ان ( $x_p = .86 Ve$ ) حيث ان  $x_p$  تم التنبؤ بها بزيادة مقدارها 25% مقارنة مع 40-50% في الدراسات العددية السابقة. ان قوة الدوامة الأرضية وحجمها يزدادان كذلك مع زيادة  $Ve$ . ان توزيع درجات الحرارة في مجال الجريان يتأثر بشدة ب  $Ve$  حيث ان اختراق الغازات الساخنة يزداد بازدياد  $Ve$ . علاوة على ذلك، فانه قد وجد ان نقطة الاختراق القصوى للدوامة الأرضية تساوي لاختراق الغازات الساخنة.

436779

لقد وجد ان تأثير درجة حرارة النفث على مجال الجريان ضئيل عند ثبات قيمة  $Ve$ ، بالنسبة لشكل الدوامة الأرضية وقوتها وبالنسبة للتوزيع درجات الحرارة، وذلك لأن تأثير درجة حرارة النفث محتوى في تأثير  $Ve$ .

تعد وجد أن ارتفاع المنفذ (في المدى الذي تمت دراسته) له تأثير قليل على شكل وقوة الدوامة الأرضية، ولكن له تأثير كبير على درجة حرارة نقطة الارتطام. وقد وجد أن نسبة الانضغاط في المنفذ لها تأثير ضعيف عند ثبات قيمة  $Ve$ .

إن قوة الوامة الأرضية تزداد قليلاً عند زيادة معدل الدفع الكتلي للمدخل، مع أن معدل الدفع الكتلي للمدخل له تأثير ضئيل على شكل الدوامة الأرضية وعلى اختراق الغازات الساخنة، وإن ابتلاع الغازات الساخنة في مدخل المحرك يقل قليلاً عند زيادة معدل الدفع الكتلي للمدخل. وقد وجد أن موقع المدخل له تأثير كبير على قوة للدوامة الأرضية وعلى ضغط الركود، في حالة وضع المدخل بعد قلب الدوامة الأرضية (*ground vortex core*)، مع تأثير قليل على توزيع درجات الحرارة، وإن ابتلاع الغازات الساخنة في مدخل المحرك يقل بوضوح عند زيادة بعد المدخل عن المنفذ.

```

IF (RESK.LT.RESOK)THEN
NLESSK=NLESSK+1
RESLK(NNB)=.TRUE.
ELSE
NMOREK=NMOREK+1
RESLK(NNB)=.FALSE.
ENDIF

```

```

IF (RESE.LT.RESOE)THEN
NLESSE=NLESSE+1
RESLE(NNB)=.TRUE.
ELSE
NMOREE=NMOREE+1
RESLE(NNB)=.FALSE.
ENDIF

```

```

IF (REST.LT.RESOT)THEN
NLESST=NLESST+1
RESLT(NNB)=.TRUE.
ELSE
NMORET=NMORET+1
RESLT(NNB)=.FALSE.
ENDIF

```

```

IF (CHNGURF) THEN

```

```

IF ((NLESSU-NMOREU).GT.NN1)THEN
URFU=URFU+(.9-URFU)/300.
ELSEIF((NLESSU-NMOREU).LT.NN2)THEN
URFU=URFU-(URFU-.1)/300.
ENDIF

```

```

IF ((NLESSV-NMOREV).GT.NN1)THEN
URFV=URFV+(.9-URFV)/300.
ELSEIF((NLESSV-NMOREV).LT.NN2)THEN
URFV=URFV-(URFV-.1)/300.
ENDIF

```

```

IF ((NLESSK-NMOREK).GT.NN1)THEN
URFK=URFK+(.9-URFK)/300.
ELSEIF((NLESSK-NMOREK).LT.NN2)THEN
URFK=URFK-(URFK-.1)/300.
ENDIF

```

```

IF ((NLESSE-NMOREE).GT.NN1)THEN
URFE=URFE+(.9-URFE)/300.
ELSEIF((NLESSE-NMOREE).LT.NN2)THEN
URFE=URFE-(URFE-.1)/300.
ENDIF

```

```

IF ((NLESST-NMORET).GT.NN1)THEN
URFT=URFT+(.9-URFT)/300.
ELSEIF((NLESST-NMORET).LT.NN2)THEN
URFT=URFT-(URFT-.1)/300.
ENDIF

```

```

ENDIF

```

```

RESOU=RESU
RESOV=RESV
RESOK=RESK
RESOE=RESE
RESOT=REST

```

```

A=REAL(NITER)/5.
B=INT(A)
C=A-REAL(B)
IF (C.LE.1E-5) THEN
PRINT*,*****
PRINT*,NITER,NITER,RESM-,RESM
PRINT*,RESU-,RESU,URFU-,URFU,NLESSU-NMOREU-,NLESSU-NMOREU
PRINT*,RESV-,RESV,URFV-,URFV,NLESSV-NMOREV-,NLESSV-NMOREV
PRINT*,RESK-,RESK,URFK-,URFK,NLESSK-NMOREK-,NLESSK-NMOREK
PRINT*,RESE-,RESE,URFE-,URFE,NLESSE-NMOREE-,NLESSE-NMOREE
PRINT*,REST-,REST,URFT-,URFT,NLESST-NMORET-,NLESST-NMORET
ENDIF

```

```

SORCE=AMAX1(RESORU,RESORV,RESORM,RESORK,RESORE,RESORT)
SOR=AMAX1(RESU,RESV,RESORM,RESM,RESK,RESE,REST)

```

```

IF(SORCE.GE.1.E+10.AND.NITER.GT.100)STOP
IF(SOR.LE.SORMAX)GO TO 20
IF(NITER.LT.MAXIT)GO TO 10
20 CONTINUE

```

```

C *** END ITERATION

```

```

CALL WRITE

```

```

311 FORMAT(1X,I4,1P12E10.3)

```

```

STOP

```

```

END

```